DOTTORATO DI RICERCA IN MEDICINA SPERIMENTALE

CURRICULUM BIOTECNOLOGIE E SCIENZE BIOCHIMICHE

XXXVIII CICLO

TESI DI DOTTORATO IN

Utilizzo degli ultrasuoni su modelli tumorali di epatocarcinoma e glioblastoma: approcci innovativi per l'identificazione di biomarcatori diagnostici

SSD: MEDS-26/A

Coordinatore del Corso
Prof. Adriano Angelucci

Dottorando
Francesco Colaianni

Tutor
Prof.ssa Alessandra Tessitore
Co-tutor
Prof. Mario Rossi

Anno Accademico 2024/2025

Contents

Chapter 1

Abstract

Background. Hepatocellular carcinoma (HCC) and glioblastoma (GBM) are highly aggressive tumors frequently diagnosed at late stages and associated with poor prognosis. Novel diagnostic biomarkers and strategies to enhance therapeutic delivery are urgently needed. Ultrasounds (US) and focused ultrasounds (FUS) emerged as promising tools to modulate cell membranes permeability, potentially enabling biomarker release (miRNAs and proteins) and improving drug uptake.

Methods and Materials. HCC cell lines (HepG2 and SNU-387) were treated with US to assess the release of microRNAs and proteins, into the culture supernatant. A normal liver cell line (THLE-2) was used as negative control for the analyses. After fine-tuning US parameters, miRNAs' profiling was performed by qRT-PCR using TaqMan-based microfluidic cards. Public datasets (GSE113740, GSE106817, GSE112264, GSE113486) were used for validation and Receiving Operating Curve (ROC) and Area Under Curve (AUC) were considered for analyses. Protein analysis was evaluated in cell supernatants by Antibody Array C-Series "Human Apoptosis Array C1".

To evaluate the ability of US to enhance small-molecule uptake, FAM-labeled AS1411 aptamer and sorafenib, both in combination with US, were tested on HCC cell lines. Uptake enhancement was assessed by measuring the FAM fluorescence signal, while treatment efficacy was evaluated through cell viability analysis . Cell viability was assessed after 24h of incubation with PrestoBlue viability assay.

In vivo pharmacokinetic analyses were performed in an orthotopic human GBM

xenograft mouse model. In this context, given the novel application of this technology in animal models, a pilot study was conducted to determine the optimal FUS parameters for assessing FUS-mediated effects . FUS treatment was applied to transiently open the blood–brain barrier (BBB) and facilitate delivery of the radiolabeled antibody xiRA63, targeting Endothelin A (ETA) receptor, considered as biomarker for GBM. Biodistribution was quantified by PET imaging at different timepoints post-injection (1 h, 4 h, 24 h, 48 h, 72 h and 168 h).

Results. US stimulation induced the significant release of four miRNAs, compared to untreated samples: miR-145-5p (SNU-387) and miR-29a-3p, miR-532-5p, miR-106b-3p (HepG2). Strikingly, same miRNAs were also proven to be significantly upregulated in HCC patient sera across public GEO datasets, with miR-532-5p showing the highest diagnostic performance. The control cell line, THLE-2, showed no significant miRNA release after US treatment. Moreover, US promoted the release of 9 protein factors resulted increased after US treatment on HCC cell lines. Among these proteins, FasL and Livin resulted significantly increased .

In addition, US enhanced sorafenib uptake and drug efficacy only in HepG2 cells, significantly reducing cell viability.

In vivo GBM mouse model, showed a mild not significant increase in xiRA63 distribution volume within glioma tissue after FUS, while irreversible uptake parameters and plasma AUC remained unchanged between FUS treated and non-treated group.

Conclusion. These *in vitro* and *in vivo* findings demonstrate that US and FUS can be considered innovative and promising tools for both identifying novel putative biomarkers and possibly enhancing the efficacy of therapeutic compounds, also targeting GBM biomarkers, for early diagnosis and therapy. US application enabled the selective release of miRNAs and proteins, leading to the identification of promising biomarker candidates—miR-532-5p, miR-29a-3p, miR-145-5p, miR-106b-3p, FasL and Livin—that warrant further clinical validation for diagnostic purposes. Moreover, US improved the *in vitro* response to sorafenib, suggesting its potential to enhance drug uptake and reduce required therapeutic doses. In the pilot experiments on the *in vivo* GBM model, FUS, applied based on the parameters and conditions

here tested, seem to induce a transient BBB opening, given that there is a trend towards to the increase of distribution volume of the xiRA63 in the brain, without reaching statistical significance. Then, also irreversible uptake of xiRA63 did not show any difference between FUS treated and untreated groups. Overall, this study highlights US are extremely useful in promoting the release of molecules to be used as putative biomarkers and boosting drug uptake in *in vitro* models. On the other hand, further research is still necessary to optimize FUS treatment to promote BBB opening, increasing the distribution volume of xiRA63 in the tumor site.

Chapter 2

Introduction

Cancer is the most common public health problem of the 21st century, in fact cancer is the second most common related-death disease [1]. The landscape is generally complicated by the lack of early prevention, early diagnosis and advanced treatment. In addition, non-resectable tumors represent a difficult challenge for clinical oncology. In this context, hepatocellular carcinoma (HCC) and glioblastoma multiforme (GBM) were chosen as candidate disease due to their complex pathogenesis, to develop better therapeutic approaches and to better care and management of patients. Regarding HCC, imaging-based diagnostic approaches, liver biopsy and other conventional strategies rarely provide early diagnosis to have full recovery. Moreover, several serological markers are not precisely diagnostic, due to their low sensitivity and specificity [2]. Similarly, GMB is often diagnosed when the lesion is already well-established and surgical resection is usually required. On the other hand, cancer therapy for HCC and GBM is deeply studied, especially in GBM, because, although biotechnological approaches, as recombinant antibodies, anti-cancer vaccines and combined strategies with chemotherapy and radiotherapy seem to be quite promising, there is still an urgent need of developing innovative strategies to enhance therapeutic efficacy and increasing overall survival and life expectancy to the greatest extent possible [3, 4]. Thus, this research aimed to set up ultrasound-based protocols to promote the release of molecules to be used as putative biomarkers (miRNAs and proteins), from HCC cell lines, and to enhance the delivery of an experimental antibody, targeting ETA receptor, a GBM biomarker,

in the brain of an *in vivo* GBM mouse model.

2.1 Biomarkers

Biomarkers are measurable biological indicators that reflect physiological or pathological processes or responses to therapeutic interventions. In oncology, biomarkers play a central role in early detection, diagnosis, prognosis, patient stratification, treatment selection, and monitoring of disease progression or therapeutic response [5]. They encompass a broad range of biological entities, including proteins, DNA and RNA species—such as circulating tumor DNA and microRNAs—metabolites, and cellular or imaging-based features, which can be detected in tumor tissues or accessible biofluids [6].

Several biomarkers are currently integrated into clinical oncology practice, including prostate-specific antigen (PSA) for prostate cancer, Human Epidermal Growth Factor Receptor 2 (HER2) amplification in breast cancer, and Epidermal Growth Factor Receptor (EGFR) or Kirsten rat sarcoma virus (KRAS) mutations to guide targeted therapies [7]. In recent years, increasing attention has been directed toward circulating biomarkers measurable through liquid biopsy approaches, owing to their minimally invasive nature and their potential to reflect tumor heterogeneity and dynamic disease changes over time [5].

In the context of HCC and liver diseases, alpha-fetoprotein (AFP) represents one of the most widely used circulating biomarkers and is routinely assessed in clinical practice. Although AFP levels may also be influenced by non-malignant liver conditions, its measurement remains a relevant component of HCC surveillance and patient evaluation, highlighting the need for complementary biomarkers to further improve diagnostic performance [2].

In the context of GBM, key molecular biomarkers include mutations in isocitrate dehydrogenase 1 and 2 (IDH1/2), which are associated with distinct tumor biology and significantly improved patient prognosis. Methylation of the O6-methylguanine-DNA methyltransferase (MGMT) promoter is another clinically relevant biomarker, as it predicts responsiveness to alkylating agents such as temozolomide and is routinely assessed in clinical practice [8, 9]. EGFR amplification

and the EGFRvIII mutant variant contribute to tumor proliferation and therapeutic resistance. Emerging circulating biomarkers, such as circulating tumor DNA and extracellular vesicle-associated RNAs detectable in cerebrospinal fluid or plasma, are being actively investigated as minimally invasive tools for disease monitoring and treatment response assessment. Although their clinical application remains limited, novel biomarkers are being investigated to assure a better management for the evolution of GBM in patients [10, 11].

2.2 MicroRNAs

MicroRNAs (miRNAs) are small non-coding RNAs, 22–30 nucleotides in length, that can regulate gene expression at the post-transcriptional level. As shown in Figure 1, miRNAs are transcribed from DNA gene sequences into primary miRNAs (pri-miRNAs) by RNA polymerase II/III. Most of pri-miRNAs are processed according to a canonical pathway by the RNA binding protein DiGeorge Syndrome Critical Region 8 (DGCR8) and Drosha ribonuclease [13]. Drosha cleaves the pri-miRNAs duplex at the hairpin structure of the pri-miRNAs, while DGCR8 recognizes a specific methylated sequence of GGAC to stabilize pri-miRNAs [14, 15]. Then, exportin transporters bring the pre-miRNAs from the nucleus to the citosol, where they are partially digested by the RNAse III endonuclease Dicer complex to produce the single-stranded mature miRNAs, which can regulate gene expression, by different mechanisms [12]. Few miRNAs can be also synthetized by non-canonical pathways, avoiding the molecular cleavage of DGCR8/Drosha pathways or the Dicer cleavage. Such pre-miRNAs avoid DGCR8/Drosha pathways beceause they derive from the cleavage of introns during the splicing. Other pre-miRNAs are directly transported into the citosol, thanks to a methylation of the CAP sequence at 5' end, that allows the protection from the first molecular cleavage. Dicer-independent miRNAs are processed in the DGCR8/Drosha pathway and in Argonaut 2 (Ago2) enzymatic cleavage in the citosol [16–18] (Figure 1). Once in the citosol, miRNAs negatively regulate target genes by forming a protein complex with Argonaut, called miRNA-RNA induced silencing complex (mi-RISC). Then, miRISC will bind at mRNA 3' untranslated region (UTR) only in the complementary sequence (seed sequence)

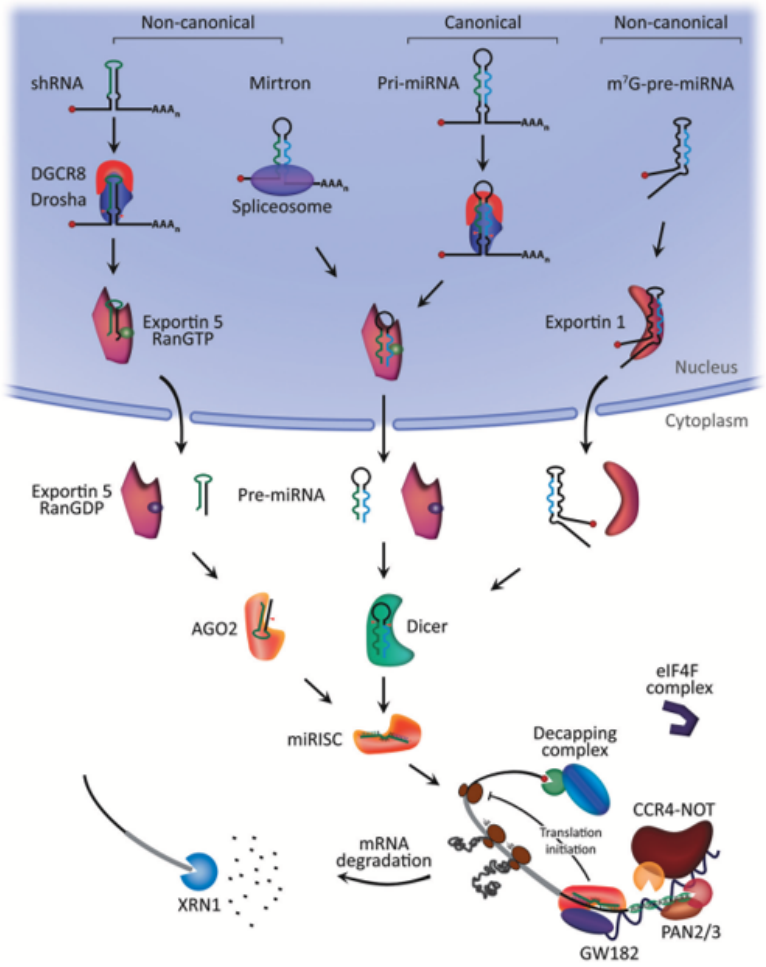

Figure 1. Panel showing canonical and non-canonical biogenesis of miRNA [12]

to promote inhibition of translation by enzymatic cleavage or RNA decay [12, 19]. Moreover, if the 3'UTR are too short, miRNAs can inhibit translation by binding mRNA coding sequences [20]. MiRNAs match target mRNAs only in the seed sequence, thus leading more than 15000 genes to be modulated by more than 2600 miRNAs in humans. As expected, a single miRNA can modulate tens of mRNAs, and single mRNA can be also modulated by multiple miRNAs [21–23].

MiRNA expression, regulation and dysregulation have been extensively described in several important physio-pathological conditions (e.g., cell proliferation, apoptosis, inflammation, metastasis, cardiovascular and neurodegenerative diseases, diabetes, cancer) [24–26]. In cancer disease, depending on the function of related target genes, miRNAs can be considered as oncomiR or tumor suppressor miRNAs, thus

promoting or suppressing oncogenesis processes [27, 28]. OncomiRs are generally overexpressed in cancers and promote cell proliferation, migration, inflammation, metastasis, multidrug resistance, and escaping apoptosis, by regulating several target proteins involved in tumor suppression, such as the Kruppel-like family of transcription factors (KLF), the phosphate and tensin homolog (PTEN), suppressor factors for NF-kB signaling pathway, programmed cell death 4 (PDCD4), pro-apoptotic and epitelial-mesenchimal transition (EMT) factors. In contrast, tumor suppressor microRNAs (ts-miRs) are frequently downregulated or inactivated in cancer and function as key negative regulators of oncogenic signaling. Under normal conditions, ts-miRs maintain cellular homeostasis by repressing oncogenes, growth factor receptors, cell-cycle regulators, and anti-apoptotic factors; their loss results in activation of proliferative and survival pathways, including PI3K/AKT/mTOR and RAS/MAPK, thereby promoting uncontrolled tumor growth [29–38]. MiRNAs can be found in tissue as well as in body fluids, such as plasma/serum, where they are extraordinarily stable and resistant to endogenous RNase, because they exist in association with RNA-binding proteins and/or exosomes, offering a potential source of non-invasive diagnostic, prognostic, and predictive biomarkers [12, 39, 40]. Therefore, circulating miRNAs can be detected and profiled in liquid biospy, thanks to the sensitive methods, such as quantitative PCR (qPCR), microarray analysis, next-generation sequencing (NGS) [41–43].

2.3 Hepatocellular carcinoma

2.3.1 Epidemiology and risk factors

HCC is a major global burden and the third death-related cancer disease, accounting for over 800.000 deaths per year worldwide [44–46]. In addition, HCC related mortality and incidence is expected to increase by more than 50% within 20 years [47].

The incidence of HCC is related to different risk factors, such as hepatitis B (HBV), hepatitis C (HCV) infection and metabolic-associated liver disease [48]. The burden of HCC is currently decreasing in Europe and America, because the

incidence of HBV and HCV infection was dramatically reduced by early prevention. However, viral liver infections remain an important liver disease-related factor in Asia and Africa [49]. Among the metabolic alterations, type 2 diatebes, dyslipidemia, hypertension and fat-rich diet contribute to increase HCC incidence, because they promote metabolic-associated liver disease development, such as alcoholic liver disease (ALD) and non-alcoholic fatty liver disease (NAFLD) [50]. Host factor and genetic susceptibility are also important risk factors related to HCC development: median age of HCC diagnosis is 62 years, with the highest incidence over the 50 years old. However, in 2024 more of 14.7% of cases were reported in young adult in the 15-49 years old range [44, 51]. Then, women are less susceptible than men, because the estrogen axis can suppress tumor-prone microenvironment and protect against HCC [52, 53].

2.3.2 Hepatocellular carcinoma: pathogenesis

HCC pathogenesis is a complex multistep process that consists of the progressive accumulation of genetic or developed molecular alterations in specific key target genes. Risk factor diseases contribute in a different way to the development of HCC by inducing several molecular and biochemical pathways, which mostly include inflammation, necrosis, apoptosis, and proliferation. Such molecular alteration can be easily detected with NGS to define the main features of HCC pathogenesis [54]. As mentioned above, HCC initiation and progression are promoted by different etiological risk factors: alcohol abuse, smoke, fat-rich diet, HBV and HCV infections, and aflatoxin exposure induce liver chronic inflammation [48, 49, 55]. Fat-rich diet and alcohol abuse contribute to HCC pathogenesis, by inducing the metabolic disease ALD and NAFLD. Both diseases induce hepatic steatosis, a pathological condition characterized by the excessive accumulation of triglycerides within hepatocytes, that can cause inflammation [55, 56]. HBV and HCV infections are the most common viral causes of hepatitis, which can manifest as either acute or chronic disease. Acute hepatitis typically resolves following viral clearance by cytotoxic T cells, provided that the liver damage is reversible [55, 57]. Common features of chronic liver disease are inflammation and production of reactive oxigen species (ROS). These events

lead to liver cirrhosis, through liver fibrosis, a specific process that occurs when the injured tissue is replaced by fibrotic scars, due to the accumulation of proteins from extracellular matrix. The combination of necrotic injured areas, fibrotic scars and regenerating nodules of hepatic stem cells (HSCs), leads to liver cirrhosis [58, 59]. Notably, if liver cirrhosis is irreversible, several molecular alteration can drive to HCC development [55]. The most commonly mutated genes in HCC are TP53 and beta-catenin (CTNNB1), associated with ALD-related HCC and HBV-related HCC respectively. Mutations of telomerase reverse transcriptase (TERT) promoter were found in 90% of HCC cases and are recurrently mutated in the last step of malignant transformation. Other less frequent somatic mutations are known to play a role in HCC development, such as mutation in PTEN, mitogen-associated protein kinase (MAPK) pathway, EGFR signaling pathway [54, 55, 60–65]. Main molecular alterations typical of HCC pathogenesis are shown in Figure 2. Recent studies demonstrated that epigenetic alterations (e.g. methylation, histone modification, post-transcriptional regulation) play pivotal role in HCC pathogenesis. In this context, several authors suggest that post-trascriptional regulation by miRNAs represents a crucial mechanism contributing to HCC development and progression. In addition, miRNAs' deregulation could be responsible for the alteration of pathway involved in HCC pathogenesis. All the features of miRNAs related to HCC pathogenesis will be described in details in the following subsection.

2.3.3 miRNAs in liver disease progression and HCC

As described in the previous subsections, miRNAs' aberrant expression is a crucial mechanism of liver disease progression and HCC. In HCC, miRNAs can act as oncomiRs and tumor suppressor miRs. As reviewed by Braconi et al., miRNAs contribute to tumor progression by modulating genes involved in regulation of proliferation, epitelial mesenchimal transition and metastasis [66]. According to the literature, the most studied miRNA related to liver disease development is miR-122, because it accounts for 70% of the miRNome of hepatic tissue. Downregulation of miR-122 in tissue induces the hyperexpression of multiple targets, as Krüppel-like Factors (KLF,) bone morphogenetic protein receptor type 1A (Bmpr1a), solute

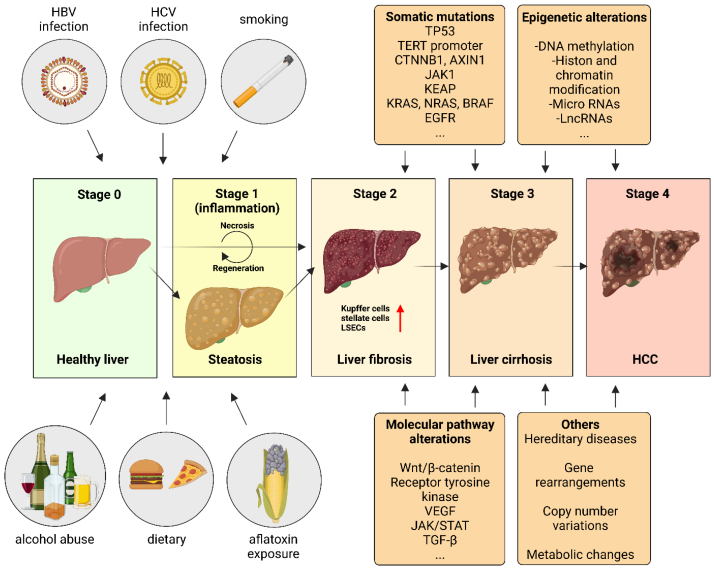

Figure 2. Panel showing the main stages of liver disease progression, main risk factors, such as fat-rich diet, alcohol abuse, aflatoxin exposure, smoke and viral infections, and main molecular alterations [55]

carrier family 7A2 (SLC7A2), insulin-like Growth Factor Receptor 1 (IGFR1), Cyclin G1 (CCNG1), Cell Division Cycle 6 protein (CDC6) and Minichromosome Maintenance Complex Component 4 (MCM4), leading to proliferation [67–69]. Also other miRNAs were described as modulators of cell proliferation, such as miR-223, miR-29 and miR-34, because their downregulation in HCC promote cell growth and apoptosis escaping [70–73]. In addition, miR-199 family downregulation is related to advanced stage of HCC and associated with poor prognosis, since these miRNAs regulate the expression of matrix metalloproteinase 9 (MMP-9) and hypoxia-inducible factor-1a (HIF1a) [74–76]. Similarly, miR-125a was found downregulated in HCC tissue and cell lines, inducing the expression of MAP3K11 and Protein tyrosine phosphatase N1 and promoting cell surival and proliferation [77]. On the other hand, several oncomiRs were found upregulated in tissue during HCC development. MiR-21 upregulation in liver promote HCC, via targeting PTEN, PDCD4 and tissue inhibitor of metalloproteinase 3 (TIMP3) [29, 69, 78, 79]. The pattern of miRNA deregulation depends on the etiology of HCC, including viral hepatitis and steatohepatitis, both alcoholic and non-alcoholic, and metabolic alterations [80, 81]. In this context,

miR-182-5p was found to be upregulated in diet-related HCC, modulated the tumor suppressor lysine 63 deubiquitinase (CYLD) and the transcription factor forkhead box protein O1 (FOXO1), whose downregulation is related to HCC development [82]. MiRNAs can be also involved in HBV and HCV-related HCC. As reviewed by Colaianni et al., miR-122 is known to interact with internal-ribosome entry site (IRES) of HCV virus to promote viral genome translation. In addition, several miRNAs were found to be involved in viral-related HCC, such as miR-141, miR-143, miR-145 and miR-199 [68, 83]. However, miRNAs expression pattern in HCC is mainly employed to define novel prognostic, diagnostic and therapeutic strategies. The identification of a miRNA or a panel of miRNAs in liver tissue or released into the bloodstream could improve diagnostic and therapeutic outcomes.

2.3.4 Hepatocellular carcinoma: current diagnosis

Currently, the main guidelines for the early diagnosis of HCC are based on the use of different approaches, that rely on the possibility to discriminate high risk patients (e.g. liver viral infection, liver cirrhosis, NAFLD/ALD, HCC background in relatives) from low risk patients. Recently, European Association for the Study of the Liver (EASL) recommended a specific diagnostic process, according to the classification of the patients. Magnetic resonance imaging (MRI) and computed tomography (CT) are mandatory as the first step of HCC diagnosis, because they are non-invasive and provide clear representations of liver. However, these imaging techniques cannot provide high resolution evaluation for the smallest nodules (<2cm), then it is challenging to develop novel diagnostic strategies. In details, a novel contrast enhanced ultrasound sonography (CEUS) technique was introduced as possible complementary strategy to MRI/CT. Although the novel diagnostic imaging strategies, nodules can be still uncertain, independent of the classification of the patients. Regarding the latter, the gold standard is the liver biopsy. However, it is a delicate procedure, that requires qualified pathologist producing a suitable specimen and avoiding tumor dissemination. Even if, the combination between MRI/CT, CEUS, liver biopsy and standardization processes can be considered gold standard procedures, each requires expertise for diagnostic evaluation of specific parameters

and liver biopsy is the most invasive (Table 1). In this context, there is an urgent need to evaluate novel diagnostic strategies, particularly those based on liquid biopsy for the analysis of circulating miRNAs and proteins, as plasma and serum represent readily accessible biofluids that allow for rapid and minimally invasive analysis [3].

Diagnostic method	Scenario	Criteria / Intent
High quality MRI/TC contrast	High and low-risk patients	APHE, delayed portal washout
MRI/TC + CEUS	Atypical imaging pattern	APHE, delayed portal washout
Liver biopsy	Negative imaging result, atypical imaging pattern, low and non-risk patients	Identification of tumor structures, differential diagnosis, translational medicine
Emerging strategies (liquid biopsy, radiomics, machine learning)	Absence of specific diagnostic criteria for early diagnosis	Pre-clinical research for novel putative biomarkers and criteria, bio-informatic analyses

Table 1. Table showing the main diagnostic methods for HCC recommended by EASL in 2025. Even if liver biopsy represents the gold standard method, it is only recommended for differential diagnosis to exclude risk of other diseases (cholangiocarcinoma, metastasis). Emerging strategies consist of the development of novel diagnostic methods, mainly based on the analysis of molecular serological markers, combined also with machine learning, to ease the diagnostic processes [3]

.

Regarding the latter, several authors showed that HCC diagnosis could be possible by analyzing AFP, because HCC development could correlate with increasing serum levels of AFP [84–86]. However, AFP levels are only suggestive of HCC, because it was demonstrated that AFP can be found in serum from HCC patients as well as well in others (e.g. viral and non-viral hepatitis, liver cirrhosis, cholangiocarcinoma) and also in healthy donors. This is possible, because AFP is the embrional homologue of human albumin and its expression can be modulated according to several factors,

that include pregnancy and genetic disorders. Thus, serum AFP resulted unreliable as diagnostic biomarker [2]. MiRNAs' involvement in HCC development made miRNAs putative biomarkers for HCC diagnosis. In this context, many studies highlighted the correlation of miRNAs' expression in sera with HCC development. Notably, a panel of miRNAs and AFP could improve diagnostic performance in large case-studies. As described above, although miR-122 is the most represented miRNA in liver, it should be combined in a panel of different miRNA to achieve good diagnostic sensitivity and specificity for HCC [68, 87–89]. Several miRNAs panels were provided to better the diagnostic accuracy, compared to AFP serum levels and they showed great outcomes in large case studies. Since these studies are related only to specific populations, novel strategies are still necessary to determine determine novel miRNAs actually predictive of HCC. To address this issue, several studies have investigated miRNAs as potential biomarkers of disease/condition, as summarized in Table 2, identifying a subset of miRNAs as particularly promising due to their specificity, stability in biofluids, and association with disease progression.

miRNAs	Regulation	References
miR-101-3p	Down	[90, 91]
miR-106b	Up	[90, 92]
miR-122	Up	[87–89, 93, 94]
miR-125a	Up	[95]
miR-125b	Down	[96–98]
miR-1246	Up	[90]
miR-15b	Up	[99, 100]
miR-150	Down	[101, 102]
miR-16	Down	[87]
miR-192	Up	[103]
miR-199a	Down	[89, 94, 104]
miR-130b	Up	[98]
miR-21	Up	[91, 103, 105]
miR-221	Up	[88, 106]
miR-222	Up	[93]
miR-224	Up	[106]
miR-26a	Down	[91, 104, 107]
miR-34a	Up	[108, 109]
miR-92a	Up	[110, 111]

Table 2. Table showing the most studied miRNAs as putative available biomarkers for HCC diagnosis. As asuggested by several authors, most of miRNAs should be used in panel to increase the diagnostic performance. Most of miRNAs represented in table were studied as circulating biomarkers for HCC diagnosis

.

2.3.5 Hepatocellular carcinoma: current therapies

Current guidelines for HCC treatment and management consist of different approaches, according to the stage and the main features of the disease. Main curative approaches rely on surgical resection of the tumor, combined with liver transplant, if necessary. In addition, there are invasive loco-regional treatments

that allow a stepwise reduction of the tumor. Trans-artherial chemoembolization and radioembolization (TACE and TARE) consist of the radio-guided injection of chemotherapic or radiotherapic drugs into hepatic arterial circulation, in presence of temporary arterial occlusion. These approaches should sensitively reduce small tumor mass also. Besides, it is possible the application of several combinations of systemic immunotherapy (e.g. atezolizumab, bevacizumab, durvalumab, tremelimumab), because classical chemotherapy, as platin-derived drugs and doxorubicin, can be associated to systemic toxicity and poor outcomes of survival. On the other hand, systemic target-therapy by tyrosin kinase inhibitors (e.g. sorafenib, levantinib, regorafenib, cabozantinib) can be still employed as possible treatment, when any therapy is not available. In particular, administration of atezolizumab, bevacizumab, durvalumab, tremelimumab and levantinib, regorafenib, cabozantinib showed less systemic toxicity and better outcomes of survival than sorafenib [3]. Indeed, sorafenib was the first tyrosin kinase inhibitor approved for the treatment of non-resectable HCC, but it showed systemic toxicity, as reactivation of HBV and HCV viruses, suppression of immune response, and resistance mechanism throughout time, as mutation in ATP binding cassette, SLC family transporters, RAF/MEK/ERK pathway, and autophagy activation [112–114]. Therefore, there is an urgent need to develop novel therapeutic approaches that could improve the delivery of the drug into the tumor, without affecting normal cells, reducing the dose administration and toxic effects.

2.4 Challenges and Opportunities in 3D modeling of Hepatocellular Carcinoma

The development of three-dimensional (3D) models of HCC represents a pivotal advancement toward overcoming the limitations of two-dimensional (2D) culture systems, which inadequately recapitulate the architectural, biochemical, and functional complexity of liver tumors. As demonstrated by multiple studies, 3D culture platforms, including spheroids, organoids, scaffold-based constructs, and hydrogels, improved physiological relevance by preserving cell–cell and cell–extracellular matrix

interactions, oxygen and nutrient gradients, and the spatial heterogeneity characteristic of in vivo tumor microenvironments [115–117]. These features are particularly essential for modeling HCC, that is characterized by extensive intratumoral heterogeneity, frequent resistance to systemic therapies, and co-presence of previous liver disease, as cirrhosis and hepatitis.

Spheroid-based tumor models remain among the most widely established 3D systems, offering controlled multicellular architectures that mimic avascular tumor regions, early metastatic niches, and hypoxic cores [116, 118]. Such models allow investigation of proliferation rate, metabolic rewiring, and drug penetration barriers: these processes are poorly represented in 2D cultures. Organoid technology further expands these fields by enabling long-term propagation of patient-derived tumors while retaining their genetic, phenotypic, and functional complexity [119]. In HCC, organoid models have emerged as powerful tools for studying tumor evolution, identifying actionable molecular drivers, and supporting precision medicine approaches.

Beyond self-organizing systems, engineered scaffolds and hydrogel-based bioprinting allow to reproduce specific hallmarks of hepatic tissue. Scaffold-based models can recapitulate liver-specific matrix composition, stiffness gradients associated with fibrosis, and tumor–stroma interactions with high fidelity [115]. Likewise, hydrogels provide modular platforms that preserve liver-relevant extracellular matrix cues and mechano-transduction pathways, enabling refined studies of tumor invasion and microenvironmental regulation [117].

Research conducted in different cancer types, including bladder, lung and breast cancer, has demonstrated the translational value of 3D cultures for modeling drug response, tumor–immune interactions, and mechanisms of therapeutic resistance [120, 121]. Concurrently, emerging technologies such as surface-enhanced Raman scattering (SERS) have been successfully applied to 3D systems, enabling real-time, high-resolution monitoring of cellular metabolism, drug uptake, and microenvironmental dynamics within complex tumor constructs [122]. These findings significantly demonstrated the current potential of studying HCC, by developing 3D HCC models.

In pharmacology and toxicology, 3D models of HCC could offer substantial advantages by enabling more realistic evaluation of drug behavior within tissue-like structures. Their ability to reproduce physiologically relevant gradients and mechanical cues supports more accurate assessments of drug penetration, metabolic activation, and chemotherapeutic efficacy. Given the liver's central role in xenobiotic metabolism, 3D culture systems better preserve key functional features—such as cytochrome P450 activity, drug transporter expression, and detoxification pathways—compared with conventional 2D cultures, particularly over prolonged culture periods, thereby improving the prediction of therapeutic response and off-target toxicity [123, 124]. Patient-derived spheroids and organoids are particularly valuable for profiling inter-patient variability and modeling mechanisms of acquired resistance [124]. Furthermore, insights from other 3D cancer systems have demonstrated that integration with high-content imaging, omics approaches, and sensitive analytical platforms yields improved characterization of dose–response relationships and adverse reactions [120, 121], underscoring the translational relevance of 3D HCC models for preclinical drug development.

Collectively, these advancements reinforce a growing consensus that 3D culture systems provide superior physiological fidelity, predictive accuracy, and mechanistic insight compared to traditional models. The continued refinement and implementation of 3D HCC models will be essential for bridging the gap between preclinical studies and clinical outcomes, ultimately supporting the development of more effective and personalized therapeutic strategies.

2.5 Glioblastoma

2.5.1 Epidemiology and risk factors

GBM is the third most common primary tumor of central nervous system (CNS). On a global scale, the mean incidence rate is estimated to be between 2 and 4 cases per 100.000 of population. GBM usually occurs at median age of 64 years, with slightly higher incidence in men than women and in caucasians than other ethnicities. Recurrence of GBM is typical, also after surgical resection and therapy.

Life expectancy after diagnosis is 4 months, but resection and therapy can increase it to 15 months [125, 126] . Very few risk factors were found to be associated to GBM. Notably, environmental risk factors were firstly associated to GBM development, but the relation to the disease was irrelevant. Actually, direct ionizing radiation exposure relates to GBM development, while other risk factors, as vinyl chloride, pesticides, smoking, synthetic rubber and petroleum refining, are poorly associated with GBM development. Strikingly smoke and alcohol consumption are not related to an increased risk of developing GBM [125, 127]. Also, genetic susceptibility is an important factor, because GBM can easily occur in presence of genetic diseases, as neurofibromatosis, retinoblastoma, Turcot and Li-Fraumeni syndrome [125, 127, 128].

2.5.2 Glioblastoma: pathogenesis

GBM development is a complex multi-step process, that consists of the alteration of CNS cells. Generally, in the adult human brain, most of neurons are post-mitotic and are mostly quiescent in the adult brain, but several glial cells maintain their proliferative activity. GBM develops as an astrocytic tumor, but its progenitor cells are more glial/neural subtype rather than fully differentiated astrocytes. 61% of GBMs usually develop in the four lobes of the brain, while it is less frequent in brainstem and spinal cord. According to World Health Organization (WHO) guidelines, in 2007 GBMs were described as astrocytomas and classified as primary or *de novo* and secundary tumors. WHO updated the classification in 2021, introducing the WHO grade, that defined GBM as IV grade astrocytoma, IDH-1 wildtype [126].

Morphologically, GBMs are characterized by irregularly shaped mass that exerts strong pressure nearby brain lobes, and necrotic core. Also, surrounding edema, ventricular distortions and hemorrhage are typical feature of GBMs. Despite of the classification, origin of GBM is still a debated question. Evidences suggest that GBM may derive from both astrocytes and neural-stem like cells (NSCs). This hypothesis is supported by phenotypic and molecular affinities between GBM cells and CNS cell populations, including surface, cell morphology and trascriptomic signatures [130,131]. In addition, genetic GBM mouse model demonstrated that differentiated glial cells, -and, in specific contexts, even neurons- can undergo oncogene-driven de-

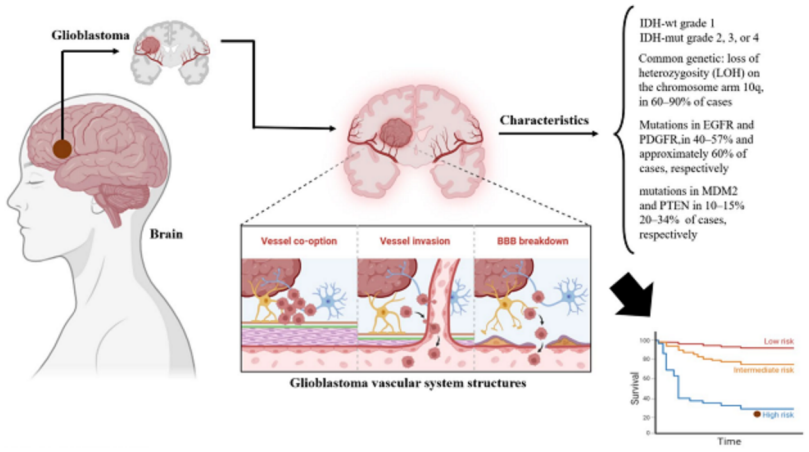

Figure 3. Picture showing the main features of GBM pathogenesis, including IDH alterations, loss of heterozygosity for 10q chromosome, MDM-2 and PTEN mutations. Morphologically GBM is characterized by vessel alterations, that induce BBB breakdown and inflammatory infiltrate [129].

differentiation into NSCs, that can initiate and sustain the gliomagenesis [132, 133]. Interestingly, accumulating evidences showed that cellular origin determines the molecular subtypes of the GBM [131, 134]. An extensive study for the Human Genome Atlas demostrated that more than 600 genes involved in pathways related to GBM development [135]. GBM shows the most frequent alteration in PTEN and TERT promoter mutations, overexpression of EGFR, loss of chromosome 10q. Also less frequent mutations can be found in TP53, PI3K and retinoblastoma (pRB). These alterations promote uncontrolled cell proliferation, cell survival, escape from apoptosis and senescence [126,127,136]. GBM pathogenesis is a complex cross-talk of different pathways: growth factors, as platelet derived growth factor (PDGF), VEGF, EGF and hepatocyte growth factor (HGF), activate Ras-Raf-Mek-ERK and PI3K signaling to induce cell proliferation. Thus, these pathways result in activation and phosphorylation of NF-kB, sustaining cell proliferation and survival [137]. Emerging evidences demonstrate that NF-kB activation is a peculiar feature of the mesenchimal subtype cells of GBM, indicating a more aggressive phenotype. In this context, GBM shows elevated expression of NF-kB target genes and upstream activators such as TNF-α, RELB, and TNF receptor type associated death domain protein (TRADD),

compared to other subtypes [138, 139]. Also Wnt/bCatenin and Notch pathways contribute to tumor invasion by inducing stemness, survival and neo-angiogenesis. The complex interaction between mutated oncosuppressor and oncogene activation contribute to the aggressiveness of GBM [4]. However, since 2016 studying GBM development has become easier, thanks to the set up of GlioVis data portal, in which 50 expression datasets of more than 6500 brain tumors, mostly GBMs, are recorded [140]. Although CNS was historically considered as immune-privileged site, it is now well known that it is tightly regulated by immune surveillance. glia and microglia cells act as the immune system, affecting GBM microenvironment, cell growth and angiogenesis. Microglia, the resident immune cells of CNS, together with macrophages and other glial cells, plays a pivotal role in regulating tissue homeostasis and orchestrating immune responses within the brain. In this context, microglia and tumor-associated macrophages (TAMs) are the major cellular elements of the tumor microenvironment, that actively regulate inflammation, tumor proliferation and angiogenesis. On the same level, GBM affects microenvironment, via inducing microglia activation towards distinct functional subtype, usually classified as M1 or M2 subtypes. M2-polarized microglia is usually activated in GBM, and reduces T-lymphocytes activity, by expressing Programmed death ligand 1 (PD-L1) and cluster differentiation 39 (CD39). In addition, M2-activated macrophages can produce anti-inflammatory cytokines, tumor-promoting factors and angiogenic factors [141, 142]. Within the glioblastoma microenvironment, several cytokines produced by tumor cells and immune populations—particularly TAM and microglia—cooperate to sustain tumor progression. IL-6, secreted by GBM cells, glioma stem cells (GSCs), TAMs and endothelial cells, activates the JAK/STAT3 pathway in tumor cells, thereby promoting survival, invasion, and maintenance of stem-like traits [143, 144]. IL-1β, generated mainly by activated microglia and TAMs, signals through NF-kB in GBM cells, enhancing local inflammation, matrix remodeling and invasiveness, while also stimulating secondary cytokine production such as IL-6, thus reinforcing a feed-forward pro-tumorigenic loop [144,145]. TGF-β, produced by tumor cells, T regulatory cells and TAMs, further shapes the tumor microenvironment through canonical SMAD-dependent and non-canonical pathways, driving cellular

plasticity, mesenchymal transition and GSC maintenance, while exerting strong immunosuppressive effects by inhibiting cytotoxic T cells, NK cells and dendritic cell maturation [146, 147]. In contrast, M1-polarized microglia play a minimal role in glioblastoma, as the immunosuppressive tumor microenvironment—shaped by TAMs, stromal elements, GBM cells, and immunoregulatory cytokines and chemokines such as IL-10, CCL2, CCL5, and CXCL12—prevents their induction and persistence, rendering their anti-tumor activity largely ineffective [148, 149]. Angiogenesis is very important in GBM, because hypoxia induces stem cells to differentiate into endothelium, producing additional blood vessels. Angiogenic factors in GBM are regulated by oncogene activation, tumor suppressor loss, and hypoxia. Several pro-angiogenic factors, as VEGF, basic fibroblast growth factor (bFGF), and MMPs are released by microglia and tumor to sustain tumor invasion. The overexpression of VEGF and VEGFR-1 is correlated with poor prognosis, because this pathway cooperates with PDGF and FGF to induce vessels formation. MMPs degrade the endothelial basement membrane, facilitating angiogenic differentiation of cancer cells. Aberrant activation of these pathways is usually related to genetic mutations or alterantions, as aforementioned [4, 150]. Moreover, recent studies demonstrated that chemokine receptor type 4 (CXCR-4), endothelin A (ETA) receptor are expressed as hallmark in GBM associated vessels [151–154]. ETA receptor represents a key regulator of both tumor-intrinsic and microenvironmental processes that drive disease aggressiveness. Through activation by endothelin-1, ETA contributes to the development of the aberrant tumor vasculature by promoting endothelial cell proliferation. Then, ETA receptor signaling sustains GBM cell proliferation, survival and resistance to apoptosis via activation of PI3K/AKT and MAPK pathways. In addition, ETA contributes to the maintenance of the stem-like phenotype, reinforcing tumor growth and therapeutic resistance. Overall, these features highlights the ETA receptor as a crucial marker for the tumor progression and disease aggressiveness [151, 153].

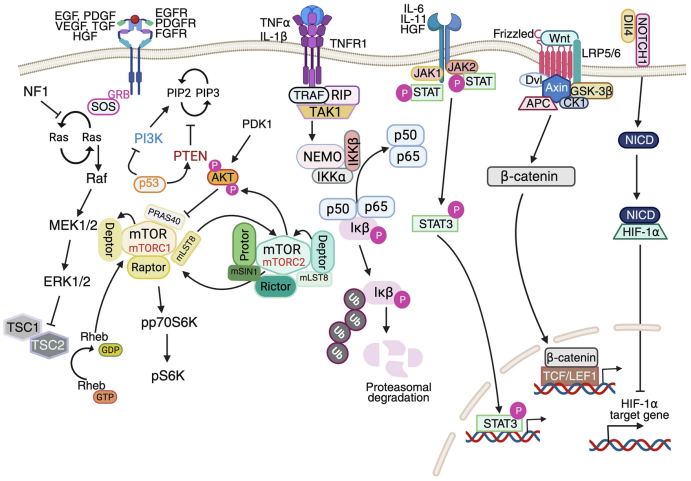

Figure 4. Picture showing complex crosstalk that induce and promote GBM development and aggressiveness. [4]

2.5.3 Glioblastoma: current therapies

Current guidelines for the treatment of GBM consist of conventional and innovative approaches. Conventional therapeutic strategies include surgical intervention to remove the tumor, combined with chemotherapy and radiotherapy (RT). These approaches are not resolutive, either individually or in combination; therefore, the primary goal of GBM treatment is to prolong overall survival after diagnosis.

Conventional care involves maximal safe surgical resection, followed by external radiation therapy and chemotherapy, administered concomitantly or sequentially with radiotherapy. Complete elimination of the tumor mass by surgery is not currently possible due to the complexity and highly infiltrative behavior of gliomas [4]. As a result, radiotherapy and chemotherapy—primarily temozolomide—are routinely employed as post-surgical treatments, although their impact on long-term survival remains limited and is often accompanied by debilitating side effects. Despite the use of multimodal standard-of-care treatments, the 5-year overall survival rate for patients with GBM remains approximately 5% [4, 155].

Advances in brain mapping and imaging techniques, such as CT and MRI, have improved surgical planning and tumor resection. In particular, intra-operative MRI and fluorescence-guided imaging have proven useful in identifying tumor margins and optimizing the extent of resection [156, 157]. Nevertheless, surgical interven-

tion remains highly challenging due to intraoperative brain shift, which can cause mismatches between preoperative imaging and the actual tumor location. MRI remains the gold standard for GBM imaging because of its high spatial resolution and contrast, and imaging-guided resection is also valuable for identifying residual tumor tissue amenable to further surgical or adjuvant treatment.

Given the impossibility of achieving complete tumor eradication through surgery alone, external radiotherapy and chemotherapy—mostly temozolomide (TMZ)—represent the standard post-surgical treatment modalities. In addition, carmustine, lomustine, and other nitrosourea-based drugs have been evaluated for GBM therapy because of their ability to cross the blood–brain barrier (BBB), owing to their small molecular size and lipophilicity [155, 158].

Radiotherapy aims to directly damage the DNA of residual GBM cells while minimizing toxicity to surrounding healthy tissue. External RT is delivered using x-ray photons, gamma rays, or protons, whereas brachytherapy relies on the implantation of radioactive isotopes such as iodine-125 or iridium-192. More advanced radiotherapy techniques, including stereotactic radiosurgery, hypofractionated regimens, and adaptive radiotherapy, have been explored to enhance local tumor control while limiting radiation exposure to healthy brain regions [159]. Although combination therapies are generally more effective than single-modality approaches for reducing tumor burden, combined chemotherapy and radiotherapy still confer only modest benefits in overall survival and are associated with significant adverse effects, including nausea, headache, loss of appetite, skin inflammation, and leukopenia [155, 158, 159].

Tumor recurrence is largely attributed to intrinsic and acquired resistance mechanisms, such as p53 inactivation, enhanced DNA repair capacity, and impaired cell cycle checkpoint control. Furthermore, resistance and recurrence are strongly linked to the presence of glioma stem-like cells, which contribute to tumor heterogeneity and therapeutic failure [131, 134].

In this context, the molecular heterogeneity of GBM plays a critical role in determining treatment response and prognosis. Genetic and epigenetic alterations—including IDH mutation status, MGMT promoter methylation, and EGFR amplification—are now recognized as major determinants of therapeutic sensitiv-

ity and resistance, underscoring the importance of molecular stratification for the development of personalized treatment strategies [155, 160].

Immunotherapeutic approaches have been extensively investigated in glioblastoma but have not yet demonstrated substantial improvements in overall survival. Similarly, emerging strategies based on precision oncology and targeted therapies—such as vaccines, tyrosine kinase inhibitors, and monoclonal antibodies—remain under active investigation and require further optimization to achieve meaningful clinical efficacy [161]. Tumor Treating Fields (TTF), a non-invasive modality that delivers alternating electric fields, have been introduced as an adjunct to standard therapy, showing modest survival benefits while raising concerns related to patient compliance and quality of life [162].

Recent advances in nuclear medicine, particularly in the field of internal radiotherapy, offer promising new opportunities for GBM treatment. If therapeutic radiation doses can be delivered selectively to tumor cells, as shown in oligometastatic prostate cancer with 3-year OS of 95.7%, tumor control can be improved while sparing healthy tissue [163]. Accordingly, radiopeptides targeting somatostatin receptors, such as ^{90}Y-DOTATOC and ^{177}Lu-DOTATE, have shown improvements in patient quality of life and, in some cases, partial or complete tumor remission in advanced glioblastoma [4, 161]. However, a major limitation of radiopeptide-based therapies remains their ability to effectively cross the BBB and target only tumor cells in the brain. In GBM, BBB integrity is disrupted in a stage-dependent manner, and while increased permeability may facilitate biomarker detection, it is also associated with more aggressive disease phenotypes [164].

Therefore, early diagnosis and timely initiation of therapy are essential to ensure optimal management of GBM patients. Early-stage intervention may provide a therapeutic window for strategies aimed at enhancing drug delivery across the BBB. Accurate dose localization could also help preserve healthy functional tissue, which is as critical as eliminating cancer cells in such a sensitive organ as the brain. In this context, radioactive cargoes, in the form of radionuclides emitting therapeutic levels of particulate radiation, can deliver cytotoxic doses directly to the tumor mass.

2.5.4 Antibody targeted therapy

Considering the limited efficacy of standard-of-care treatments—including surgical resection, chemotherapy, and radiotherapy—in achieving durable disease control in glioblastoma, increasing attention has been directed toward molecularly targeted therapies. In this context, the altered integrity of the BBB observed in GBM provides a potential therapeutic window for the application of antibody-based strategies, including antibody–drug conjugates (ADCs), aimed at improving selective drug delivery to tumor cells [165]. Moreover, given the poor prognosis and limited overall survival associated with GBM, the appropriate selection and management of targeted therapies represent a critical aspect of patient care [164].

Currently, none of the available targeted therapies are approved as first-line treatments for GBM, as the standard therapeutic approach still relies on a multimodal regimen combining maximal safe surgical resection, radiotherapy, and chemotherapy. Nevertheless, several monoclonal antibodies targeting key molecular pathways involved in glioblastoma progression have been investigated, particularly in the recurrent setting.

Most clinically evaluated monoclonal antibodies for targeted therapy in GBM have been developed to interfere with pro-angiogenic signaling pathways or growth factor receptors. Among these, bevacizumab, nimotuzumab, cetuximab, and panitumumab are naked monoclonal antibodies that target VEGF or EGFR, rather than antibody–drug conjugates.

Bevacizumab is a humanized monoclonal antibody directed against VEGF and is approved for second-line therapy and for recurrent GBM. In a phase II experimental study, treatment with bevacizumab in combination with irinotecan demonstrated good tolerability and a reduction in neuroinflammation and cerebral edema; however, no significant improvement in overall survival was observed [166].

Cetuximab is a chimeric monoclonal antibody targeting EGFR, thereby inhibiting tumor growth and angiogenesis. Similar to bevacizumab, cetuximab has shown an acceptable safety profile in GBM patients, although its efficacy in reducing edema and inflammation has been limited. Nonetheless, phase II studies in recurrent GBM have reported an improvement in overall survival in subsets of patients with

EGFR overexpression [167]. Likewise, nimotuzumab and panitumumab—both EGFR-targeting monoclonal antibodies—have demonstrated favorable toxicity and safety profiles, with modest but promising clinical benefits. In particular, phase II clinical studies have reported that approximately 21% of patients experienced an increase in overall survival of 4.5 months and up to 2 years following treatment with panitumumab and nimotuzumab, respectively [168, 169].

Overall, antibody-based therapies represent a promising therapeutic rationale for the management of recurrent GBM; however, multiple factors continue to limit their clinical efficacy. These include insufficient and non-uniform BBB permeability, heterogeneity of EGFR expression and mutations, and the lack of reliable predictive biomarkers of therapeutic response. Although nimotuzumab has demonstrated good tolerability, its impact on overall survival remains limited, while cetuximab and panitumumab are currently considered less effective in GBM compared with other solid tumors.

In this context, there is an urgent need to develop novel strategies capable of overcoming the limitations imposed by BBB permeability. Recent studies have demonstrated that focused ultrasound (FUS) can transiently disrupt the BBB, thereby enhancing the uptake of antibody-based therapeutics. Notably, Chevaleyre et al. reported that FUS-mediated BBB disruption enabled the delivery and quantitative imaging of anti–PD-L1 antibodies in murine models of GBM, highlighting the potential of this approach to improve the efficacy of antibody-based targeted therapies [170].

2.6 Ultrasounds in biology

Ultrasounds (US) are sound waves with frequency higher than 20 kHz, characterized by sinusoidal propagation and repeated impulses. Ultrasound waves are generated by piezo-electric crystal when is driven by a high-frequency electrical signal. Then, the crystal vibrates at the same frequency and these vibrations produce sound waves in air or liquid, which become ultrasound if the frequency is above 20 kHz. The International Transcranial Ultrasonic Stimulation Safety and Standards Consortium (ITRUSST) recommends reporting ultrasound parameters as follows.

Frequency represents the number of wave cycles per unit of time, typically expressed in Hertz (Hz). Wavelength is the distance between two consecutive maxima in the wave. Duty cycle (DC) indicates the percentage of time during which ultrasound waves are transmitted. Acoustic pressure, measured in Pascals (Pa), corresponds to the positive or negative peak of compression along the ultrasound wave. Spatial-peak temporal-average intensity (I_{spta}) and spatial-peak pulse-average intensity (I_{sppa}), expressed in W/cm^2, represent the average intensity of the ultrasound waves over time and during each pulse, respectively [171].

Regarding the use of US in biology, several authors demonstrated that US at specific parameters produce the bio-mechanic effect of sonoporation, which consists in the formation of transient pores on cell membrane to allow bi-directional passage of molecules. In the context of sonoporation, US should be applied to promote transient permeability of cell membrane, avoiding cell disruption. Thus, frequency, AP and DC should be defined according to conservative approach. A particular application of ultrasounds consist of FUS. These are high-frequency sound waves that are physically analogous to conventional ultrasound, but with the capability to be concentrated at a precise location within biological tissues. Like standard ultrasound, FUS propagates through materials as mechanical vibrations. However, its main distinguishing feature is the spatial focusing of energy, which enables localized biological effects such as ablation or membrane opening without affecting surrounding areas. This ability sets FUS apart from conventional ultrasound, which typically acts over larger volumes with lower spatial precision [172]. Then, US and FUS are widely employed in biology and medicine for diagnostic and therapeutic approaches, owing to their interaction with tissues through bio-mechanical, thermal and cavitation-related effects. US are routinely employed for real-time US-based imaging of soft tissues, vascular structures, organ dynamics, blood flown and perfusion, that are critical features in oncology, cardiology and obstetrics [3, 173]. From a therapeutic perspective, FUS are used to induce controlled thermal effects, that are useful in clinical application, such as coagulation, hyperthermia and tumor ablation. High-intensity focused ultrasounds (HIFU), a specific implementation of FUS, allow precise thermal destruction of pathological tissues while sparing surrounding healthy

structures, and has been clinically applied in the treatment of solid tumors and neurological disorders. At lower intensities, ultrasound-mediated hyperthermia can sensitize tissues to radiotherapy or chemotherapy, enhancing treatment efficacy. Moreover, ultrasound can sensitize tissue to promote a mild production of ROS, performing sonodynamic therapy and healing injured tissues [172, 174, 175].

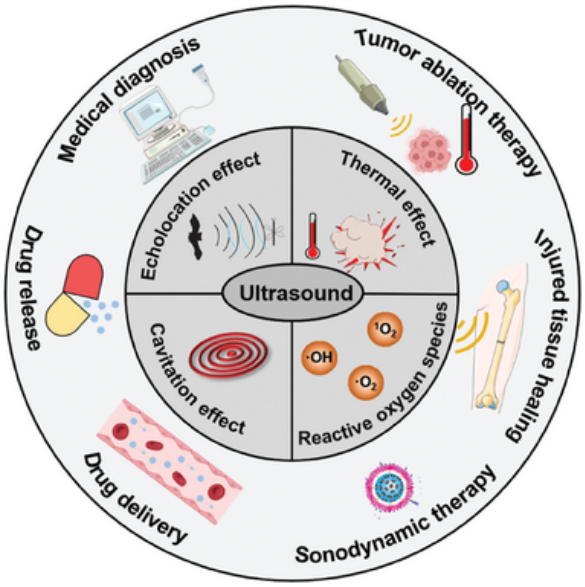

Figure 5. A summary of mechanism and application of ultrasound in biomedicine [175]

As reviewed by Przystupski et al., US can promote the alteration of permeability, facilitating targeted delivery across biological barriers, including the blood–brain barrier, allowing bi-directional flux of molecules, avoiding significant cellular alterations [176]. As reported by Zelli et al. and Cornice et al., US-mediated sonoporation can promote and amplify the release of small molecules, as miRNAs and proteins, from pancreatic cancer cell lines and prostate cancer cell lines respectively. [177, 178]. In addition, FUS-related BBB opening facilitates the uptake of C4 radio-labeled ligand, allowing the quantitative imaging of PD-L1 within the brain of GBM mouse model [170].

Features	Ultrasounds (US)	Focused ultrasounds (FUS)
Frequency	0.5-20MHz	0.5-5MHz
Precision	Low	High
Area	Wide	Focalized
Biological effects	Imaging	Target therapy, ablation
Intensity	Moderate/Low	Very high in the focal point
Applications	Ecography	Ablation

Table 3. Table shows the main features of US and FUS and their most known applications in clinical context. It is possible to highlight that US and FUS are the same physical principle and their differences consist of the experimental method of application.

2.7 Aim of the thesis

The aim of this thesis was to explore the potential of US and FUS as versatile, non-invasive technologies to improve both diagnostic and therapeutic strategies in HCC and GBM, that require early diagnosis and therapy. Given the poor prognosis associated with late diagnosis and limited drug delivery efficiency in these tumors, this work focused on exploiting the ability of US/FUS to transiently modulate biological barriers and cellular membrane permeability in a controlled and localized manner.

In *in vitro* HCC models, the study aimed to assess whether US stimulation could selectively induce the release of tumor-associated microRNAs and proteins into supernatant, supporting their use as candidate circulating biomarkers for liquid biopsy applications in HCC patients. In addition, the effect of US on enhancing the uptake and efficacy of therapeutic compounds was investigated, using sorafenib as a model drug in HCC cell lines. These experiments were designed to evaluate US as a strategy to increase intracellular drug accumulation while potentially reducing the required therapeutic dose and associated toxicity.

Regarding the GBM *in vivo* model, a pilot study was set up to define experimental conditions, with the aim to evaluate the effects of FUS in orthotopically xenografted mice. To this purpose, the ability of FUS to transiently open the BBB

and modulate the biodistribution of a radiolabeled antibody, recognizing the ETA receptor, overexpressed in the vascular endothelium of GBM and known to be a biomarker for GBM, was considered.

This work was carried out through a multidisciplinary and translational approach, supported by the industrial partner Inno-Sol srl (Rome, Italy), which provided the Sonowell instrument, and by an international collaboration with BioMaps, laboratory of medical imaging (Paris Saclay, CEA-SHFJ, Orsay, France) that carried out the *in vivo* experimentation. Overall, the thesis contributed to the development of US/FUS-based strategies as enabling technologies for precision oncology, bridging diagnostic biomarker discovery and biomarker-based targeted therapeutic delivery.

Chapter 3

Methods and materials

3.1 Sonowell: a prototype for ultrasound treatment in *in vitro* models

The use of focused ultrasound requires dedicated instrumentation, which must be selected according to the biological system under investigation. In recent years, an integrated ultrasound platform—Sonowell®, developed by Inno-Sol srl (Rome), the industrial partner of this study— has been introduced for conducting sonoporation experiments on *in vitro* cancer models [177, 178].

Figure 6. The Sonowell® system and its modular components.

The system allows multi-well plates ranging from 6 to 96 wells and enables the execution of fully customizable treatment protocols. These protocols are managed through proprietary software installed on a computer-based control terminal, allowing independent adjustment of the ultrasound parameters for each individual well. As shown in Figure 6, the device is composed of several functional modules: an ultrasound generator, a thermostatically controlled water bath, a hydraulic recirculation system, a three-axis positioning unit, a holder containing four transducers, and the control terminal. The presence of a controlled-temperature bath, which maintains the medium at approximately 37 °C, ensures that experiments can be carried out without inducing thermal stress in the cultured cells. The generator includes four fully independent parallel channels, each capable of delivering up to 20 W of power over a frequency range of 0.5–5 MHz. It produces a sinusoidal output waveform with a pulse repetition frequency of up to 90 Hz and a duty cycle adjustable up to 100%. The holder comprises four flat transducers with an active surface diameter of 12 mm. The transducers operate at distinct frequencies, 0.65, 1, 2.4, and 4.5 MHz, and can deliver a maximum acoustic intensity of 6 W/cm^2 in continuous-wave mode (60 s). Their spatial arrangement is optimized according to frequency to ensure maximal uniformity of the acoustic field across the targeted wells. The hydraulic unit includes a 10 L water reservoir, pumps for continuous circulation between the reservoir and the holder, and a set of filters designed to degas the water and remove particulate contaminants. The positioning system enables automated motion and precise placement of the multi-well plate without manual intervention. It consists of three motors operating along the X, Y, and Z axes, with a minimum step resolution of 10 µm.Once the treatment protocol is defined, the corresponding parameters are entered into the control software, which communicates directly with the generator.

The main experimental applications of the Sonowell® system include:

- controlled sonoporation of the cell membrane
- enabling the bi-directional flux of molecule (e.g. drugs, nanoparticles, nucleic acids, proteins)
- disruption and weakening of microbial biofilms

- stimulation of cellular proliferation and *in vitro* regeneration

3.2 FUS instrumentation for BBB opening in *in vivo* models

For transcranial BBB opening in preclinical mouse models, a single-element focused ultrasound platform developed by Imasonic (Voray-sur-l'Ognon, France) was employed in this study.

The system allows precise delivery of ultrasound energy to targeted regions of the mouse brain and enables fully customizable treatment protocols. These protocols are managed through a single-channel programmable generator (Image Guided Therapy, Pessac, France), which allows independent adjustment of all ultrasound parameters, including frequency, pulse duration, and repetition rate.

The device is composed of several functional modules: a focused ultrasound transducer, a calibrated hydrophone for beam profiling, a motorized XYZ positioning stage, a coupling interface consisting of a water-filled latex balloon and coupling gel, and the control terminal connected to the generator. The presence of the coupling balloon, filled with deionized and degassed water, ensures efficient transmission of the ultrasound waves through the skull, while maintaining the center of the brain at the focal depth of 20 mm.

The transducer has an active diameter of 25 mm and operates at a central frequency of 1.5 MHz. It exhibits an axial resolution of 5 mm and a lateral resolution of 1 mm, as measured by the hydrophone at -6 dB. The generator delivers a sinusoidal output waveform with programmable parameters, allowing precise control of the acoustic exposure.

The motorized positioning system enables automated motion and precise alignment of the mouse head relative to the focal zone. It consists of three motors operating along the X, Y, and Z axes, which allow fine adjustments of the focal distance and lateral placement, ensuring accurate targeting of the brain region of interest.

Once the treatment protocol is defined, the corresponding parameters are entered

into the control software, which communicates directly with the generator to execute the ultrasound exposures. This configuration allows reproducible and controlled BBB permeabilization without inducing thermal damage to the tissue.

3.3 Cell cultures

3.3.1 Liver cell lines

Human hepatocellular carcinoma (HCC) cell lines (HepG2 and SNU-387) were purchased from ATCC (Manassas, VA, USA) and a human normal hepatocyte derived cell line (THLE-2) was purchased from AddexBio (T0015001, San Diego, CA, USA). In details, HepG2 cell line, isolated from HCC of a 15-year-old white caucasian male, is characterized by epithelial-like morphology and by the expression of several liver marker genes, proteins and enzymes, such as AFP, albumin, alpha2 macroglobulin (alpha-2-macroglobulin), insulin-like-growth factor II (IGF II), 3-hydroxy-3-methylglutaryl-CoA reductase and hepatic triglyceride lipase. SNU-387 cell line derives from primary pleiomorphic HCC isolated from a 41-year-old Korean female patient, who had been treated by TACE with lipoidol plus a combination of doxorubicin and mitomycin-C. Hepatitis B virus (HBV) genome was detected by Southern Blot hybridization in SNU-387, but it is not expressed as genomic RNA. In addition, SNU-387 cells show few differentiation features, such as low expression of E-cadherin and expression of Vimentin and does not express AFP [179, 180]. HCC cell lines were cultured in RPMI-1640 (EuroClone, Milan, Italy) supplemented with 10% fetal bovine serum, 2 µM L-glutamine, 0.05 U/mL penicillin-streptomycin and were maintained at 37°C with 5% CO_2. As a control, THLE-2, an immortalized epithelial cell line derived from the liver of a healthy donor by infection with Simian Virus 40 (SV40) large T antigen, was used. The cell line expresses all the phenotypic characteristics of normal adult hepatocytes. Cells are non-cancerous and express epoxide hydrolase, NADPH cytochrome P450 reductase, superoxide dismutase, catalase, glutathione S-transferase, and glutathione peroxidase [181]. THLE-2 cell line was maintained under the same conditions and cultured using BEGM Bulletkit (CC3170, Lonza, Basilea, Switzerland), supplemented as the manufacturer protocol,

from which gentamycin/ Amphotericin (GA) and Epinephrine were discarded and additional 5 ng/mL of EGF, 70 ng/mL of phosphoethanolamine, 10% FBS and 0.05 U/mL penicillin-streptomycin were added. Each culture support for THLE-2 was coated with mixture of 0.01 mg/mL fibronectin, 0.03 mg/mL bovine collagen type I and 0.01 mg/mL, as indicated by manufacturer protocol.

Cell number / well		
Cell line	**Molecule release**	**Drug delivery**
HepG2	200.000	100.000
SNU-387	80.000	50.000
THLE-2	200.000	

Table 4. Table resumes the cell number seeded per each cell line, according to the experimental procedure. Cell number was chosen according to the doubling time of cell lines and the type of each treatment.

At 80% confluency, the cells were treated with trypsin, counted with an automatic cell counter (Cyto Smart, Corning Life Sciences, Durham, USA), transferred into a Falcon 24-well plate (cod 353047, Corning Incorporated, Corning, NY, USA) with a different number depending on each cell line (per well: 100.000 and 200.000 HepG2, 50.000 and 75.000 SNU-387 and 200.000 THLE-2 cells, in 500 µL of medium, Table 4) and cultured at 37°C with 5% CO_2 for 24h. Cell seeding number was chosen per each cell line according to their growth rate and after observation at light microscopy [180–182] .

3.3.2 Glioblastoma cell line

Human GBM primary Gli7 cells were kindly provided by BioMaps Laboratory (Paris Saclay, CEA-SHFJ, Orsay, France). At 80% of confluence, Gli7 were recovered and prepared for GBM xenograft in nude NMRI mouse models. Gli7 cells were cultured in DMEM-F12 (Gibco) supplemented with 1% glutamine, 1% N-2 supplement (Gibco), 1% B-27 (Gibco), 0.6 µg/mL glucose (Sigma), 20 µg/mL insulin (Sigma), 0.2 µg/mL bFGF (Preprotech), 0.2 µg/mL EGF (Prepotech), 2 µg/mL ciprofloxacin (Euromedex) and 2 µg/mL heparin (Sigma). Cells were incubated at 37°C in a 5%

CO_2 atmosphere.

3.4 US and FUS treatment

3.4.1 Measurements of US/FUS parameters

Measurements of the parameters were performed based on the suggestions of the ITRUSST consensus, where applicable, to the *in vitro* measurements and suggested nomenclature was adopted for the acoustic parameters [171]. For the *in vitro* experiments, one well at time was treated with US, taking advantage of the SonoWell® instrument (Inno-Sol srl, Rome, Italy) at 1MHz frequency for the *in vitro* experiments. For the *in vivo* experiments, the FUS single-channel transducer (Imasonic, Voray-sur-l'Ognon, France; Image Guided Therapy, Pessac, France) was used. AP, I_{spta} and I_{sppa} and DC were adjusted according to each experimental condition.

3.4.2 US treatment for molecule release in liver cell lines

After 24h, culture medium was discarded, cells were washed in sterile PBS, and 400 uL of serum-free culture medium was added in each well. One well at a time was treated with US. All sonication parameters were defined to prevent any alteration in cell morphology and to maintain over 85% cell viability. To promote the flux of molecules through cell membrane, both HCC cell lines were treated at 394kPa of AP. HepG2 were treated for 80 minutes of SD, with 10 minutes of interval without US after 40 minutes of treatment, with 2 ms TBD, 10%DC, I_{SPPA} = 5.0401 W/cm² and I_{SPTA} = 0.5040 W/cm². SNU-387 were treated for 30 minutes of SD, with 2 ms TBD, 10%DC, I_{SPPA} = 5.0401 W/cm² and I_{SPTA} = 0.5040 W/cm². While, THLE-2 were treated at 460 kPa of AP, for 30 minutes of SD, with 2 ms TBD, 10% DC, I_{SPPA} = 6.871 W/cm² and I_{SPTA} = 0.687 W/cm². Untreated control samples were subjected to same washing, temperature, and timing conditions, cultured in parallel within an incubator. After US treatment, cells were incubated at 37 °C and 5% CO_2 for 10 min. Morphological alterations were evaluated by optical microscopy analysis. Cell viability and and cell number were assessed by Trypan Blue staining with an automatic cell counter (Cyto Smart, Corning Life Sciences) and then analyzed to

compare the number of US treated and non-treated cells. Then cells and supernatants were collected and centrifuged for 20 minutes at 4 °C and 1500× g to remove cellular debris. Samples were stored at -80 °C and used for downstream applications, as described below.

3.4.3 US treatment for small drugs delivery in liver cell lines

After 24h, HCC cell lines were treated at 5 µM concentration of the FAM-labelled mutated aptamer AS1411 to determine whether US treatment could enhance drug delivery within specific incubation time. To promote US-mediated drug delivery, HCC cell lines were treated at 1MHz frequency, for 3 seconds and 30 seconds of SD, 526kPa of negative peak AP, with 6 ms of TBD, 50%DC, I_{SPPA} = 8.976 W/cm² and I_{SPTA} = 4.488 W/cm². These acoustic parameters were selected as they provided the most efficient aptamer uptake among the different experimental conditions tested. After US treatment, internalization of the FAM-labelled AS1411 was compared in US treated and non-treated samples with FLoid® Cell Imaging Station (Life Technologies, Carlsbad, CA, USA, Catalog Number 4471136) and analyzed with the plate reader Infinite 200 PRO (TECAN, Mannendorf, Switzerland) at 490nm excitation and 520nm emission wavelenghts. Then, to assess whether US could promote the uptake of small therapeutic molecules, cell lines were treated at different concentration of kinase-inhibitor sorafenib, that is the first line therapy for unresectable HCC [112]. Both HCC cell lines were treated for 24 hours with 10 µM sorafenib and exposed to US treatment at 1MHz frequency, for 3 seconds of SD, at 526kPa of negative peak AP, with 10 ms of TBD, 50%DC, I_{SPPA} = 8.976 W/cm² and I_{SPTA} = 4.488 W/cm². Then, cell viability was analyzed with PrestoBlue Cell Viability Reagent (Life Technologies, Carlsbad, CA, USA) following manifacturer's protocol.

3.5 RNA extraction and miRNA expression analysis in liver cells

Total RNA, including fractions smaller than 200 nucleotides, was extracted from US treated and non-treated samples, with the Plasma/Serum RNA Purification Mini

kit (Norgen Biotek, Thorold, ON, Canada) using 200 µL of supernatants per each sample. Before the extraction, spike-in ath-miR-159a was added as exogenous control at 100 pM of final concentration in each sample. Total RNA was also extracted from cells with mirVana™ miRNA Isolation Kit (ThermoFisher San Diego, CA, USA, AM1560, AM1561) following the manufacturers' instructions. RNA quantification and purity were evaluated by NanoDrop 2000 (ThermoFisher, San Diego, CA, USA). Total RNA was retrotranscribed using TaqMan® Advanced miRNA cDNA Synthesis Kit (A25576, ThermoFisher, San Diego, CA, USA) and then analyzed by quantitative Realtime PCR (7500 Fast Real Time PCR System, Applied Biosystems), using the $2^{-\Delta\Delta Ct}$ method. To set up the most appropriate conditions for the following experiments, the expression of hsa-miR-125a-5p and hsa-miR-182-5p, known to be expressed in the liver, was evaluated in the cell lines here used. hsa-miR-16-5p was used as endogenous control, according to manifacturer's instructions (Applied Biosystems, Foster City, CA, USA) To assess miRNAs' release in supernatants after US treatment, ath-miR-159a was used as exogenous control (478411 mir Applied Biosystems, Foster City, CA, USA). The $2^{-\Delta\Delta Ct}$ method was applied to compare miRNAs' expression in US treated samples and controls. Each experiment was repeated at least three times. Once miRNA's release after US treatment was assessed, RNA from supernatants was retrotranscribed again and 188 target miRNAs were analyzed using TaqMan® Advanced miRNA Human/Serum Plasma cards (A34717, Applied Biosystems) using a ViiA7 instrument (4453545, Applied Biosystems). Table of the 188 target miRNAs can be found at https://documents.thermofisher.com/TFS-Assets/GSD/Reference-Materials/TAC-Advanced-miRNA-Human-SerumPlasma-CardLayout.xls. Each experiment was repeated at least three times. MiRNAs expression levels were analyzed with $2^{-\Delta\Delta Ct}$ method and normalized by exogenous calibration with ath-miR-159a expression. Manual analyses of qRT-PCR data were performed to refine analysis and retain only miRNAs showing good amplification plots. Differentially expressed miRNAs with relative quantification (RQ)$\geq$ 2 in the US-treated samples compared to controls were considered for the downstream analyses. P-values (p) and RT-qPCR data analyses were performed using respectively the Student's t-test alghorithm automatically provided by Expression Suite v1.3 software and Quant Studio software

(Thermo Fisher). Data with p-value less than $p \leq 0.05$ was considered as statistically significant.

3.6 Protein quantification and analyses

Proteins levels in the supernatants after US treatment were analyzed using the Antibody Array C-Series "Human Apoptosis Array C1" (RayBiotech), that allows quantification of 43 apoptosis-related proteins and factors. Table of the 43 target apoptosis-related proteins can be found at https://www.raybiotech.com/human-apoptosis-array-c1-aah-apo-1. Samples were processed and analyzed according to the manufacturer's instructions. Densitometric analyses were performed following the same protocol.

3.7 Publicly Available Datasets for Results Validation

Four publicly available datasets, EXP00529 (GSE106817) [183], EXP00620 (GSE112264) [184], EXP00609 (GSE113740) [185], and EXP00538 (GSE113486) [186], from the Database of Differentially Expressed miRNAs in Human Cancers (dbDEMC, https://www.biosino.org/dbDEMC/index, accessed on 3 September 2025), were analyzed to compare the expression levels of miRNAs released in the sera from HCC patients and healthy controls. EXP00529 (GSE106817) and EXP00620 (GSE112264) were considered as a single study, since the patients included came from two different parts of the same study. Notably, in these studies miRNA profiling was performed on serum samples both from cancer patients and healthy controls. Data were filtered based on a log2 fold change (FC) ≥ 0.58 and an adjusted p-value (padj) ≤ 0.05. All the studies were used to perform receiver operating characteristic (ROC) curve analyses to estimate diagnostic specificity and sensitivity per each single miRNA or in combination in discriminating HCC cases from non-cancer samples, as well as from other cancer types, using R software v 4.3.1 (www.r-project.org).

3.8 Establishment of 3D bio-printed HCC models

The composition of the 3D matrix used in this study was selected based on previous evidence demonstrating its effectiveness in supporting the growth and differentiation of Müller glial cells [187]. The biochemical and mechanical properties of these components are consistent with the microenvironment requirements of various cell types, suggesting potential applicability to hepatocellular carcinoma (HCC) cell lines as well. Hydrogel for the bio-ink is composed by 2% sodium alginate, 8% gelatin and 100µg/mL type I collagen in sterile PBS. At 80% confluency, HepG2 and SNU-387 were treated with trypsin and counted with an automatic cell counter (Cyto Smart, Corning Life Sciences, Durham, USA). Then cells were mixed at different concentrations (Table 5), and then each solution of cells and hydrogel was loaded into a cartridge for the bio-printing.

Cell Count / mL hydrogel	
HepG2	**SNU-387**
2 milions	1.5 milions
3 milions	3 milions
6 milions	6 milions

Table 5. Table provides the cell density applied for the preparation of the bio-ink for the 3D printing.

BIO-X-3D printer was used to print the 3D models as it follows. Each structure was printed maintaining the temperature at 29°C for the cartridge and 26°C for the plate, then the pressure advance for the printing was 55kPa and print speed 5mm/s. 3D structures were defined by PrusaSlicer 3D and were designed as it is reported in Figure 7 (b-C). Each structure was round-shaped, 1.2mm height and 10mm φ.

After the print, each structure was stabilized by crosslinking with 100 mM calcium cloride for 10' and 60 mM barium cloride for 2'. Then 3D HCC models were incubated in RPMI-1640 (EuroClone, Milan, Italy) supplemented with 10% fetal bovine serum, 2 µM L-glutamine, 0.05 U/mL penicillin-streptomycin and were maintained at 37°C with 5% CO_2. Then, 3D HCC models were analyzed at different

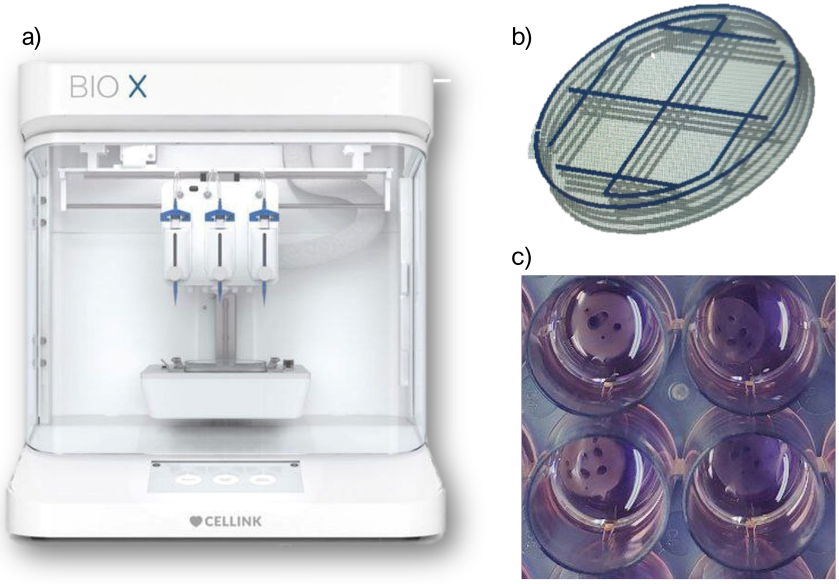

Figure 7. Figure shows the Bio-X-3D printer (a) and the 3D structure model provided by PrusaSlicer 3D (b) and in 24 multiwell plate after the print (c).

timepoints with PrestoBlue Cell Viability Reagent (Life Technologies, Carlsbad, CA, USA) to assess cell viability.

3.9 Glioblastoma xenograft model

4-week-old NMRI nude mice (n=15) (Janvier Labs) were orthotopically implanted with 5×10^5 Gli7 cells into the striatum (2.5mm depth from the dura and 2mm right of bregma) under 3% isoflurane anesthesia. Orthotopic intracranial xenografts are widely used in glioblastoma research because they place tumor cells within the native brain microenvironment, allowing more physiologically relevant interactions with neural tissue, vasculature, and the blood–brain barrier compared to ectopic sites [188]. Immunodeficient nude mice lack functional T cells, enabling engraftment of human tumor cells without rejection, which supports reproducible tumor establishment and growth for preclinical assessment of tumor biology and therapeutic efficacy [188, 189]. However, this model has limitations: the absence of an intact adaptive immune system restricts evaluation of immunotherapy and tumor–immune interactions, and established cell line-derived xenografts may not fully recapitulate the heterogeneity,

infiltrative behavior, and molecular features of patient tumors [188, 190]. Despite these constraints, orthotopic xenograft models in nude mice remain a standard and informative preclinical platform for in vivo glioblastoma studies prior to investigations in more complex or immunocompetent systems.

Animal experiments were performed according to the European Directive 2010/63/EU and its transposition into French law (Decree No. 2013-118). The research project was conducted at the BioMaps laboratory (Orsay, France) in collaboration with Atomic Energy and Alternative Energies Commission (CEA)-Service Hospitalier Frédéric Joliot (SHFJ) imaging platform and was approved by a local ethics committee (n°D91-471-105/ethic committee n°44)

3.10 Antibody for endothelin A receptor target therapy

The ETA receptor has been proposed as a biomarker for GBM patients stratification according to disease severity, as it is overexpressed in the vascular endothelium of GBM [140, 152]. Based on this, a chimeric experimental antibody, named xiRA63, was produced to target ETA receptor. XiRA63 was produced according to the protocol provided by Hautiere et Al [152]. Both light and heavy chains encoding IgG-XiRA63 were cloned into pTT5 expression plasmid and transfcted in ExpiCHO-cells, with ExpiCHO expression kit system, according to manufacturer instructions (MAN0014337 ThermoFisher Scientific). After 12 days, xiRA63 was purified from cell supernatant on a HiTrap Protein A HP column (GE HealthCare) and ThioFab-xiRA63 on the HiTrap KappaSelect (GE HealthCare). Following elution, antibody solutions were dialyzed with Slide-A-Lyzer™G2 Dialysis Cassette (ThermoFisher Scientific) into 1L of PBS.

3.11 Antibody radiolabeling with ^{89}Zr

XiRA63 antibodies were radiolabeled with Zirconium-89 (Zr) (PerkinElmer) by using deferoxamine (DFO) and dodecane tetracetic acid (DOTA) respectively, as explained by Hautiere et al [154]. Briefly, one day before the injection, 0.75 mg of xiRA63-DFO and 0.65 mg of ThioFab-xiRA63-DFO, pH adjusted to 7.2, were

incubated in a solution containing $[[^{89}Zr]\text{-}((C_2O_4)^{2-})_4]^{4-}$ for 1 hour at 37°C, 300 rpm. The oxalic acid of the ^{89}Zr solution (200 µL, 413 MBq) was neutralized with 90 µL of 2 M Na_2CO^3 before addition to the antibody solution. [^{89}Zr]Zr-xiRA63-DFO and [^{89}Zr]Zr-ThioFab-xiRA63-DFO were purified on a PD-10 column with a gentisic acid solution (pH 5.4-5.6) as a mobile phase and concentrated by Vivaspin® ultrafiltration tubes (Sartorius) with a 10 kDa cutoff for the ThioFab and a 50 kDa cutoff for the mAb. Radiochemical purity of [^{89}Zr]-xiRA63-DFO and [^{89}Zr]-ThioFab-xiRA63-DFO was assessed by size-exclusion high-performance liquid chromatography (HPLC) coupled to a UV (UVD 170U UV/VIS) and scintillation gamma detector (Packard). Measurements were performed using a bioZen 1.8 µm SEC-2 LC column (Phenomenex) and a DIONEX System (Thermo-Fisher). A linear-gradient elution was carried out with a solution of KH_2PO_4 (50 mM) and KCl (250 mM) (pH 6.8), at a flow rate of 0.2 mL/min.

3.12 GBM animal model's treatment

45 days after Gli7 implantation, tumor growth was assessed and confirmed by MRI. As described by Hautiere et al., at this timepoint BBB was still intact [152,154]. Then, the 11 mice were randomized into 2 different groups as it follows:

- Group 1, n=6 mice received ^{89}Zr-xiRA63
- Group 2, n=5 mice received ^{89}Zr-xiRa63 and FUS treatment

40ug of radiolabeled xiRA63 were injected through caudal vein in each mouse, as described by Hautiere and colleagues [154].

To achieve the BBB opening and increase the uptake of xiRA63 antibody, before the FUS treatment, each animal was injected in the caudal vein, with 50uL of microbubbles SonoVue. Then, BBB opening was achieved using the FUS transducer (Imasonic, Voray-sur-l'Ognon, France) with active diameter 25 mm, focal depth 20 mm, operating at 1.5 MHz and driven by a single-channel programmable generator (Image Guided Therapy, Pessac, France). FUS parameters and microbubble administration were chosen according to the protocol provided by Tran and colleagues,

because they demonstrated that FUS selectively opened BBB in mouse model to promote release and delivery of molecules, without significantly altering animal health [191]. To achieve a wide BBB opening (6 × 6 mm), a mechanical zig-zag scanning pattern was performed along the X and Y axes. The motion consisted of repeated linear sweeps along the X axis with direction reversals at each end, while the Y axis advanced stepwise to cover the entire square area. The stage velocity was set to 10 mm/s, and a complete trajectory lasted 5.1 s. Ultrasound emission at 1.5 MHz remained continuously active throughout the entire motion (duty cycle = 100%). The sequence was repeated 25 times for a total exposure time of 127 s of SD. Mice were treated with probe focused on the brain, with FUS at 400 kPa negative peak of AP, I_{SPPA} and I_{SPTA}= 5.1944 W/cm².

3.13 PET-CT image acquisition

PET acquisitions were performed using the Inveon micro PET-CT system (Siemens Medical Solutions) providing a spatial resolution of 1.5 mm. After the PET acquisition, a 6 minute 80 kV/500 µA CT scan was performed for attenuation correction. PET images were reconstructed using a 3D OSEM algorithm with parameters set to 4 iterations, 16 subsets, and a voxel size of 0.4 mm × 0.4 mm × 0.8 mm. The reconstruction process included normalization, dead time correction, random subtraction, CT-based attenuation correction, and scatter correction. PET acquisition was performed at 1 h, 4 h, 24 h, 48 h, 72 h and 168 h post injection of radiolabeled xiRA63.

3.14 *In vivo* biodistribution analysis

XiRA63 biodistribution was analyzed by the use of the software 3d slicer, to examine different volumes of interest and specific sites for drug accumulation: brain, liver, left ventricle of the heart, lungs, muscles, kidneys and spleen. Data analyzed with 3d slicer were used to calculate and compare the ratio of percentual injected dose (%ID) over volume in cubic centimeters (cc) in each specific site for drug accumulation. All the data were analyzed by Patlak linearization algorithm, to

evaluate the uptake of the xiRA63 between tissues and tumor. In detail, the Patlak linearization algorithm was applied to calculate within tumor site the apparent distribution volume (V_0), the tissue volume accessible to the tracer immediately after its delivery, irreversible uptake (Ki), the rate of the fraction of labeled-xiRA63 undergoing non-reversible binding, and Area Under the Curve (AUC) of plasmatic concentration [192].

3.15 Statistical Analysis

Statistical analysis was perfomed with Student's T-test, one-way Anova test followed by Tukey test, and Mann-Whitney statistical test on the software GraphPad Prism 10.0 and Microsoft Excel.

Chapter 4

Results

4.1 Effects of US on cell viability and cell number

Application of US according to different parameters of time exposure and DC was necessary to choose the best conditions to maintain cell viability above 85% and cells mostly in their adherent phenotype (Fig.8a). To sum up, cell viability and morphology were not altered by applying well defined parameters as reported in Methods and Materials (Fig.8b). Afterwards, the same parameters were applied to promote molecule release for the identification of putative biomarkers.

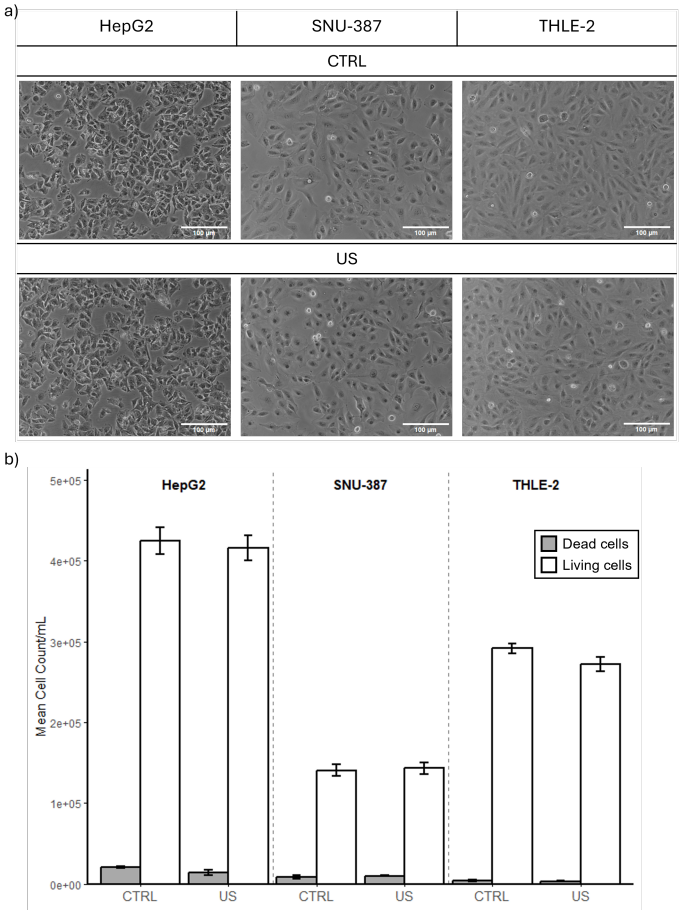

Figure 8. Figure shows cell morphology and cell viability based on US treatment. Microscopy pictures show that cell morphology is not significantly altered (a). Barplot shows the mean cell count per each cell line with and without US treatment. Data shown in the barplot represent mean cell count/ ml and standard error. Statistical analysis was performed with Student T-test (*$p<0.05$, n=3).

4.2 Assessment of US-mediated molecules' release

HCC cell lines, SNU-387 and HepG2, and normal cell line THLE-2 were analyzed for the expression of miR-125a-5p and miR-182-5p by RT-qPCR to determine if each cell line could express at least one liver-specific miRNA. Expression levels of miRNAs in SNU-387 and THLE-2 cells are shown relative to HepG2 cells, which were used as the calibrator for the analysis. It was found that each cell line expressed similar levels of miR-125a-5p, while only HepG2 cell line expressed detectable levels of miR-

182-5p (Fig.9 a). Then, after US treatment miR-125a-5p expression was analyzed in supernatants collected from HepG2, SNU-387 and THLE-2. As mentioned above, US parameters were fine-tuned to avoid cell detachment, morphology alteration and cell death. In this context, each experiment was repeated in triplicate at least three times. No significant difference in cell number was observed between ultrasound-treated and untreated cells. RT-qPCR performed on RNA extracted from cell supernatants with and without US revealed that US could promote and increase the release of miR-125a-5p, as shown in Fig.9 (b-d). Expression levels of miRNAs in cell supernatants are calculated using CTRL1 samples as calibrator for the analysis.

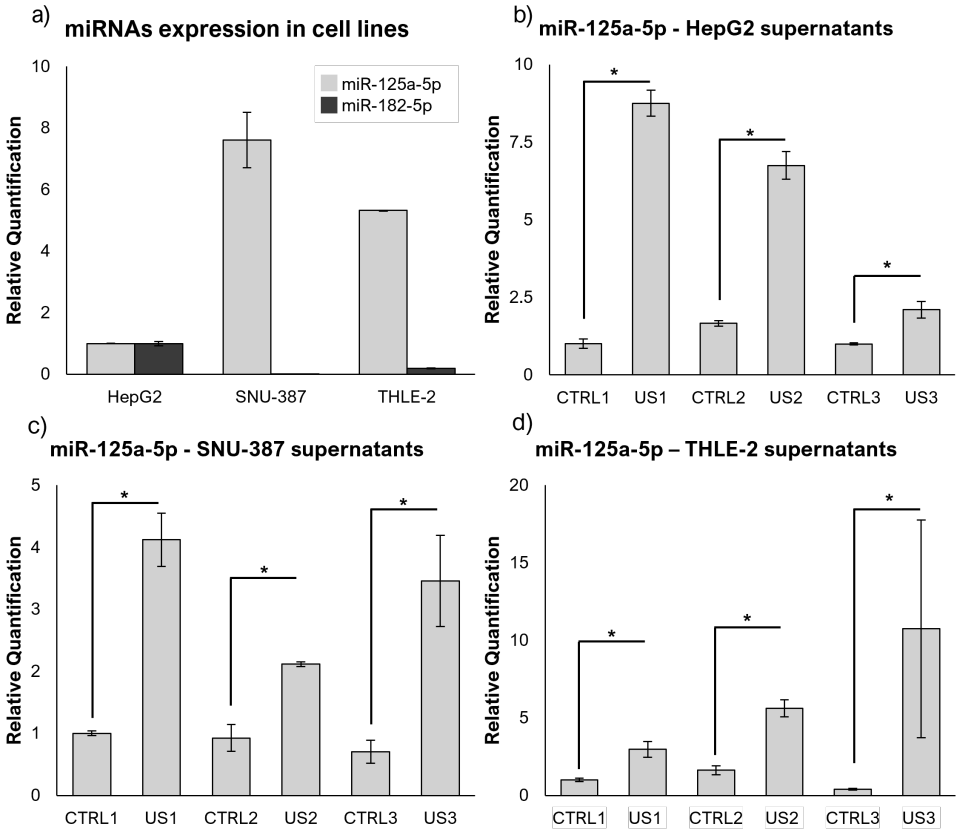

Figure 9. Panel shows the expression of miRNAs in liver cell lines and in supernatants after US treatment. Barplot represents the analyses of miR-125a-5p and miR-182-5p expression in liver cell lines, both normal and cancerous. miRNA expression levels in cell lines is compared to HepG2 cells, which were used as calibrator for the analysis (a). Bar plots show the expression of miR-125a-5p in US-treated samples. Data represent three independent biological replicates. Data are shown as Relative Quantification (RQ) and standard error (b-d). Statistical analysis was performed with Student's T-test (*$p<0.05$, $n=9$)

4.3 US-released miRNA profiling in supernatants

Supernatants were subjected to miRNA profiling of 188 target miRNAs and only US-treated samples with Relative Quantification of miR-125a-5p higher than 2 were selected for further analysis. This threshold was applied to focus the analysis on miRNAs significantly modulated by the US treatment and to minimize background variability associated with marginal expression changes. In addition, all real-time

PCR reactions were manually inspected and verified in terms of wells showing no amplification or software-generated error flags, as well as those exhibiting excessive technical variability or failing to meet predefined quality control criteria.

The analysis of the profiling showed that US indeed promoted the release of more than 85 miRNAs, among 188 target miRNAs provided by the TaqMan-based microfluidic card, as reported in the section Methods and Materials.

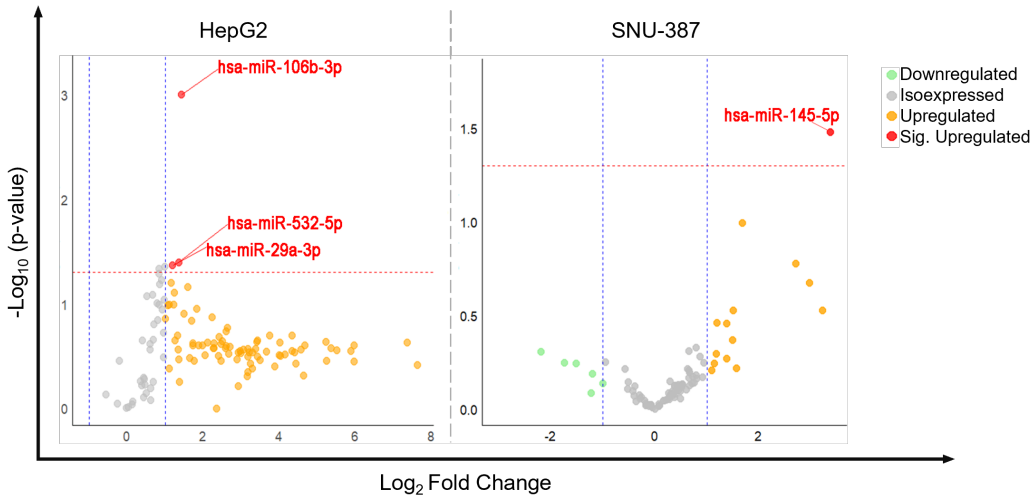

Figure 10. Volcano plot showing hyper-expressed miRNAs in supernatants from HepG2 and SNU-387 cells after US treatment. Levels of more than 85 miRNAs resulted increased: among them, miR-106b-3p, miR-532-5p, miR-29a-3p and miR-145-5p were statistically significant. Data were shown as Log_2Fold Change and -log_{10}p-value. Statistical analyses were performed with Student's T-test. P-value threshold is set at $p<0.05$ and calculated on 3 different replicates.

As shown in Fig.10, more than 85 miRNAs resulted up-regulated in supernatants after US treatment: among them, miR-106b-3p, miR-532-5p and miR-29a-3p resulted significantly up-regulated in HepG2 supernatants, and miR-145-5p resulted significantly up-regulated in SNU-387 supernatants. These differences in miRNAs' release in supernatants could suggest the ability to discriminate two different types of HCC cell lines.

Then miRNAs profiling after US treatment was performed also in supernatants from THLE-2 as control normal cells. In this context, miRNAs profiling in THLE-2 supernatants was used to exclude all the common miRNAs between the HCC cell lines

and THLE-2. As shown in Fig.11, no miRNAs resulted significantly up-regulated after US treatment in THLE-2 supernatants. Notably, although some miRNAs were detected as non-significantly up-regulated in THLE-2 supernatants, these were not shared with the miRNAs found to be non-significantly up-regulated in the HCC cell lines, further supporting the specificity of the tumor-associated miRNA release.

The selective release of certain miRNAs after US treatment may reflect differences in their intracellular abundance, spatial localization, or interactions with proteins that affect their mobility. Likely, this selective release could enhance their potential as biomarkers. In addition, some miRNAs were detected as down-regulated in the supernatants following US treatment. This observation may be explained by a bidirectional flux of molecules across the plasma membrane induced by ultrasound exposure, allowing not only the release of intracellular miRNAs but also the re-entry of extracellular miRNAs, resulting in an apparent decrease in their extracellular levels.

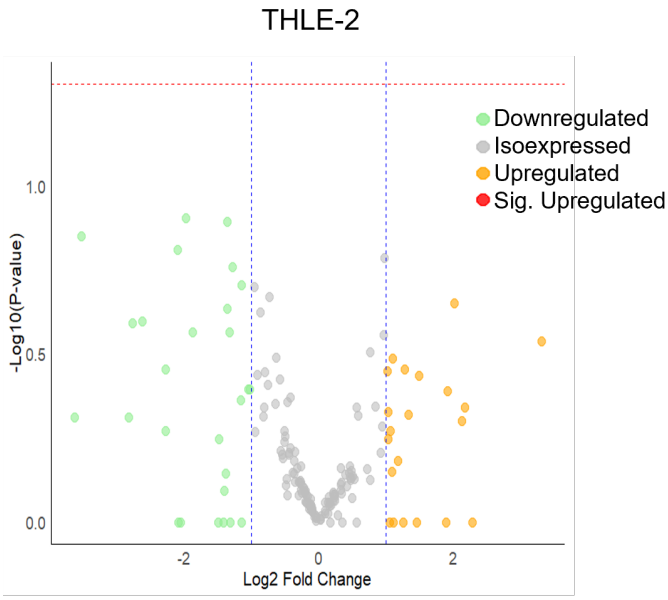

Figure 11. Volcano plot showing profiled miRNAs in supernatants from THLE-2 cell line, after US treatment. The plot highlights that US don't promote significantly up-regulation of miRNAs in supernatant. Data were shown as Log_2Fold Change and -log_{10}p-value. Statistical analyses were performed with Student's T-test. Significative p-value threshold is set at $p<0.05$ and calculated on 3 different replicates.

4.3.1 *In silico* validation of significantly released miRNAs as biomarkers

To validate miRNAs as putative biomarkers of HCC, the four publicly available datasets GSE113740, GSE112264, GSE106817 and GSE113486 were interrogated. *In silico* analyses revealed that the four miRNAs, miR-532-5p, miR-106b-3p, miR-29a-3p and miR-145-5p are significantly up-regulated in the sera of HCC patients compared to healthy donors (Fig.12).

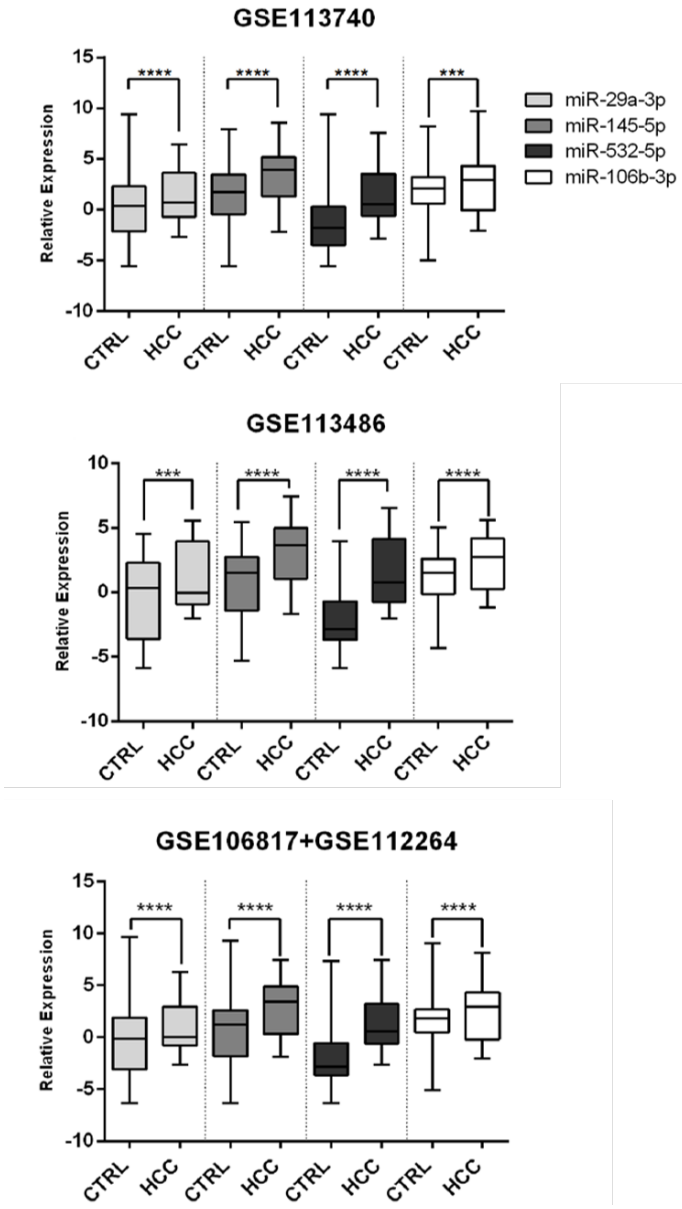

Figure 12. Boxplots show analyses of US-released miRNAs in publicly available GEO dataset of human patients of HCC. GSE113486, GSE106817, GSE112264 and GSE113740 were analyzed: miR-29a-3p, miR-145-5p, miR-532-5p and miR-106b-3p resulted significantly upregulated in HCC patients when compared to healthy donors in each dataset. Data are presented as box-and-whisker plots showing the median and interquartile range (IQR), with whiskers indicating minimum and maximum values, and statistical analysis was performed with the Mann-Whitney statistical test (****$p < 0.00001$)

Following the assessment of miRNA expression in the datasets, feasibility analyses

were performed to validate the previously identified miRNAs as putative biomarkers. ROC analysis was conducted for each miRNA in each dataset, and the Area Under the Curve (AUC), sensitivity (SE), and specificity (SP) were calculated. In addition, a combined ROC analysis was performed to evaluate the diagnostic accuracy of the four miRNAs. ROC analysis assesses the ability of a biomarker to discriminate between conditions by plotting sensitivity against 1-specificity across different thresholds, with overall performance summarized by the AUC.

In the GSE113486 dataset, the AUC values showed variability among the different miRNAs. miR-29a-3p displayed an AUC of 0.669, with a SE=0.87 and a SP=0.45, indicating good sensitivity but limited specificity and therefore a moderate overall discriminative performance. miR-145-5p showed an AUC of 0.739, with both sensitivity and specificity equal to 0.70, suggesting a balanced and moderately reliable diagnostic accuracy. miR-532-5p provided an AUC of 0.872, with SE=0.92 and SP=0.75, reflecting a high discriminative ability with both strong sensitivity and specificity. miR-106b-3p showed an AUC of 0.693, with SE=0.60 and SP=0.73, indicating a moderate performance with better specificity than sensitivity. The combined analysis of the four miRNAs yielded an AUC of 0.886, with SE=0.76 and SP=0.82, showing an overall improvement in diagnostic accuracy compared to most single miRNAs (Fig.13 a).

In the combined GSE106817+GSE112264 dataset, the results showed similar patterns. miR-29a-3p exhibited an AUC of 0.64, with a SE=0.89 and SP=0.42, again indicating high sensitivity but poor specificity. miR-145-5p provided an AUC of 0.74, with a SE=0.65 and SP=0.75, suggesting a balanced and reliable discriminative performance. miR-532-5p presented an AUC of 0.85, with a SE=0.90 and a SP=0.71, confirming a strong diagnostic accuracy across datasets. miR-106b-3p showed an AUC of 0.61, with SE=0.50 and a SP=0.80, indicating limited sensitivity despite good specificity. The combined model of the four miRNAs provided an AUC of 0.86, with a SE=0.82 and SP=0.75, supporting the robustness of the multi-miRNA panel (Fig.13 c).

In the GSE113740 dataset, miR-29a-3p showed an AUC of 0.60, with a SE=0.42 and SP=0.74, suggesting a low discriminative ability mainly driven by reduced

sensitivity. miR-145-5p exhibited an AUC of 0.69, with a SE=0.65 and SP=0.65, indicating a moderate and balanced diagnostic performance. miR-532-5p provided an AUC of 0.78, with SE=0.79 and SP=0.59, confirming a good sensitivity with moderate specificity. miR-106b-3p reported an AUC of 0.56, with a SE=0.52 and SP=0.68, reflecting a limited diagnostic value. The combined analysis of the four miRNAs resulted in an AUC of 0.78, with SE=0.72 and SP=0.66, indicating an overall improvement compared to individual miRNAs (Fig.13 b).

Overall, miR-532-5p consistently provided the highest AUC values across all datasets, reaching AUC=0.78 (SE=0.79; SP=0.59), AUC=0.85 (SE=0.90; SP=0.71), and AUC=0.872 (SE=0.92; SP=0.75) in GSE113740, GSE106817+GSE112264, and GSE113486, respectively, supporting its robustness and reliability as a potential biomarker.

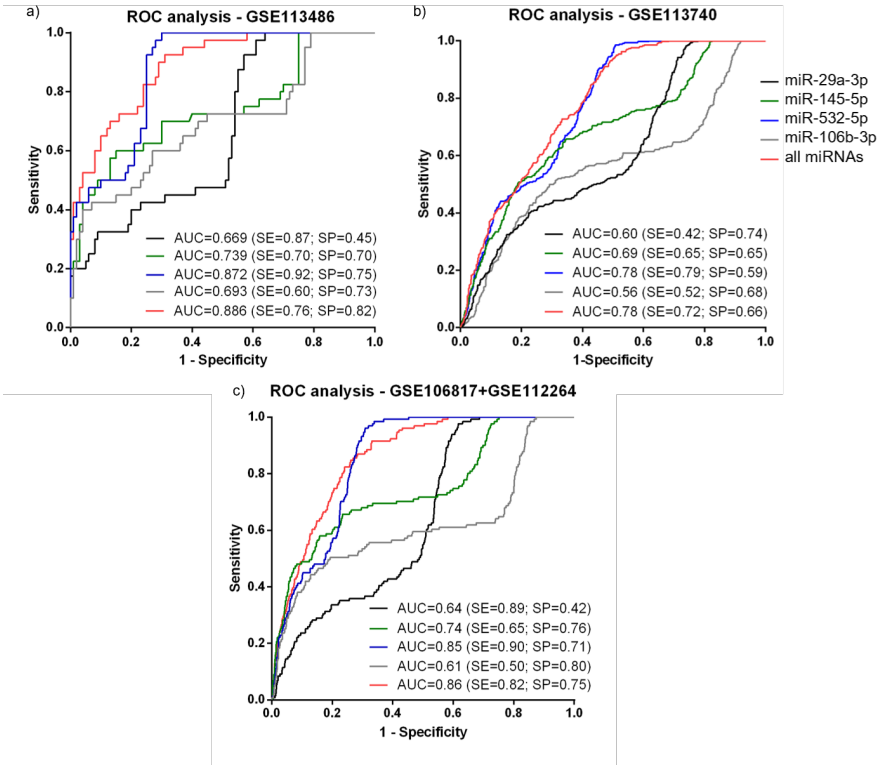

Figure 13. ROC curves showing *in silico* analysis of US-released miRNAs in publicly available GEO dataset (GSE113486 (a), GSE113740 (b), GSE106817+GSE112264 (c)) of sera from human patients of HCC. miR-532-5p showed the best AUC value compared to other miRNAs in each dataset analyzed to discriminate HCC from healthy donors. ROC curves of each putative biomarker were analyzed by DeLong statistical test

4.4 US-mediated release of proteins

Among the 43 proteins analyzed, US treatment consistently increased the release of several proteins compared with untreated controls. In HepG2 supernatants, Bad, Bax, Bcl-w, CD40, FasL, HSP27, IGF-1sR, and Livin showed a clear upward trend in fold change following US treatment. Among these, FasL and Livin were significantly increased, indicating that US treatment enhances protein release from the HepG2 cell line. In the SNU-387 cell line, US treatment increased the release of two proteins, CD40 and IGFBP-4, compared with untreated controls. Notably, the normal liver cell line THLE-2 did not show detectable release of any proteins in the supernatant following US treatment, reinforcing that the release of proteins from HepG2 cells

appears to be closely associated with the tumor phenotype of the cells.

Taken together, these results suggest that US stimulation actively promotes the release of multiple proteins from both HCC cell lines. Notably, although several of the released proteins are classically associated with apoptotic pathways, the highly conservative US treatment parameters used in this study are not expected to induce or modulate apoptosis, supporting the interpretation that their increased detection reflects enhanced release rather than activation of cell death processes. In this context, these proteins may be further investigated in the literature as putative circulating biomarkers released from HCC tissue.

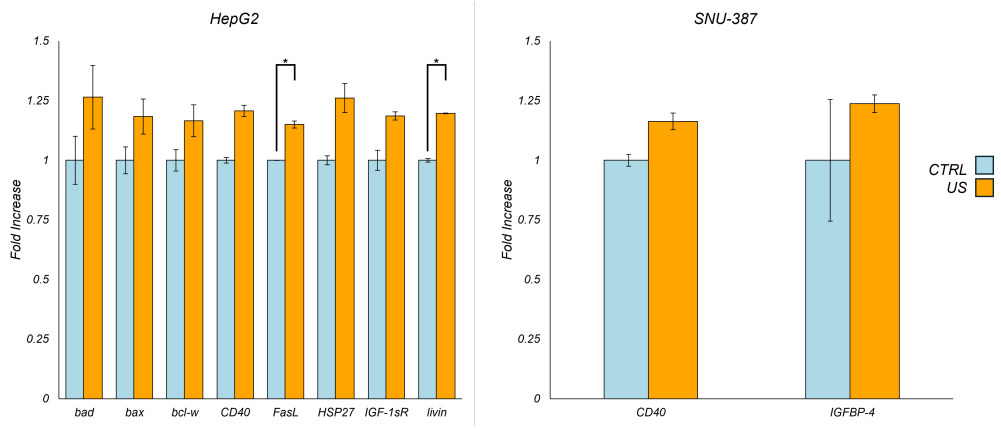

Figure 14. Barplots show relative expression of proteins in supernatants of HCC cell lines after US treatment. Overall, among 43 proteins, 9 different proteins resulted significantly increased in cell supernatants after US treatment. Data are shown as mean of fold increase and coefficient variation of fold increase. Statistical analyses were performed with Student's T-test (* $p<0.05$, n=2)

4.5 US could promote small molecule uptake and boost drug efficacy in HCC cell lines

4.5.1 US effect on the delivery of FAM-labeled AS1411 in HCC cell lines

HCC cell lines were treated with 5 µM of FAM-labeled AS1411 at different timepoints in combination with US to establish suitable parameters for enhanced

molecule uptake. In the SNU-387 cell line, preliminary observations suggested that short exposures to US promoted higher uptake of FAM-AS1411 compared to passive incubation at 1 h and 2 h. In details, 30 s of US exposure promoted higher uptake of AS1411 than 2 h uptake without US (Fig.15).

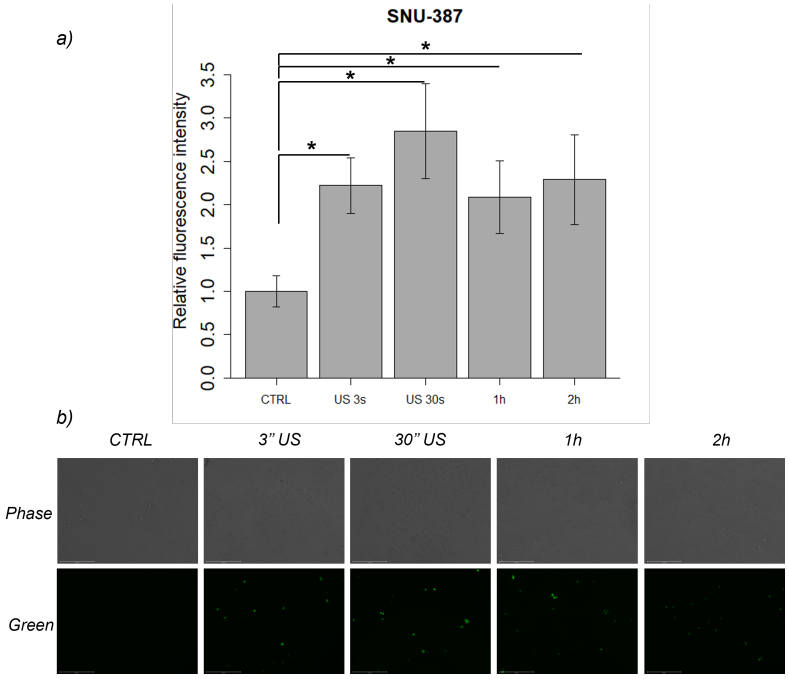

Figure 15. US treatment increased the uptake of the FAM-labelled AS1411 aptamer in SNU-387 cell line, producing fluorescence signal within 30 seconds US exposure slightly higher than 2 hours of passive uptake. Fluorimetric data are shown as relative mean fluorescence and standard error (a). Statistical analysis was performed with Student's T-test (*$p<0.05$, n=3). Fluorescence pictures (20x magnification), obtained with EVOS m7000, show FAM fluorescence intensity of internalized AS1411 (b).

In the HepG2 cell line, preliminary observations indicated that short exposures of 3 s and 30 s to US promoted the FAM-AS1411 uptake, similar to FAM-AS1411 uptake observed over 1 h and 2 h without US treatment. (Fig.16).

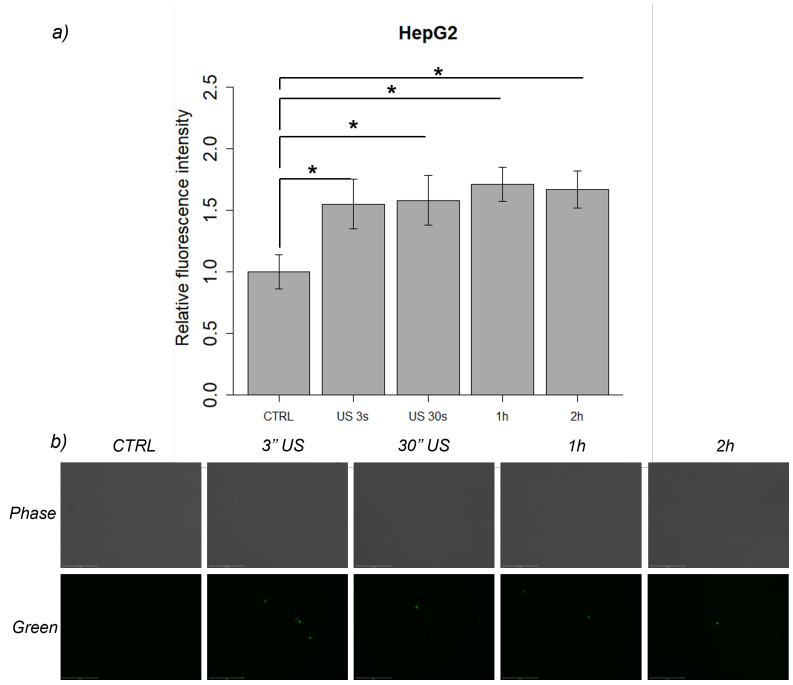

Figure 16. US treatment increased the uptake of the FAM-labelled AS1411 aptamer in HepG2 cell line, producing similar fluorescence signal within 30 seconds of US exposure and 2 hours of passive uptake. Fluorimetric data are shown as relative mean fluorescence and standard error (a). Statistical analysis was performed with Student's T-test (*p<0.05, n=3). Fluorescence pictures (20x magnification), obtained with EVOS m7000, show FAM fluorescence intensity of internalized AS1411 (b).

Based on the observation by Reyes-Reyes et al., AS1411 is rapidly internalized by cancer cells through an active, macropinocytosis-driven process, with the maximum fluorescent signal at 2 h of incubation. In this context, the US-enhanced uptake suggests that US accelerates this early internalization phase, enabling levels of AS1411 uptake comparable to those achieved after 1–2 h of passive incubation [193].

4.5.2 US effect on the viability of Sorafenib treatment in HCC cell lines

After determining US parameters to set up an US treatment useful in enhancing drug delivery, HCC cell lines were treated for 24 h at different concentrations of tyrosine kinase inhibitor sorafenib, to determine the best concentration for following treatments. Cell viability assay revealed that 24 h of 100 µM sorafenib treatment

caused significant cell death in both HCC cell lines (Fig.17). Moreover, 1 µM sorafenib did not alter cell viability within 24 h of treatment in both HCC cell lines.

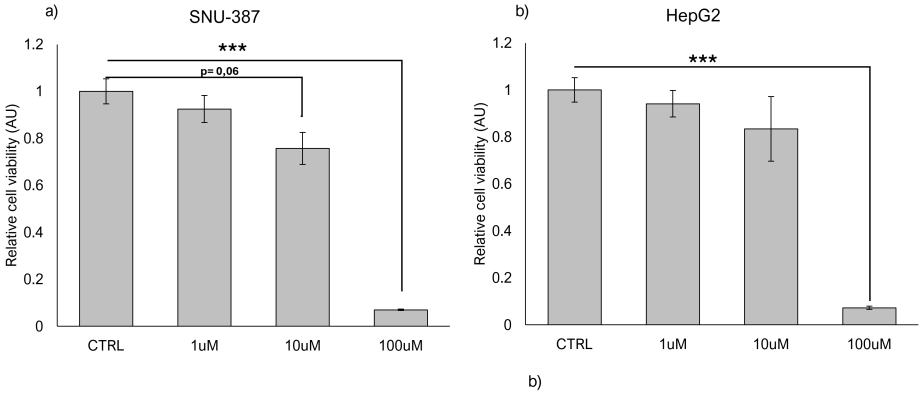

Figure 17. Panel shows cell viability after 24 hours of sorafenib treatment in SNU-387 (a) and HepG2 (b) cell lines. Data are shown as mean and standard error of relative cell viability, calculated by using non treated control as a reference. Statistical analysis was performed using One Way Anova, followed by Tukey test (* $p<0.05$, ** $p<0.01$, *** $p<0.001$), n=3.

However, 10 µM sorafenib treatment in SNU-387 cell line altered cell viability, showing a trend of statistical significance ($p = 0.06$), while the same treatment did not produce any statistical significance in HepG2 cells. Then, 10 µM sorafenib was selected as the optimal concentration for subsequent experiments, as it was non-saturating and it induced only minimal, albeit not statistically significant, changes in cell viability in both HCC cell lines. Therefore, 10 µM sorafenib was selected as a borderline effective concentration to evaluate whether 3 s of US exposure could enhance drug uptake and/or therapeutic efficacy in HCC cell lines. As shown in the following plots (Fig.18), the application of US parameters was expected to increase drug toxicity in HCC cell lines. In SNU-387 cells, US application did not significantly enhance cell death in the presence of 10 µM sorafenib compared to treatment with sorafenib alone: 10 µM sorafenib with and without US significantly promoted cell death, both compared to untreated control, reinforcing that trend of statistical significance of the previous experiment is related to experimental variability (Fig.17 a). In contrast, in HepG2 cells, US application significantly increased cell death, as the combination of US treatment and 10 µM sorafenib resulted in higher cytotoxicity

than sorafenib alone. In addition, 10 µM sorafenib with US promoted significant cell death compared to untreated control (Fig.18 b). These observations might suggest that for SNU-387 cell line a longer US treatment could be tested to better reveal the potential in enhancing the uptake of sorafenib. Given that US did not enhance uptake or drug efficacy in the SNU-387 cell line, higher sorafenib concentrations in the range of 10–100 µM should be evaluated to assess a potential ultrasound-mediated increase of uptake/efficacy. These interesting results could be further explored for *in vivo* application of FUS to increase drug efficacy within the tumor site.

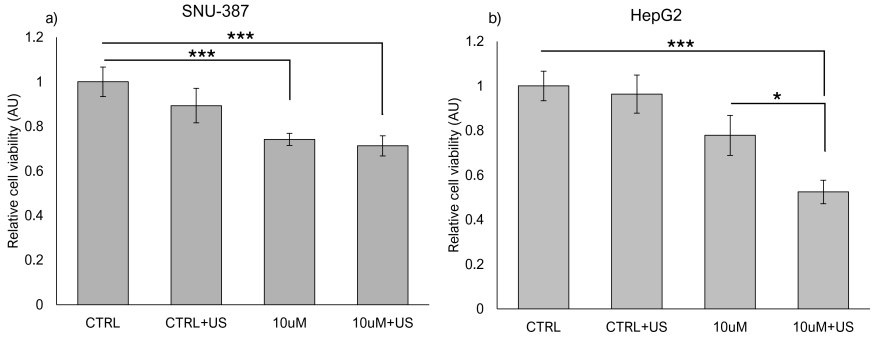

Figure 18. Panel shows cell viability analysis in each HCC cell line, after 24 hours of sorafenib treatment and US exposure, as parameters are shown in Methods and Materials. a) SNU-387 showed similar viability with 10 µM sorafenib treatment and 10 µM sorafenib and US treatment. b) HepG2 showed significant differences in viability with 10 µM sorafenib treatment and 10 µM sorafenib and US treatment. Data are shown as mean and standard error of cell viability, that is expressed in arbitrary unit of optical density. Statistical analysis was performed with Student's T-test (* $p<0.05$, ** $p<0.01$, *** $p<0.001$ n=3).

4.6 Establishment of 3D HCC cell cultures: assessment of Cell Viability

After the bio-printing, hydrogel-based 3D cultures of HepG2 and SNU-387 were monitored at different timepoints. The 3D HepG2 cell model showed distinct viability patterns depending on the initial seeding density. Cultures seeded at 6 million cells/mL exhibited the highest viability at 24, 48, and 72 hours, although a marked decline was observed after one week. At 3 million cells/mL, viability

was lower than in the 6 million cells/mL condition but remained relatively stable across all time points. In contrast, cultures seeded at 2 million cells/mL consistently displayed the lowest viability throughout the experiment. Overall, higher initial cell density supported greater short-term viability but appeared to compromise long-term survival (Fig.19 a). The 3D SNU-387 cell model demonstrated generally low viability, regardless of the initial seeding density. At 1.5 million cells/mL, viability was already very low at 24 h and became undetectable at 72 h. Cultures seeded at 3 million cells/mL showed slightly better performance, maintaining a stable viability between 24 and 72 h. At 6 million cells/mL, viability was modestly reduced compared with the 3 million cells/mL condition at both time points. After one week, no detectable viability signal was observed in any of the SNU-387 cultures (Fig.19b). These differences, observed in the HCC cell lines, might suggest that different cell lines strongly influence performance in 3D culture, and that optimal seeding density must be tailored to each cell type to balance short-term viability with long-term survival. However, the HepG2 3D model is now available for further studies aimed at evaluating US *in vitro* responses also at three-dimensional level.

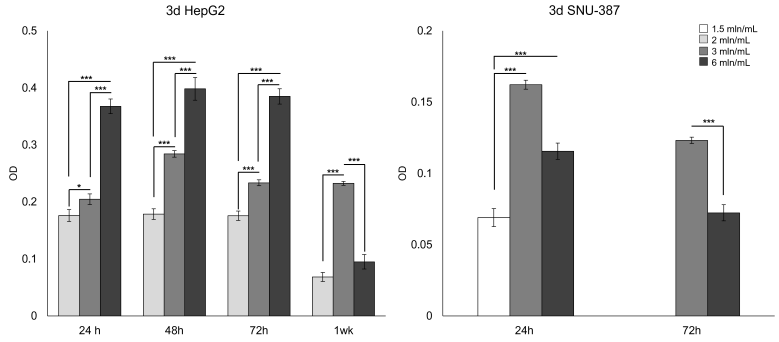

Figure 19. Barplots show PrestoBlue cell viability assay performed at different timepoint for the HCC 3D models. 3D HepG2 model was analyzed at 24h, 48h, 72h and 1 week (a), 3D SNU-387 model was analyzed at 24h and 72h. Data are shown as mean and standard error of optical density of the viability assay. Statistical analysis was performed with Student's T-test (*p<0.05, **p<0.01, ***p<0.001).

4.7 Focused ultrasounds could promote the uptake of radio-labeled xiRA63 in glioblastoma mouse model

Considering the overexpression of ETA receptor in vascular endothelium of GBM [140, 151, 152], FUS were applied to promote the uptake of xiRA63 in the GBM site. As mentioned above, FUS treatment, applied according to the protocol provided by Tran et al., should provide a non-invasive opening of the BBB for controlled molecule's uptake [191].

The data obtained by the analysis of different Volume Of Interest (VOI) related to differend deposit organs suggest that FUS could modulate the distribution of xiRA63 within the tumor, without significantly alteration of the xiRA63 distribution in different organs. As shown in Figure 20 (a-f), FUS treatment did not significantly alter the distribution of the xiRA63 in lungs, blood pool of left ventricle of the heart, liver, masseter muscle, spleen and kidney, suggesting that FUS treatment directed on mouse brain should only produce localized effects on the tumor and preserve organ functions and integrity. Considering that no statistically significant differences were observed in tracer activity within the left ventricular blood pool between FUS and non-FUS groups, plasma concentrations were deemed comparable across both conditions (Fig.20 b)

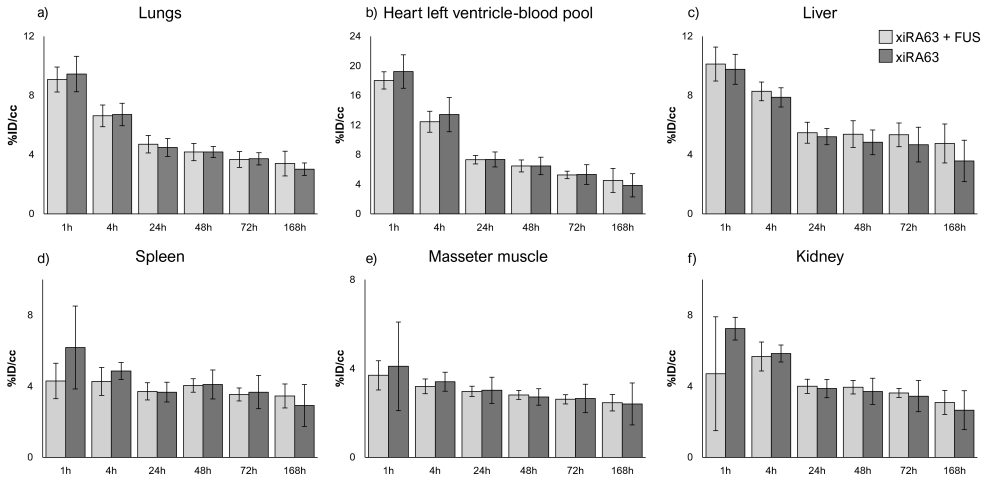

Figure 20. Panel shows barplots representing the biodistribution analysis at 1 h, 4 h, 24 h, 48 h, 72 h and 168 h of xiRA63 antibody with and without FUS treatment in lungs (a), left ventricle (b), liver (c), spleen (d), masseter muscle (e), kidney (f). Data of bio-distribution are shown as mean of %ID/cc and standard error. Statistical analysis was performed with one-way Anova statistical test, followed by Tukey test (n=6, xiRA; n=5 xiRA+FUS).

Moreover, as shown in Figure 21, FUS tended to increase the distribution of the xiRA63 antibody within the tumor VOI, although this difference did not reach statistical significance.

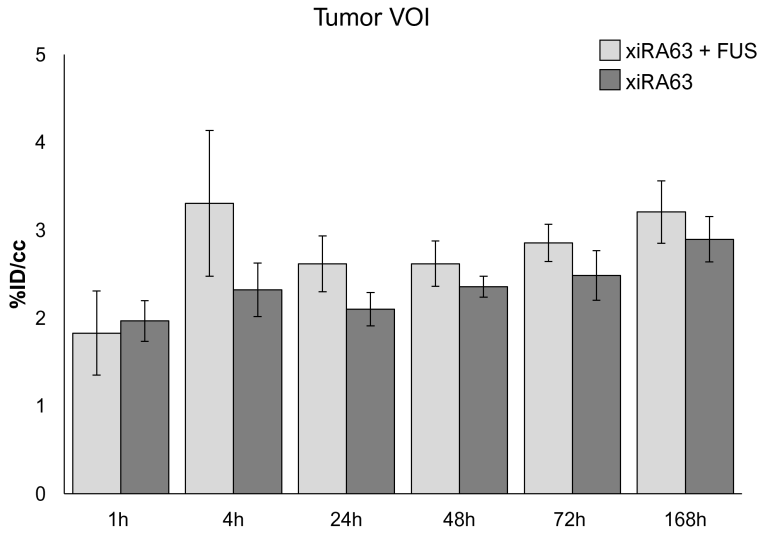

Figure 21. Picture shows the distribution of xiRA63 with and without FUS in the region of interest of the tumor analyzed by PET imaging. Data are shown as mean of %ID/cc and standard error. Statistical analysis was performed with one-way Anova statistical test, followed by Tukey test (n=6, xiRA; n=5 xiRA+FUS).

PET imaging analysis provided additional insight into how FUS might influence intratumoral pharmacokinetics, revealing slight differences at 4 h and 24 h in the distribution of the xiRA63 within the tumor VOI and near to the site of the xenograft injection, as shown by the red arrows in Figure 22a. Accordingly, FUS efficacy in enhancing tumor distribution was further evaluated by analyzing the ratio between antibody concentration in the tumor VOI and plasma concentration (Fig.22b). This analysis confirmed slight differences only at 4 h and 24 h post treatment in the distribution of xiRA63 between the FUS-treated group and the group without FUS, although these differences did not reach statistical significance.

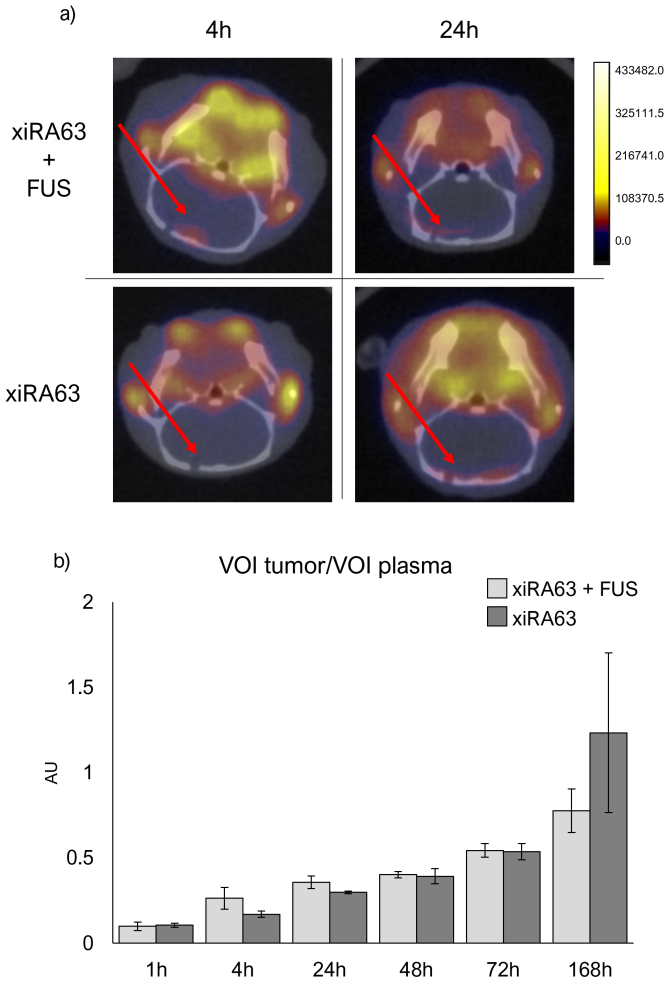

Figure 22. Panel shows the analyses regarding the plasmatic concentration and the tumor/plasma ratio concentrations of xiRA63 in the study. PET imaging at 4 h and 24 h post injection evidences differences of xiRA63 concentration in tumor microenvironment, highlighted by red arrows, with and without FUS treatment (a). Plots show the ratio of tumor and plasma concentration, to determine the actual variation over time. Data are shown in the plot as mean value ratio of tracer concentration in tumor over its plasmatic concentration and standard error (b). Statistical analysis was performed with one-way Anova, followed by Tukey test (n=6, xiRA; n=5 xiRA+FUS).

Applying Patlak linearization algorithm, as mentioned in Methods and Materials [192], deepen pharmacokinetic analyses were performed, to determine wether apparent distribution volume (V_0) and irreversible uptake (Ki) could be altered in FUS-treated animals compared with group without FUS. Overall, animals receiv-

ing combined xiRA63 and FUS treatment exhibited higher V_0 in the GBM ROI after 168 h (Fig.23a), although without reaching statistical significance. Therefore, considering the observed effect on distribution volume towards to the increase, this approach could be definitely an important tool to improve the delivery of drugs into the brain, by reducing administration dose and delivering tracer through the BBB. Moreover, as expected, Ki did not differ between FUS-treated and untreated groups, considering that the observed difference in V_0 did not reach statistical significance (Fig. 23b). In addition, pharmacokinetic analysis was performed by calculating the AUC of plasmatic concentration of the labeled xiRA63 at multiple time-points. AUC analysis demonstrated comparable systemic exposure to xiRA63 between the two experimental groups (Fig. 23c). The lack of differences in plasma indicates that FUS does not alter the circulating levels of xiRA63, reinforcing the fact that its potential effects could be localized rather than systemic.

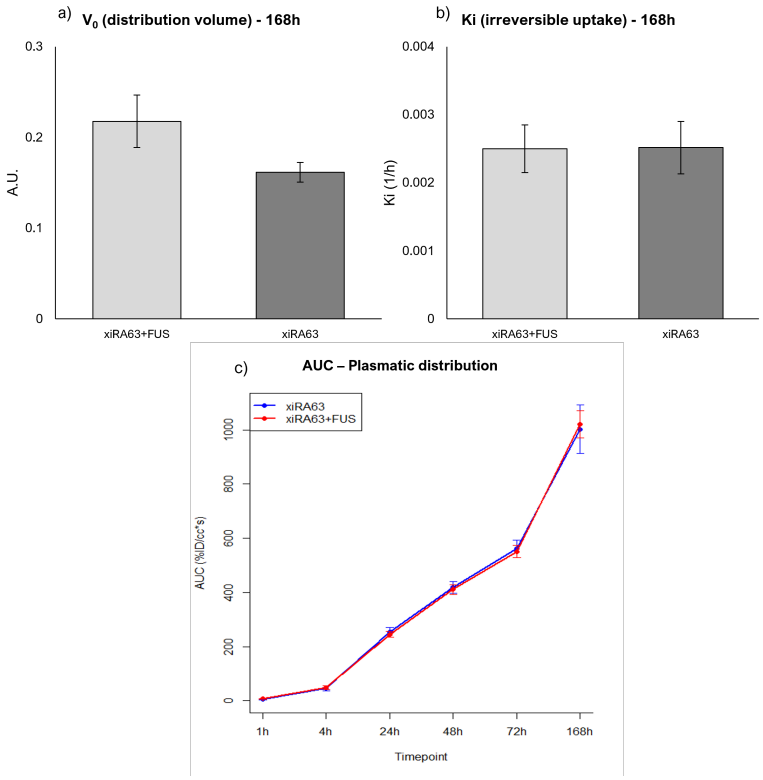

Figure 23. Panel shows biodistribution features of xiRA63 in glioblastoma bearing mice. Barplots show that distribution volume (V_0) of xiRA63 is slightly increased in GBM microenvironment after FUS treatment at 168 h. Data are shown as mean and standard error of V_0 (a). Barplot shows the rate of the fraction of labeled-xiRA63 undergoing non-reversible binding (Ki). Data are shown as mean and standard error of Ki (1/h) (b). Scatterplot shows the Area Under the Curve of plasmatic distribution integrated over time. Data are shown as mean and standard error of AUC (c). Statistical analysis was performed with one-way Anova, followed by Tukey test (n=6, xiRA; n=5 xiRA+FUS)

Chapter 5

Discussion

HCC and GBM are among the most aggressive type of cancer, often associated with late diagnosis and poor prognosis, due to the lack of specific and sensitive biomarkers and adeguate therapy [4, 54]. Therefore, there is an urgent need to identify novel putative biomarkers and develop novel therapeutic strategies, to upgrade clinical management of HCC and GBM patients. In this research, novel putative biomarkers were identified and innovative therapeutic approaches were assessed using US and FUS. The use of US/FUS to transiently permeabilize cell membranes enables bi-directional transport of molecules, including miRNAs, proteins, small drugs, and antibodies. Different cellular responses induced by US treatment, such as sonoporation, are deeply related to parameters applied for US treatment [176]. Indeed, despite the widespread use of US and FUS in oncology, it is crucial to underline that these technologies can induce very different biological effects depending on the acoustic parameters applied. High-intensity or prolonged sonication can trigger inertial cavitation and thermal effects, leading to irreversible membrane damage, apoptosis, or tissue ablation, and is therefore exploited for tumor destruction [174]. Conversely, when low-intensity and carefully controlled US parameters are used, stable cavitation and mechanical effects can transiently increase cell membrane permeability without compromising cell viability [194]. In this project, US were applied under highly conservative conditions to avoid cell death and preserve cell viability, while selectively promoting the release of intracellular molecules. Consistently, no significant alterations in cell viability or cell number were observed following

US treatment, as shown in Fig.8. These findings indicate that the applied US parameters induced reversible biophysical effects—such as transient pore formation and enhanced membrane permeability—rather than irreversible cellular damage. In this context, US represents a suitable and non-destructive strategy to stimulate the release of putative biomarkers from cancer cells, while preserving cell integrity and viability, thereby minimizing confounding effects related to cell death. Thus, US are innovative tools to target cancer cells, promoting the release of putative biomarkers and delivering specific drugs. In this research, the application of US was proposed as innovative strategy to identify novel biomarkers from HCC cell lines to support HCC diagnosis, and FUS as innovative approach to deliver drugs through BBB, taking advantage of ETA receptor, described as putative GBM biomarker [140, 151, 152]. Within the panel of four miRNAs, including miR-532-5p, miR-29a-3p, miR-145-5p, miR-106b-3p, miR-532-5p appears to be the most promising candidate biomarker, based on the results obtained from external validation in the GEO datasets. Although miR-532-5p has not been widely studied as a circulating diagnostic biomarker for HCC, several reports indicate that it may function as a tumor suppressor in other cancer types by inhibiting proliferation, migration, and invasion. Then, Song and colleagues described miR-532-5p as a tumor suppressor in HCC by targeting CXCL2 and pro-survival associated pathways [195]. Although its tumor suppressive role, miR-532-5p feasibility as a diagnostic biomarker in patient serum remains to be fully established. Similarly, miR-29a-3p has been shown to be downregulated in HCC tissues and cell lines, where its overexpression suppresses cell proliferation and migration by directly targeting IGF1R, a known oncogenic receptor tyrosine kinase in HCC, suggesting its release could reflect underlying tumor suppressive activity in tumors with active IGF signaling [196]. Then, also miR-145-5p acts as tumor suppressor in HCC by inhibiting IGF1R-mediated proliferation and EMT. In particular, miR-145-5p has been implicated in regulating proliferation, invasion, EMT processes and metastasis, suggesting that its release into circulation may correlate with these key pathological features [196, 197]. In addition, other tumor-suppressor miRNAs, such as miR-15a-5p and miR-10b, have been reported to be increased in the serum/plasma of cancer patients compared with healthy donors. This apparently

paradoxical behavior may be explained by enhanced active (e.g., exosome- or vesicle-mediated) and/or passive (e.g., necrosis-, apoptosis-, or turnover-related) release of tumor-suppressor miRNAs from tumor cells, suggesting that this mechanism may contribute to the maintenance of tumorigenic features [198–200]. In contrast, miR-106b-3p is generally described as an oncomiR that promotes cell survival and metastasis, and circulating miR-106b-3p has demonstrated diagnostic potential in plasma of HCC patients when evaluated alongside other miRNAs, implying that its elevated levels may reflect oncogenic signaling and tumor burden [90]. The increase of miR-106b-3p, miR-145-5p, miR-29a-3p and miR-532-5p in HCC cell line supernatants after US treatment served as a starting point for evaluating these miRNAs as potential biomarkers for HCC diagnosis. Their upregulation in the sera of HCC patients was confirmed by external validation across the four GEO datasets described in the previous sections. Moreover, a panel combining the four miRNAs achieved an AUC > 0.78, which can be considered a reasonably good diagnostic accuracy (Fig.13). Nevertheless, these results require stronger validation, such as miRNAs profiling from additional HCC patients and/or new available dataset in the future.

Furthermore, analysis of protein levels in cell culture supernatants revealed that 9 different proteins were increased following US treatment; among them, only FasL and Livin showed statistically significant increase. At first glance, this result might suggest a possible involvement of apoptotic pathways upon US exposure. However, this interpretation must be carefully contextualized, considering that the US parameters applied in this study were highly conservative and not expected to induce apoptosis. Therefore, the increased detection of these proteins is more likely attributable to enhanced release mechanisms rather than to activation of cell death processes. In particular, the death-receptor axis mediated by Fas/FasL has long been studied in HCC tissues. As reviewed by Muraki and colleagues, decreased expression of the Fas receptor is a common feature of carcinoma cells, especially in poorly differentiated or larger tumors. Moreover, elevated serum levels of soluble FasL have been detected in HCC patients compared with healthy controls or cirrhotic patients, suggesting a potential association with disease severity. However, despite

these observations, no data are currently available regarding the possible use of FasL as a putative diagnostic biomarker [201]. In this context, the significant increase of FasL in supernatants following US treatment may reflect its active release from HCC cells, mirroring pathological mechanisms occurring in vivo rather than direct apoptotic activation. Livin is an anti-apoptotic protein frequently overexpressed in HCC, where it has been associated with apoptosis resistance and tumor progression. Notably, Livin has also been reported to be increased in the serum of HCC patients compared with healthy donors [202], even if it is not clear which cell type could release it. Although its diagnostic value remains poorly defined, the significant release of Livin after US exposure supports the hypothesis that US stimulation can promote the extracellular detection of tumor-associated proteins with known relevance in HCC biology. Despite the established roles of FasL and Livin in HCC carcinogenesis and progression, their diagnostic significance is still far from being conclusively established. Besides FasL and Livin, other proteins detected in the supernatant after US exposure showed a heterogeneous degree of biological and translational relevance in HCC. Canonical apoptosis regulators such as BAD, BAX and BCL-W are typically intracellular proteins and have not been consistently reported as circulating biomarkers in HCC. Their extracellular detection is therefore more likely to reflect cellular perturbation, membrane permeability changes, or the release of apoptotic bodies, rather than regulated secretion. This interpretation is consistent with the conservative US parameters applied, which are expected to favor transient membrane permeabilization rather than irreversible cellular damage. In contrast, other molecules such as CD40 and HSP27 display stronger evidence of translational relevance. Soluble CD40 (sCD40) has been detected in sera from subjects at risk of HCC and has been associated with HCC incidence and disease progression [203–205]. Similarly, circulating HSP27 (sHSP27) has been reported to be significantly elevated in the sera of HCC patients compared with healthy controls or individuals with chronic liver disease [206]. The increased release of CD40 and HSP27 after US exposure therefore strengthens their potential relevance as candidate circulating biomarkers. Finally, while insulin-like growth factor-1 (IGF-1) remains one of the most extensively studied serum proteins for HCC risk stratification,

evidence supporting a diagnostic role for soluble IGF-1 receptor (IGF-1R) or for IGF binding protein-4 (IGFBP-4) in HCC serum is weak or currently lacking. Their detection in supernatants following US treatment likely reflects cellular perturbation rather than clinically meaningful secretion.

Taken together, these observations indicate that while some of the proteins released after US treatment may primarily reflect cellular alteration, others—particularly FasL, Livin, CD40 and HSP27—exhibit stronger links to HCC biology and circulating detection. Overall, these results highlight the potential of US treatment as a valuable strategy to promote the release of tumor-associated molecules from cells, thereby facilitating the identification and prioritization of novel putative circulating biomarkers for HCC diagnosis.

Since the urgent need of defining novel therapeutic strategies based on the delivery of a small drug to the tumor site, preliminary results showed the ability US in promoting the uptake of FAM-AS1411 aptamer in HCC cell lines. Strikingly, this study showed that a short ultrasound exposure of 30 s tended to promote higher FAM-AS1411 uptake than 2 h of passive incubation in SNU-387 cells, although this difference did not reach statistical significance. At the same time, the same US treatment resulted in uptake levels comparable to those observed after 2 h of passive incubation in HepG2 cells. These findings are consistent with previous evidence reported by Reyes-Reyes et al. [193], demonstrating that fluorescently labeled AS1411 is rapidly internalized by cancer cells through an active process, reaching maximal intracellular fluorescence within approximately 2 h. In this context, the enhanced uptake observed following US treatment suggests that US may accelerate the early phase of AS1411 internalization, resulting in uptake levels comparable to those achieved after 2 h of passive incubation, which corresponds to the maximal signal. Then, same US treatment applied for 3 s also proved to be useful in significantly decreasing cell viability in the HepG2 cell line treated with 10 µM sorafenib. Although SNU-387 cell line did not show any significative difference, the same trend in the decrease of cell viability was observed with and without US . Interestingly, these differences can be both related to increased uptake of sorafenib in the HCC cell lines and to a combined effect of US treatment and sorafenib together. However, it

is still necessary to consider the time exposure to US, in fact sorafenib treatment was combined to 3 s of US exposure only. Moreover, intermediate concentrations of sorafenib , between 10 µM and 100 µM, should be tested in SNU-387 cell line, to better appreciate the US effect in enhancing drug efficacy/uptake. Despite these interesting results, the main limitations of the study highlight the need for deeper molecular analyses based on dose–response curves combined with US at different exposure times, to establish the impact of sorafenib on cell viability as well as on the phosphorylation of MAPK/RAF, VEGFR, PDGFR, c-Kit, and RET.

Developing an hydrogel-based 3D cultures for HCC cell lines provided more physiologically relevant insights into HCC biology than traditional 2D models. The differences in terms of cell viability between HepG2 and SNU-387 underscore the importance of tailoring seeding density and culture conditions to each cell line to optimize short-term viability and long-term survival. However, PrestoBlue Assay, used for the analysis, may underestimate cell viability in 3D cultures due to limited reagent penetration in cytoplasm, gradients in nutrient and oxygen availability, or interactions with the hydrogel matrix. Alternative approaches, including ATP-based or live/dead imaging assays, could provide complementary or more reliable assessments of cell survival in these three-dimensional systems. By allowing cells to interact in three dimensions, establish complex networks, and experience gradients of nutrients and oxygen, 3D systems better mimic the tumor microenvironment. This approach could allow the reduction of animal models use, offering an ethical, scalable, and potentially more translational platform for studying HCC biomarkers and evaluating therapeutic strategies. Overall, these results support the adoption of 3D cultures as a customizable and robust alternative to conventional *in vitro* and *in vivo* models in HCC research, providing an additional feasible model to further investigate the effects of US.

FUS represents a highly innovative and promising technology to improve cancer therapy by enhancing the delivery of specific drugs to the tumor site. This approach is particularly attractive for aggressive cancers affecting well-defined anatomical districts. To achieve this goal, given the pioneering nature of the methodology, it is essential to establish and optimize the most appropriate experimental conditions in

preclinical models.

In GBM-bearing mice, FUS treatment showed a trend towards to the increase of the xiRA63, which targets the ETA receptor, in the brain. As reported by Hautière et al., the ETA receptor has been proposed as a biomarker to stratify GBM patients according to disease severity, as it is overexpressed in the vascular endothelium of GBM [140, 154]. As reported in Figure 23(a-b), FUS promoted a trend towards to the increase of the distribution volume in the brain, without reaching statistical significance, while irreversible uptake was not altered. This observation is supported by the ratio of VOI tumor and plasma, that highlights a slight difference at 4h and 24h post treatment (Fig.22a), suggesting that FUS technology promoted a trend in increasing the uptake of the tracer.

Despite a trend towards to increased distribution volume (V_0) in the FUS-treated group, the irreversible uptake (Ki) of xiRA63 in the brain did not change significantly in the FUS-treated group.

Several factors could contribute to the limited effect on the distribution volume and the lack of effect on the irreversible uptake, highlighting that this study is a pilot research to determine the appropriate experimental conditions to apply FUS treatment. One possible explanation may be related to the FUS application settings. Although, in this study, FUS parameters were applied as reported by Tran et al. [191], the analyses of V_0 and Ki did not reach statistical significance, highlighting that FUS settings may be revised. Notably, to evaluate BBB integrity in mice, healthy animals are required as controls to ensure that GBM-bearing mice have an intact BBB at 45 days.

Moreover, it may be necessary to evaluate earlier time points for the treatment of the GBM mouse model, because, according to the literature, GBM growth can progressively disrupt the BBB, thereby altering its permeability [164]. At later stages of tumor development, this disruption may lead to passive leakage of circulating molecules into the tumor tissue. Such passive diffusion represents a critical confounding factor, as it may introduce an analytical bias in the evaluation of the specific contribution of FUS to BBB opening and enhanced molecular uptake. Indeed, if molecule passage occurs independently as a consequence of tumor-induced BBB

breakdown, it becomes difficult to discriminate between passive tumor-associated leakage and FUS-mediated BBB opening. In this context, assessing BBB integrity and potential leakage at the selected time point for FUS treatment by MRI and PET imaging would be essential to accurately interpret the effects of FUS on BBB permeability and drug delivery.

Another possible explanation for the Ki results may be related to the administered dose of 40 µg of xiRA63. In this context, xiRA63 may have approached or reached saturation of ETA receptors in the tumor microenvironment, limiting further increases in irreversible retention despite a trend towards an improved distribution volume. Receptor saturation is a well-recognized phenomenon in pharmacokinetics when high doses of a ligand are administered relative to receptor density, resulting in a plateau of irreversible binding even when local drug concentration increases. However, at this point, if the BBB is not leaking and the FUS settings are already optimal, it may be necessary to reduce the antibody dose to fully evaluate the potential of FUS. This, however, would require an increase in radiochemical activity, given that we are already at the minimum concentration required for the detection of the xiRA63 antibody. Thus, enhancing the radiochemical activity of xiRA63, by increasing the number of ^{89}Zr radionuclides per molecule, may improve the sensitivity of PET imaging to better observe antibody distribution within the GBM microenvironment and could allow a reduction in the injected dose. Thus, it may be possible to address the ability of FUS to reduce the dose by evaluating irreversible uptake at lower antibody doses.

Moreover, the tumor model itself may present important sources of variability that reduce the translation of increased regional delivery into higher irreversible uptake. In this study an orthotopic xenograft was established in NMRI nude mice using Gli7 cells, a human GBM stem-like line for which only limited published characterization is available [154]. Limited prior information on Gli7 implies that receptor density, cellular phenotype and intratumoral architecture may differ from better-characterized GBM models, producing heterogeneity in ETA expression or in target accessibility even whether BBB permeability is transiently increased [140, 154].

Taken together, these findings suggest that a combination of (i) revising FUS

parameters to promote BBB opening, (ii) including internal healthy control animals, (iii) assessing the BBB integrity after the xenograft injection, and (iv) increasing the radiochemical activity per molecule of xiRA63 antibody could allow to better address the ability of FUS to significantly enhance the distribution volume and the irreversible uptake within GBM microenvironment.

Then future studies should systematically analyze the BBB integrity within 45 days after xenograft implantation, enhance radio-chemical activity and optimize FUS treatment. Moreover, integrating PET-based biodistribution data with quantitative assessments of ETA receptor expression in the Gli-7 xenograft model could provide interesting insights into the relationship between antibody delivery within tumor microenvironment and irreversible uptake. Such an approach would help clarify whether the most appropriate experimental conditions to appreciate FUS efficacy in opening the BBB and enhancing drug delivery within GBM microenvironment.

Chapter 6

Conclusions

In this research project the use of US and FUS as novel diagnostic and therapeutic approach was extensively described. In details, US showed interesting results in increasing the release of molecules to be used as putative biomarkers from HCC cell lines. Analyses identified the four miRNAs miR-106b-3p, miR-145-5p, miR-29a-3p and miR-532-5p as novel putative circulating biomarkers for HCC diagnosis. In addition, US and FUS treatment demonstrated that it is possible to transiently create pores on cell membrane to facilitate the delivery of drugs in cancer cells. In this context, it remains necessary to evaluate the combined effects of US at different exposures with different sorafenib concentrations, by dose response curve and deepen molecular analyses in HCC cell lines. At the same time, FUS-based approach is a promising tool to be further explored and assessed, considering the pharmacokinetic analysis of the xiRA63 antibody in GBM-bearing mice. Given that the observed effects of FUS did not reach statistical significance in altering the biodistribution and the uptake of the xiRA63 in the tumore site of *in vivo* GBM model, FUS showed a potential role as enabling technologies that warrant further optimization and validation.

Indeed, the results of this research may represent a starting point for multiple future research directions. In particular, further studies could aim to validate the identified miRNAs and proteins as circulating biomarkers by analyzing serum samples from large cohorts of HCC patients and healthy donors. In parallel, future investigations may focus on demonstrating the feasibility of FUS, to transiently open

the BBB, enhancing the delivery of xiRA63 to tumor site in GBM-bearing mice. Such studies could subsequently be extended to evaluate application of the same antibody conjugated with a therapeutic radionuclide, such as ^{177}Lu, to assess its potential utility for targeted radiotherapy in GBM.

To sum up, this research project yield that US treatment are extremely proficient in promoting the release of molecules to be used as putative biomarkers and boosting drug uptake in *in vitro* HCC models. Further research is still necessary to understand diagnostic feasibility of miRNAs and proteins and to refine US/FUS combined approach to upgrade cancer diagnosis and therapy for HCC and GBM.

Bibliography

[1] Wei Cao, Kang Qin, Feng Li, and Wanqing Chen. Comparative study of cancer profiles between 2020 and 2022 using global cancer statistics (globocan). *Journal of the National Cancer Center*, 4(2):128–134, 2024.

[2] Hira Hanif, Mukarram Jamat Ali, Ammu T Susheela, Iman Waheed Khan, Maria Alejandra Luna-Cuadros, Muzammil Muhammad Khan, and Daryl Tan-Yeung Lau. Update on the applications and limitations of alpha-fetoprotein for hepatocellular carcinoma. *World journal of gastroenterology*, 28(2):216, 2022.

[3] Bruno Sangro, Josepmaria Argemi, Maxime Ronot, Valerie Paradis, Tim Meyer, Vincenzo Mazzaferro, Peter Jepsen, Rita Golfieri, Peter Galle, Laura Dawson, et al. Easl clinical practice guidelines on the management of hepatocellular carcinoma. *Journal of Hepatology*, 82(2):315–374, 2025.

[4] Shilpi Singh, Devanjan Dey, Debashis Barik, Iteeshree Mohapatra, Stefan Kim, Mayur Sharma, Sujata Prasad, Peize Wang, Amar Singh, and Gatikrushna Singh. Glioblastoma at the crossroads: current understanding and future therapeutic horizons. *Signal Transduction and Targeted Therapy*, 10(1):213, 2025.

[5] N Lynn Henry and Daniel F Hayes. Cancer biomarkers. *Molecular oncology*, 6(2):140–146, 2012.

[6] Richard Mayeux. Biomarkers: potential uses and limitations. *NeuroRx*, 1(2):182–188, 2004.

[7] Charles L Sawyers. The cancer biomarker problem. *Nature*, 452(7187):548–552, 2008.

[8] Jason T Huse, Heidi S Phillips, and Cameron W Brennan. Molecular subclassification of diffuse gliomas: seeing order in the chaos. *Glia*, 59(8):1190–1199, 2011.

[9] Roger Stupp, Monika E Hegi, Warren P Mason, Martin J Van Den Bent, Martin JB Taphoorn, Robert C Janzer, Samuel K Ludwin, Anouk Allgeier, Barbara Fisher, Karl

Belanger, et al. Effects of radiotherapy with concomitant and adjuvant temozolomide versus radiotherapy alone on survival in glioblastoma in a randomised phase iii study: 5-year analysis of the eortc-ncic trial. *The lancet oncology*, 10(5):459–466, 2009.

[10] Chetan Bettegowda, Mark Sausen, Rebecca J Leary, Isaac Kinde, Yuxuan Wang, Nishant Agrawal, Bjarne R Bartlett, Hao Wang, Brandon Luber, Rhoda M Alani, et al. Detection of circulating tumor dna in early-and late-stage human malignancies. *Science translational medicine*, 6(224):224ra24–224ra24, 2014.

[11] Alexandra M Miller, Ronak H Shah, Elena I Pentsova, Maryam Pourmaleki, Samuel Briggs, Natalie Distefano, Youyun Zheng, Anna Skakodub, Smrutiben A Mehta, Carl Campos, et al. Tracking tumour evolution in glioma through liquid biopsies of cerebrospinal fluid. *Nature*, 565(7741):654–658, 2019.

[12] Jacob O'Brien, Heyam Hayder, Yara Zayed, and Chun Peng. Overview of microrna biogenesis, mechanisms of actions, and circulation. *Frontiers in endocrinology*, 9:402, 2018.

[13] Ahmet M Denli, Bastiaan BJ Tops, Ronald HA Plasterk, René F Ketting, and Gregory J Hannon. Processing of primary microrna by the microprocessor complex. *Nature*, 432(7014):231–235, 2004.

[14] Jinju Han, Yoontae Lee, Kyu-Hyun Yeom, Young-Kook Kim, Hua Jin, and V Narry Kim. The drosha-dgcr8 complex in primary microrna processing. *Genes & development*, 18(24):3016–3027, 2004.

[15] Claudio R Alarcón, Hyeseung Lee, Hani Goodarzi, Nils Halberg, and Sohail F Tavazoie. N 6-methyladenosine marks primary microrna for processing. *Nature*, 519(7544):482–485, 2015.

[16] Jr-Shiuan Yang, Thomas Maurin, Nicolas Robine, Kasper D Rasmussen, Kate L Jeffrey, Rohit Chandwani, Eirini P Papapetrou, Michel Sadelain, Dónal O'Carroll, and Eric C Lai. Conserved vertebrate mir-451 provides a platform for dicer-independent, ago2-mediated microrna biogenesis. *Proceedings of the National Academy of Sciences*, 107(34):15163–15168, 2010.

[17] Sihem Cheloufi, Camila O Dos Santos, Mark MW Chong, and Gregory J Hannon. A dicer-independent mirna biogenesis pathway that requires ago catalysis. *Nature*, 465(7298):584–589, 2010.

[18] Mingyi Xie, Mingfeng Li, Anna Vilborg, Nara Lee, Mei-Di Shu, Valeria Yartseva, Nenad Šestan, and Joan A Steitz. Mammalian 5′-capped microrna precursors that generate a single microrna. *Cell*, 155(7):1568–1580, 2013.

[19] Myung Hyun Jo, Soochul Shin, Seung-Ryoung Jung, Eunji Kim, Ji-Joon Song, and Sungchul Hohng. Human argonaute 2 has diverse reaction pathways on target rnas. *Molecular cell*, 59(1):117–124, 2015.

[20] Anneke Brümmer and Jean Hausser. Microrna binding sites in the coding region of mrnas: extending the repertoire of post-transcriptional gene regulation. *Bioessays*, 36(6):617–626, 2014.

[21] David P Bartel. Micrornas: genomics, biogenesis, mechanism, and function. *cell*, 116(2):281–297, 2004.

[22] Chih-Hung Chou, Sirjana Shrestha, Chi-Dung Yang, Nai-Wen Chang, Yu-Ling Lin, Kuang-Wen Liao, Wei-Chi Huang, Ting-Hsuan Sun, Siang-Jyun Tu, Wei-Hsiang Lee, et al. mirtarbase update 2018: a resource for experimentally validated microrna-target interactions. *Nucleic acids research*, 46(D1):D296–D302, 2018.

[23] Azra Krek, Dominic Grün, Matthew N Poy, Rachel Wolf, Lauren Rosenberg, Eric J Epstein, Philip MacMenamin, Isabelle Da Piedade, Kristin C Gunsalus, Markus Stoffel, et al. Combinatorial microrna target predictions. *Nature genetics*, 37(5):495–500, 2005.

[24] Yong Peng and Carlo M Croce. The role of micrornas in human cancer. *Signal transduction and targeted therapy*, 1(1):1–9, 2016.

[25] Shan-shan Zhou, Jing-peng Jin, Ji-qun Wang, Zhi-guo Zhang, Jonathan H Freedman, Yang Zheng, and Lu Cai. mirnas in cardiovascular diseases: potential biomarkers, therapeutic targets and challenges. *Acta Pharmacologica Sinica*, 39(7):1073–1084, 2018.

[26] Camille A Juźwik, Sienna S Drake, Yang Zhang, Nicolas Paradis-Isler, Alexandra Sylvester, Alexandre Amar-Zifkin, Chelsea Douglas, Barbara Morquette, Craig S Moore, and Alyson E Fournier. microrna dysregulation in neurodegenerative diseases: A systematic review. *Progress in neurobiology*, 182:101664, 2019.

[27] Hiromu Suzuki, Reo Maruyama, Eiichiro Yamamoto, and Masahiro Kai. Epigenetic alteration and microrna dysregulation in cancer. *Frontiers in genetics*, 4:258, 2013.

[28] Brandi N Davis-Dusenbery and Akiko Hata. Microrna in cancer: the involvement of aberrant microrna biogenesis regulatory pathways. *Genes & cancer*, 1(11):1100–1114, 2010.

[29] Fanyin Meng, Roger Henson, Hania Wehbe-Janek, Kalpana Ghoshal, Samson T Jacob, and Tushar Patel. Microrna-21 regulates expression of the pten tumor suppressor gene in human hepatocellular cancer. *Gastroenterology*, 133(2):647–658, 2007.

[30] Jian Wang, Yanfeng Chu, Mei Xu, Xiumei Zhang, Yumei Zhou, and Mei Xu. mir-21 promotes cell migration and invasion of hepatocellular carcinoma by targeting klf5. *Oncology letters*, 17(2):2221–2227, 2019.

[31] Fernando Bergez-Hernández, Martín Irigoyen-Arredondo, and Alejandra Martínez-Camberos. A systematic review of mechanisms of pten gene down-regulation mediated by mirna in prostate cancer. *Heliyon*, 10(15), 2024.

[32] Zeng-Hui Ma, Pei-Dong Shi, and Bo-Shun Wan. Mir-410-3p activates the nf-κb pathway by targeting zcchc10 to promote migration, invasion and emt of colorectal cancer. *Cytokine*, 140:155433, 2021.

[33] Yi Tang, Jianrong Yang, Yonggang Wang, Zhenyong Tang, Sulai Liu, and Yuntian Tang. Mir-19b-3p facilitates the proliferation and epithelial-mesenchymal transition, and inhibits the apoptosis of intrahepatic cholangiocarcinoma by suppressing coiled-coil domain containing 6. *Archives of biochemistry and biophysics*, 686:108367, 2020.

[34] Xu-Hua Mao, Min Chen, Yan Wang, Pan-Gen Cui, Si-Bian Liu, and Zei-Yong Xu. Microrna-21 regulates the erk/nf-κb signaling pathway to affect the proliferation, migration, and apoptosis of human melanoma a375 cells by targeting spry1, pdcd4, and pten. *Molecular carcinogenesis*, 56(3):886–894, 2017.

[35] Pamela Ajuyah, Meredith Hill, Alireza Ahadi, Jing Lu, Gyorgy Hutvagner, and Nham Tran. Microrna (mirna)-to-mirna regulation of programmed cell death 4 (pdcd4). *Molecular and cellular biology*, 39(18):e00086–19, 2019.

[36] Giulia Romano, Mario Acunzo, Michela Garofalo, Gianpiero Di Leva, Luciano Cascione, Ciro Zanca, Brad Bolon, Gerolama Condorelli, and Carlo M Croce. Mir-494 is regulated by erk1/2 and modulates trail-induced apoptosis in non–small-cell lung cancer through bim down-regulation. *Proceedings of the National Academy of Sciences*, 109(41):16570–16575, 2012.

[37] Shin Hamada, Atsushi Masamune, Shin Miura, Kennichi Satoh, and Tooru Shimosegawa. Mir-365 induces gemcitabine resistance in pancreatic cancer cells by tar-

geting the adaptor protein shc1 and pro-apoptotic regulator bax. *Cellular signalling*, 26(2):179–185, 2014.

[38] Jun Inoue and Johji Inazawa. Cancer-associated mirnas and their therapeutic potential. *Journal of human genetics*, 66(9):937–945, 2021.

[39] Veronica Zelli, Chiara Compagnoni, Roberta Capelli, Alessandra Corrente, Mauro Di Vito Nolfi, Francesca Zazzeroni, Edoardo Alesse, and Alessandra Tessitore. Role of exosomal micrornas in cancer therapy and drug resistance mechanisms: focus on hepatocellular carcinoma. *Frontiers in Oncology*, 12:940056, 2022.

[40] Jessica A Weber, David H Baxter, Shile Zhang, David Y Huang, Kuo How Huang, Ming Jen Lee, David J Galas, and Kai Wang. The microrna spectrum in 12 body fluids. *Clinical chemistry*, 56(11):1733–1741, 2010.

[41] Kseniya Khamina, Andreas B Diendorfer, Susanna Skalicky, Moritz Weigl, Marianne Pultar, Teresa L Krammer, Catharine Aquino Fournier, Amy L Schofield, Carolin Otto, Aaron Thomas Smith, et al. A microrna next-generation-sequencing discovery assay (mind) for genome-scale analysis and absolute quantitation of circulating microrna biomarkers. *International Journal of Molecular Sciences*, 23(3):1226, 2022.

[42] Vijay Singh, Aniruddha Sen, Sapna Saini, Shailendra Dwivedi, Ruchika Agrawal, Akash Bansal, and Shashank Shekhar. Microrna significance in cancer: An updated review on diagnostic, prognostic, and therapeutic perspectives. *Ejifcc*, 35(4):265, 2024.

[43] Xuan Zou, Tiansong Xia, Minghui Li, Tongshan Wang, Ping Liu, Xin Zhou, Zebo Huang, and Wei Zhu. Microrna profiling in serum: Potential signatures for breast cancer diagnosis. *Cancer Biomarkers*, 30(1):41–53, 2021.

[44] Soo Young Hwang, Pojsakorn Danpanichkul, Vatche Agopian, Neil Mehta, Neehar D Parikh, Ghassan K Abou-Alfa, Amit G Singal, and Ju Dong Yang. Hepatocellular carcinoma: updates on epidemiology, surveillance, diagnosis and treatment. *Clinical and Molecular Hepatology*, 31(Suppl):S228, 2024.

[45] Satender P Singh, Tushar Madke, and Phool Chand. Global epidemiology of hepatocellular carcinoma. *Journal of Clinical and Experimental Hepatology*, 15(2):102446, 2025.

[46] Hyuna Sung, Jacques Ferlay, Rebecca L Siegel, Mathieu Laversanne, Isabelle Soerjomataram, Ahmedin Jemal, and Freddie Bray. Global cancer statistics 2020: Globocan estimates of incidence and mortality worldwide for 36 cancers in 185 countries. *CA: a cancer journal for clinicians*, 71(3):209–249, 2021.

[47] Harriet Rumgay, Melina Arnold, Jacques Ferlay, Olufunmilayo Lesi, Citadel J Cabasag, Jérôme Vignat, Mathieu Laversanne, Katherine A McGlynn, and Isabelle Soerjomataram. Global burden of primary liver cancer in 2020 and predictions to 2040. *Journal of hepatology*, 77(6):1598–1606, 2022.

[48] Amit G Singal, Fasiha Kanwal, and Josep M Llovet. Global trends in hepatocellular carcinoma epidemiology: implications for screening, prevention and therapy. *Nature reviews Clinical oncology*, 20(12):864–884, 2023.

[49] Evelyn Calderon-Martinez, Samanta Landazuri-Navas, Esmeralda Vilchez, Raul Cantu-Hernandez, Johanna Mosquera-Moscoso, Sebastian Encalada, Christian Zevallos-Delgado, John Cinicola, et al. Prognostic scores and survival rates by etiology of hepatocellular carcinoma: a review. *Journal of clinical medicine research*, 15(4):200, 2023.

[50] Daniel Q Huang, Philippe Mathurin, Helena Cortez-Pinto, and Rohit Loomba. Global epidemiology of alcohol-associated cirrhosis and hcc: trends, projections and risk factors. *Nature reviews Gastroenterology & hepatology*, 20(1):37–49, 2023.

[51] Katherine A McGlynn, Jessica L Petrick, and Hashem B El-Serag. Epidemiology of hepatocellular carcinoma. *Hepatology*, 73:4–13, 2021.

[52] Qing Wei, Pengbo Guo, Kun Mu, Ying Zhang, Wei Zhao, Wanwan Huai, Yumin Qiu, Tao Li, Xiaomin Ma, Yafei Liu, et al. Estrogen suppresses hepatocellular carcinoma cells through erβ-mediated upregulation of the nlrp3 inflammasome. *Laboratory investigation*, 95(7):804–816, 2015.

[53] De-Hua Wang, Dong-Wei He, Ting-Ting Lv, Xiao-Kuan Zhang, Zi-Jie Li, and Zhi-Yu Wang. Estrogen receptor α suppresses hepatocellular carcinoma by restricting m2 macrophage infiltration through the yap-ccl2 axis. *BMC cancer*, 25(1):550, 2025.

[54] Daniel Wai-Hung Ho, Regina Cheuk-Lam Lo, Lo-Kong Chan, and Irene Oi-Lin Ng. Molecular pathogenesis of hepatocellular carcinoma. *Liver cancer*, 5(4):290–302, 2016.

[55] Deniz Tuemen, Philipp Heumann, Karsten Guelow, Cagla-Nur Demirci, Lidia-Sabina Cosma, Martina Mueller, and Arne Kandulski. Pathogenesis and current treatment strategies of hepatocellular carcinoma. *Biomedicines*, 10(12):3202, 2022.

[56] Mads Israelsen, Sven Francque, Emmanuel A Tsochatzis, and Aleksander Krag. Steatotic liver disease. *The Lancet*, 404(10464):1761–1778, 2024.

[57] Christopher M Walker, Zongdi Feng, and Stanley M Lemon. Reassessing immune control of hepatitis a virus. *Current opinion in virology*, 11:7–13, 2015.

[58] Scott L Friedman. Liver fibrosis–from bench to bedside. *Journal of hepatology*, 38:38–53, 2003.

[59] Zhixian Ding, Lusheng Wang, Jiting Sun, Lijie Zheng, Yu Tang, and Heng Tang. Hepatocellular carcinoma: pathogenesis, molecular mechanisms, and treatment advances. *Frontiers in Oncology*, 15:1526206, 2025.

[60] Ting Shen, Shan-Feng Li, Jia-Lin Wang, Ting Zhang, Song Zhang, Hai-Tao Chen, Qian-Yi Xiao, Wei-Hua Ren, Chao Liu, Bo Peng, et al. Tp53 r249s mutation detected in circulating tumour dna is associated with prognosis of hepatocellular carcinoma patients with or without hepatectomy. *Liver international*, 40(11):2834–2847, 2020.

[61] Yasushi Totoki, Kenji Tatsuno, Kyle R Covington, Hiroki Ueda, Chad J Creighton, Mamoru Kato, Shingo Tsuji, Lawrence A Donehower, Betty L Slagle, Hiromi Nakamura, et al. Trans-ancestry mutational landscape of hepatocellular carcinoma genomes. *Nature genetics*, 46(12):1267–1273, 2014.

[62] Martina Müller, Elisa Schulze Schleithoff, Wolfgang Stremmel, Gerry Melino, Peter H Krammer, and Tobias Schilling. One, two, three—p53, p63, p73 and chemosensitivity. *Drug resistance updates*, 9(6):288–306, 2006.

[63] Miryam Müller, Thomas G Bird, and Jean-Charles Nault. The landscape of gene mutations in cirrhosis and hepatocellular carcinoma. *Journal of hepatology*, 72(5):990–1002, 2020.

[64] F Aguilar, CC Harris, T Sun, M Hollstein, and P Cerutti. Geographic variation of p53 mutational profile in nonmalignant human liver. *Science*, 264(5163):1317–1319, 1994.

[65] Hyuk Moon and Simon Weonsang Ro. Mapk/erk signaling pathway in hepatocellular carcinoma. *Cancers*, 13(12):3026, 2021.

[66] Chiara Braconi, Jon C Henry, Takayuki Kogure, Thomas Schmittgen, and Tushar Patel. The role of micrornas in human liver cancers. In *Seminars in oncology*, volume 38, pages 752–763. Elsevier, 2011.

[67] Wei-Chih Tsai, Sheng-Da Hsu, Chu-Sui Hsu, Tsung-Ching Lai, Shu-Jen Chen, Roger Shen, Yi Huang, Hua-Chien Chen, Chien-Hsin Lee, Ting-Fen Tsai, et al. Microrna-122 plays a critical role in liver homeostasis and hepatocarcinogenesis. *The Journal of clinical investigation*, 122(8):2884–2897, 2012.

[68] Francesco Colaianni, Veronica Zelli, Chiara Compagnoni, Martina Sara Miscione, Mario Rossi, Davide Vecchiotti, Monica Di Padova, Edoardo Alesse, Francesca Zazzeroni,

and Alessandra Tessitore. Role of circulating micrornas in liver disease and hcc: focus on mir-122. *Genes*, 15(10):1313, 2024.

[69] Raphael Mohr, Burcin Özdirik, Joeri Lambrecht, Münevver Demir, Johannes Eschrich, Lukas Geisler, Teresa Hellberg, Sven H Loosen, Tom Luedde, Frank Tacke, et al. From liver cirrhosis to cancer: the role of micro-rnas in hepatocarcinogenesis. *International journal of molecular sciences*, 22(3):1492, 2021.

[70] Yi Wei Dong, Rong Wang, Qian Qian Cai, Bing Qi, Wei Wu, Yong Hu Zhang, and Xing Zhong Wu. Sulfatide epigenetically regulates mir-223 and promotes the migration of human hepatocellular carcinoma cells. *Journal of hepatology*, 60(4):792–801, 2014.

[71] Qiu Chen, Lei Li, Yu Tu, Lu Lin Zheng, Wei Liu, Xue Yong Zuo, Yong Ming He, Shu Yu Zhang, Wei Zhu, Jian Ping Cao, et al. Mir-34a regulates apoptosis in liver cells by targeting the klf4 gene. *Cellular & Molecular Biology Letters*, 19(1):52–64, 2014.

[72] Ting-Yi Sun, Hong-Jian Xie, Zhen Li, Ling-Fei Kong, Xiang-Nan Gou, Du-Juan Li, Yu-Jie Shi, and Yan-Zhi Ding. mir-34a regulates hdac1 expression to affect the proliferation and apoptosis of hepatocellular carcinoma. *American journal of translational research*, 9(1):103, 2017.

[73] Sonya Parpart, Stephanie Roessler, Fei Dong, Vinay Rao, Atsushi Takai, Junfang Ji, Lun-Xiu Qin, Qing-Hai Ye, Hu-Liang Jia, Zhao-You Tang, et al. Modulation of mir-29 expression by alpha-fetoprotein is linked to the hepatocellular carcinoma epigenome. *Hepatology*, 60(3):872–883, 2014.

[74] Binkui Li, Liru He, Dinglan Zuo, Wei He, Yongjin Wang, Yuanping Zhang, Wenwu Liu, and Yunfei Yuan. Mutual regulation of mir-199a-5p and hif-1α modulates the warburg effect in hepatocellular carcinoma. *Journal of Cancer*, 8(6):940, 2017.

[75] Jiugang Song, Liucun Gao, Guang Yang, Shanhong Tang, Huahong Xie, Yongji Wang, Jingbo Wang, Yanping Zhang, Jiang Jin, Yawen Gou, et al. Mir-199a regulates cell proliferation and survival by targeting fzd7. *PloS one*, 9(10):e110074, 2014.

[76] Mi Zhou, Shuai Wang, Linyi Hu, Feng Liu, Qi Zhang, and Dahong Zhang. mir-199a-5p suppresses human bladder cancer cell metastasis by targeting ccr7. *BMC urology*, 16(1):64, 2016.

[77] Xin Xu, Yuquan Tao, Yongjie Niu, Zhixian Wang, Congcong Zhang, Yongchun Yu, and Lifang Ma. mir-125a-5p inhibits tumorigenesis in hepatocellular carcinoma. *Aging (Albany NY)*, 11(18):7639, 2019.

[78] Changzheng Liu, Jia Yu, Shuangni Yu, Robert M Lavker, Lei Cai, Wei Liu, Kegong Yang, Xiaodong He, and Songsen Chen. Microrna-21 acts as an oncomir through multiple targets in human hepatocellular carcinoma. *Journal of hepatology*, 53(1):98–107, 2010.

[79] Xiaolin Wang, Yong He, Bryan Mackowiak, and Bin Gao. Micrornas as regulators, biomarkers and therapeutic targets in liver diseases. *Gut*, 70(4):784–795, 2021.

[80] Catherine M Greene, Robert B Varley, and Matthew W Lawless. Micrornas and liver cancer associated with iron overload: therapeutic targets unravelled. *World journal of gastroenterology: WJG*, 19(32):5212, 2013.

[81] Jing Shen, Abby B Siegel, Helen Remotti, Qiao Wang, and Regina M Santella. Identifying microrna panels specifically associated with hepatocellular carcinoma and its different etiologies. *Hepatoma research*, 2:151, 2016.

[82] Chiara Compagnoni, Roberta Capelli, Veronica Zelli, Alessandra Corrente, Davide Vecchiotti, Irene Flati, Mauro Di Vito Nolfi, Adriano Angelucci, Edoardo Alesse, Francesca Zazzeroni, et al. Mir-182-5p is upregulated in hepatic tissues from a diet-induced nafld/nash/hcc c57bl/6j mouse model and modulates cyld and foxo1 expression. *International Journal of Molecular Sciences*, 24(11):9239, 2023.

[83] Ying-Feng Wei, Guang-Ying Cui, Ping Ye, Jia-Ning Chen, and Hong-Yan Diao. Micrornas may solve the mystery of chronic hepatitis b virus infection. *World Journal of Gastroenterology: WJG*, 19(30):4867, 2013.

[84] Ding-Shinn Chen and Juei-Low Sung. Serum alphafetoprotein in hepatocellular carcinoma. *Cancer*, 40(2):779–783, 1977.

[85] ME Alpert, J Uriel, and B De Nechaud. Alpha1 fetoglobulin in the diagnosis of human hepatoma. *New England Journal of Medicine*, 278(18):984–986, 1968.

[86] Gregory T O'Conor, Yu S Tatarinov, GI Abelev, and Jose Uriel. A collaborative study for the evaluation of a serologic test for primary liver cancer. *Cancer*, 25(5):1091–1098, 1970.

[87] Yujia Fang, Dong Yan, Lixin Wang, Jie Zhang, and Qingfang He. Circulating micrornas (mir-16, mir-22, mir-122) expression and early diagnosis of hepatocellular carcinoma. *Journal of clinical laboratory analysis*, 36(7):e24541, 2022.

[88] Hassan El-Garem, Ayman Ammer, Hany Shehab, Olfat Shaker, Mohammed Anwer, Wafaa El-Akel, and Heba Omar. Circulating microrna, mir-122 and mir-221 signature

in egyptian patients with chronic hepatitis c related hepatocellular carcinoma. *World journal of hepatology*, 6(11):818, 2014.

[89] Qingjuan Chen, Xiaojun Ge, Yuchen Zhang, Hongwei Xia, Dandan Yuan, Qiulin Tang, Liang Chen, Xiaohui Pang, Weibing Leng, and Feng Bi. Plasma mir-122 and mir-192 as potential novel biomarkers for the early detection of distant metastasis of gastric cancer. *Oncology reports*, 31(4):1863–1870, 2014.

[90] Farzaneh Moshiri, Alessandro Salvi, Laura Gramantieri, Angelo Sangiovanni, Paola Guerriero, Giuseppina De Petro, Cristian Bassi, Laura Lupini, Arash Sattari, Douglas Cheung, et al. Circulating mir-106b-3p, mir-101-3p and mir-1246 as diagnostic biomarkers of hepatocellular carcinoma. *Oncotarget*, 9(20):15350, 2018.

[91] Chunbo Zhuang, Weichao Jiang, Da Huang, Luming Xu, Qianqian Yang, Lei Zheng, Xiaobei Wang, and Lihua Hu. Serum mir-21, mir-26a and mir-101 as potential biomarkers of hepatocellular carcinoma. *Clinics and research in hepatology and gastroenterology*, 40(4):386–396, 2016.

[92] Bao-Min Shi, Wen Lu, Kun Ji, Yu-Feng Wang, Shuai Xiao, and Xiu-Yan Wang. Study on the value of serum mir-106b for the early diagnosis of hepatocellular carcinoma. *World journal of gastroenterology*, 23(20):3713, 2017.

[93] Peng Qi, Shu-qun Cheng, Hao Wang, Nan Li, Yue-feng Chen, and Chun-fang Gao. Serum microrna as biomarkers for hepatocellular carcinoma in chinese patients with chronic hepatitis b virus infection. *PloS one*, 6(12):e28486, 2011.

[94] Juan Wu, Yunbin Wu, Yue Luo, Xianghui Li, Ni Lin, Xiulin Yang, Yanfeng Lin, and Min Chen. Circulating mirna-199a and mirna-122 levels as potential diagnostic and prognostic biomarkers for hepatocellular carcinoma. *Annals of Clinical & Laboratory Science*, 50(2):219–227, 2020.

[95] Jianjian Zheng, Zhenxu Zhou, Ziqiang Xu, Guojun Li, Peihong Dong, Zhanguo Chen, Dezhao Lin, Bicheng Chen, and Fujun Yu. Serum microrna-125a-5p, a useful biomarker in liver diseases, correlates with disease progression. *Molecular medicine reports*, 12(1):1584–1590, 2015.

[96] Weifeng Liu, Jie Hu, Kaiqian Zhou, Feiyu Chen, Zheng Wang, Boyi Liao, Zhi Dai, Ya Cao, Jia Fan, and Jian Zhou. Serum exosomal mir-125b is a novel prognostic marker for hepatocellular carcinoma. *OncoTargets and therapy*, pages 3843–3851, 2017.

[97] Burcu Gurer Giray, Gurol Emekdas, Seda Tezcan, Mahmut Ulger, Mehmet Sami Serin, Orhan Sezgin, Engin Altintas, and Eyup Naci Tiftik. Profiles of serum microrna;

mir-125b-5p and mir223-3p serve as novel biomarkers for hbv-positive hepatocellular carcinoma. *Molecular biology reports*, 41(7):4513–4519, 2014.

[98] Sherin Sobhy El-Naidany, Ebrahim Zid, Fatma M Reda, Ali Nada, and Eman AM Fouda. Clinical significance of mir-130b and mir-125b as biomarkers in hepatocellular carcinoma. *Asian Pacific Journal of Cancer Prevention: APJCP*, 23(8):2687, 2022.

[99] Angela M Liu, Tzy-Jyun Yao, Wei Wang, Kwong-Fai Wong, Nikki P Lee, Sheung Tat Fan, Ronnie TP Poon, Chunfang Gao, and John M Luk. Circulating mir-15b and mir-130b in serum as potential markers for detecting hepatocellular carcinoma: a retrospective cohort study. *BMJ open*, 2(2):e000825, 2012.

[100] Yi Chen, Jin Chen, Yizhao Liu, Shiliang Li, and Ping Huang. Plasma mir-15b-5p, mir-338-5p, and mir-764 as biomarkers for hepatocellular carcinoma. *Medical science monitor: international medical journal of experimental and clinical research*, 21:1864, 2015.

[101] Noha Mohamed Hosni Shaheen, Naglaa Zayed, Nermine Magdi Riad, Hend H Tamim, Rasha Mohamed Hosny Shahin, Dalia A Labib, Suzan Mahrous ELsheikh, Reham Abdel Moneim, Ayman Yosry, et al. Role of circulating mir-182 and mir-150 as biomarkers for cirrhosis and hepatocellular carcinoma post hcv infection in egyptian patients. *Virus Research*, 255:77–84, 2018.

[102] Fujun Yu, Zhongqiu Lu, Bicheng Chen, Peihong Dong, and Jianjian Zheng. microrna-150: a promising novel biomarker for hepatitis b virus-related hepatocellular carcinoma. *Diagnostic pathology*, 10(1):129, 2015.

[103] Yang Wen, Jing Han, Jianguo Chen, Jing Dong, Yongxiang Xia, Jibin Liu, Yue Jiang, Juncheng Dai, Jianhua Lu, Guangfu Jin, et al. Plasma mi rna s as early biomarkers for detecting hepatocellular carcinoma. *International journal of cancer*, 137(7):1679–1690, 2015.

[104] Jingwen Yang, Weiwei Dong, He Zhang, Huixia Zhao, Zhiyan Zeng, Fengyun Zhang, Qiuwen Li, Xiaohong Duan, Yanyan Hu, and Wenhua Xiao. Exosomal microrna panel as a diagnostic biomarker in patients with hepatocellular carcinoma. *Frontiers in Cell and Developmental Biology*, 10:927251, 2022.

[105] Yoshito Tomimaru, Hidetoshi Eguchi, Hiroaki Nagano, Hiroshi Wada, Shogo Kobayashi, Shigeru Marubashi, Masahiro Tanemura, Akira Tomokuni, Ichiro Takemasa, Koji Umeshita, et al. Circulating microrna-21 as a novel biomarker for hepatocellular carcinoma. *Journal of hepatology*, 56(1):167–175, 2012.

[106] Won Sohn, Jonghwa Kim, So Hee Kang, Se Ra Yang, Ju-Yeon Cho, Hyun Chin Cho, Sang Goon Shim, and Yong-Han Paik. Serum exosomal micrornas as novel biomarkers for hepatocellular carcinoma. *Experimental & molecular medicine*, 47(9):e184–e184, 2015.

[107] Youwen Tan, Guohong Ge, Tengli Pan, Danfeng Wen, Li Chen, Xuejun Yu, Xinbei Zhou, and Jianhe Gan. A serum microrna panel as potential biomarkers for hepatocellular carcinoma related with hepatitis b virus. *PloS one*, 9(9):e107986, 2014.

[108] Shuying Chen, Yinqi Mao, Wei Chen, Chenbin Liu, Han Wu, Jingjun Zhang, Shenghao Wang, Chengpan Wang, Yong Lin, and Yuan Lv. Serum exosomal mir-34a as a potential biomarker for the diagnosis and prognostic of hepatocellular carcinoma. *Journal of Cancer*, 13(5):1410, 2022.

[109] Tarek K Motawi, Olfat G Shaker, Shohda A El-Maraghy, and Mahmoud A Senousy. Serum micrornas as potential biomarkers for early diagnosis of hepatitis c virus-related hepatocellular carcinoma in egyptian patients. *PloS one*, 10(9):e0137706, 2015.

[110] Andrei Sorop, Razvan Iacob, Speranta Iacob, Diana Constantinescu, Leona Chitoiu, Tudor Emanuel Fertig, Anca Dinischiotu, Mihaela Chivu-Economescu, Nicolae Bacalbasa, Lorand Savu, et al. Plasma small extracellular vesicles derived mir-21-5p and mir-92a-3p as potential biomarkers for hepatocellular carcinoma screening. *Frontiers in Genetics*, 11:712, 2020.

[111] Min Jiang, Xuelian Li, Xiaowei Quan, Xiaoying Li, and Baosen Zhou. Mir-92a family: a novel diagnostic biomarker and potential therapeutic target in human cancers. *Frontiers in molecular biosciences*, 6:98, 2019.

[112] Les Lang. Fda approves sorafenib for patients with inoperable liver cancer. *Gastroenterology*, 134(2):379, 2008.

[113] Loraine Kay D Cabral, Claudio Tiribelli, and Caecilia HC Sukowati. Sorafenib resistance in hepatocellular carcinoma: the relevance of genetic heterogeneity. *Cancers*, 12(6):1576, 2020.

[114] Weiwei Tang, Ziyi Chen, Wenling Zhang, Ye Cheng, Betty Zhang, Fan Wu, Qian Wang, Shouju Wang, Dawei Rong, FP Reiter, et al. The mechanisms of sorafenib resistance in hepatocellular carcinoma: theoretical basis and therapeutic aspects. *Signal transduction and targeted therapy*, 5(1):87, 2020.

[115] Waad H Abuwatfa, William G Pitt, and Ghaleb A Husseini. Scaffold-based 3d cell culture models in cancer research. *Journal of Biomedical Science*, 31(1):7, 2024.

[116] Louis-Bastien Weiswald, Dominique Bellet, and Virginie Dangles-Marie. Spherical cancer models in tumor biology. *Neoplasia*, 17(1):1–15, 2015.

[117] Jingwen Xu, Guangyan Qi, Weiqun Wang, and Xiuzhi Susan Sun. Advances in 3d peptide hydrogel models in cancer research. *npj Science of Food*, 5(1):14, 2021.

[118] Sritama Nath and Gayathri R Devi. Three-dimensional culture systems in cancer research: Focus on tumor spheroid model. *Pharmacology & therapeutics*, 163:94–108, 2016.

[119] Jarno Drost and Hans Clevers. Organoids in cancer research. *Nature Reviews Cancer*, 18(7):407–418, 2018.

[120] Yexin Gu, Ye Lu, Yunqiang Xiong, Xiangpeng Zhan, Taobin Liu, Min Tang, An Xie, Xiaoqiang Liu, and Bin Fu. Advances in the bladder cancer research using 3d culture models. *Bladder*, 10:e21200005, 2023.

[121] Nathan Vella, Anthony G Fenech, and Vanessa Petroni Magri. 3d cell culture models in research: applications to lung cancer pharmacology. *Frontiers in Pharmacology*, 15:1438067, 2024.

[122] Lara Troncoso-Afonso, Gail A Vinnacombe-Willson, Clara García-Astrain, and Luis M Liz-Márzan. Sers in 3d cell models: a powerful tool in cancer research. *Chemical Society Reviews*, 53(10):5118–5148, 2024.

[123] Catherine C Bell, Delilah FG Hendriks, Sabrina ML Moro, Ewa Ellis, Joanne Walsh, Anna Renblom, Lisa Fredriksson Puigvert, Anita CA Dankers, Frank Jacobs, Jan Snoeys, et al. Characterization of primary human hepatocyte spheroids as a model system for drug-induced liver injury, liver function and disease. *Scientific reports*, 6(1):25187, 2016.

[124] Xiaolu Xie, Yaomin Wang, Ziyi Wang, Lei Zhang, Jun Li, and Yaling Li. Hepatocellular carcinoma drug resistance models. *Cancer Cell International*, 25(1):195, 2025.

[125] Patrick Y Wen, Michael Weller, Eudocia Q Lee, et al. Glioblastoma in adults: A society for neuro-oncology (sno) and european society of neuro-oncology (eano) consensus review on current management and future directions. *Neuro-Oncology*, 2025.

[126] David N Louis, Arie Perry, Pieter Wesseling, Daniel J Brat, Ian A Cree, Dominique Figarella-Branger, Cynthia Hawkins, HK Ng, Stefan M Pfister, Guido Reifenberger, et al. The 2021 who classification of tumors of the central nervous system: a summary. *Neuro-oncology*, 23(8):1231–1251, 2021.

[127] Mary Elizabeth Davis. Glioblastoma: overview of disease and treatment. *Clinical journal of oncology nursing*, 20(5):S2, 2016.

[128] Young Zoon Kim, Chae-Yong Kim, and Do Hoon Lim. The overview of practical guidelines for gliomas by ksno, nccn, and eano. *Brain tumor research and treatment*, 10(2):83–93, 2022.

[129] Ashkan Pouyan, Masoud Ghorbanlo, Masoud Eslami, Majid Jahanshahi, Ehsan Ziaei, Ali Salami, Khatere Mokhtari, Koorosh Shahpasand, Najma Farahani, Tohid Emami Meybodi, et al. Glioblastoma multiforme: insights into pathogenesis, key signaling pathways, and therapeutic strategies. *Molecular cancer*, 24(1):58, 2025.

[130] Sheila R Alcantara Llaguno and Luis F Parada. Cell of origin of glioma: biological and clinical implications. *British journal of cancer*, 115(12):1445–1450, 2016.

[131] Dinorah Friedmann-Morvinski, Eric A Bushong, Eugene Ke, Yasushi Soda, Tomotoshi Marumoto, Oded Singer, Mark H Ellisman, and Inder M Verma. Dedifferentiation of neurons and astrocytes by oncogenes can induce gliomas in mice. *Science*, 338(6110):1080–1084, 2012.

[132] Sheila Alcantara Llaguno, Jian Chen, Chang-Hyuk Kwon, Erica L Jackson, Yanjiao Li, Dennis K Burns, Arturo Alvarez-Buylla, and Luis F Parada. Malignant astrocytomas originate from neural stem/progenitor cells in a somatic tumor suppressor mouse model. *Cancer cell*, 15(1):45–56, 2009.

[133] Sheila R Alcantara Llaguno, Zilai Wang, Daochun Sun, Jian Chen, Jing Xu, Euiseok Kim, Kimmo J Hatanpaa, Jack M Raisanen, Dennis K Burns, Jane E Johnson, et al. Adult lineage-restricted cns progenitors specify distinct glioblastoma subtypes. *Cancer cell*, 28(4):429–440, 2015.

[134] Maojin Yao, Shu Li, Xiaojun Wu, Shuo Diao, Guoxin Zhang, Hua He, Liuguan Bian, and Yicheng Lu. Cellular origin of glioblastoma and its implication in precision therapy. *Cellular & molecular immunology*, 15(8):737–739, 2018.

[135] D Williams Parsons, Siân Jones, Xiaosong Zhang, Jimmy Cheng-Ho Lin, Rebecca J Leary, Philipp Angenendt, Parminder Mankoo, Hannah Carter, I-Mei Siu, Gary L Gallia, et al. An integrated genomic analysis of human glioblastoma multiforme. *science*, 321(5897):1807–1812, 2008.

[136] Jian Chen, Renée M McKay, and Luis F Parada. Malignant glioma: lessons from genomics, mouse models, and stem cells. *Cell*, 149(1):36–47, 2012.

[137] Vanajothi Ramar, Shanchun Guo, Guangdi Wang, and Mingli Liu. The pivotal role of nf-κb in glioblastoma: Mechanisms of activation and therapeutic implications. *International journal of molecular sciences*, 26(16):7883, 2025.

[138] Roel GW Verhaak, Katherine A Hoadley, Elizabeth Purdom, Victoria Wang, Yuan Qi, Matthew D Wilkerson, C Ryan Miller, Li Ding, Todd Golub, Jill P Mesirov, et al. Integrated genomic analysis identifies clinically relevant subtypes of glioblastoma characterized by abnormalities in pdgfra, idh1, egfr, and nf1. *Cancer cell*, 17(1):98–110, 2010.

[139] Krishna PL Bhat, Veerakumar Balasubramaniyan, Brian Vaillant, Ravesanker Ezhilarasan, Karlijn Hummelink, Faith Hollingsworth, Khalida Wani, Lindsey Heathcock, Johanna D James, Lindsey D Goodman, et al. Mesenchymal differentiation mediated by nf-κb promotes radiation resistance in glioblastoma. *Cancer cell*, 24(3):331–346, 2013.

[140] Robert L Bowman, Qianghu Wang, Angel Carro, Roel GW Verhaak, and Massimo Squatrito. Gliovis data portal for visualization and analysis of brain tumor expression datasets. *Neuro-oncology*, 19(1):139–141, 2017.

[141] Pratibha Sharma, Ashley Aaroe, Jiyong Liang, and Vinay K Puduvalli. Tumor microenvironment in glioblastoma: Current and emerging concepts. *Neuro-oncology advances*, 5(1):vdad009, 2023.

[142] Rikke Sick Andersen, Atul Anand, Dylan Scott Lykke Harwood, and Bjarne Winther Kristensen. Tumor-associated microglia and macrophages in the glioblastoma microenvironment and their implications for therapy. *Cancers*, 13(17):4255, 2021.

[143] Alice J West, Vanessa Tsui, Stanley S Stylli, Hong Nguyen, Andrew P Morokoff, Andrew H Kaye, and Rodney B Luwor. The role of interleukin-6-stat3 signalling in glioblastoma. *Oncology letters*, 16(4):4095–4104, 2018.

[144] Braden C McFarland, Suk W Hong, Rajani Rajbhandari, George B Twitty Jr, G Kenneth Gray, Hao Yu, Etty N Benveniste, and Susan E Nozell. Nf-κb-induced il-6 ensures stat3 activation and tumor aggressiveness in glioblastoma. *PloS one*, 8(11):e78728, 2013.

[145] Leonid Tarassishin, Diana Casper, and Sunhee C Lee. Aberrant expression of interleukin-1β and inflammasome activation in human malignant gliomas. *PloS one*, 9(7):e103432, 2014.

[146] Jianfeng Han, Christopher A Alvarez-Breckenridge, Qi-En Wang, and Jianhua Yu. Tgf-β signaling and its targeting for glioma treatment. *American journal of cancer research*, 5(3):945, 2015.

[147] Irene Golán-Cancela and Laia Caja. The tgf-β family in glioblastoma. *International Journal of Molecular Sciences*, 25(2):1067, 2024.

[148] Vincenzo Di Nunno, Enrico Franceschi, Alicia Tosoni, Lidia Gatto, Stefania Bartolini, and Alba Ariela Brandes. Tumor-associated microenvironment of adult gliomas: a review. *Frontiers in Oncology*, 12:891543, 2022.

[149] Xianzhe Zhou, Guishan Jin, Junwen Zhang, and Fusheng Liu. Recruitment mechanisms and therapeutic implications of tumor-associated macrophages in the glioma microenvironment. *Frontiers in Immunology*, 14:1067641, 2023.

[150] Bhavesh K Ahir, Herbert H Engelhard, and Sajani S Lakka. Tumor development and angiogenesis in adult brain tumor: glioblastoma. *Molecular neurobiology*, 57(5):2461–2478, 2020.

[151] Franziska Lange, Daniel Kaemmerer, Julianne Behnke-Mursch, Wolfgang Brück, Stefan Schulz, and Amelie Lupp. Differential somatostatin, cxcr4 chemokine and endothelin a receptor expression in who grade i–iv astrocytic brain tumors. *Journal of Cancer Research and Clinical Oncology*, 144(7):1227–1237, 2018.

[152] Marie Hautiere, Delphine Vivier, Donovan Pineau, Caroline Denis, Dimitri Kereselidze, Amaury Herbet, Narciso Costa, Victor Goncalves, Erwan Selingue, Benoit Larrat, et al. Immunopet imaging–based pharmacokinetic profiles of an antibody and its fab targeting endothelin a receptors on glioblastoma stem cells in a preclinical orthotopic model. *European Journal of Nuclear Medicine and Molecular Imaging*, 50(11):3192–3201, 2023.

[153] Keisuke Tsutsumi, Masami Niwa, Naoki Kitagawa, Sei-ich Yamaga, Takeo Anda, Akihiko Himeno, Takaya Sato, Humayun Khalid, Kohtaro Taniyama, and Shobu Shibata. Enhanced expression of an endothelin eta receptor in capillaries from human glioblastoma: a quantitative receptor autoradiographic analysis using a radioluminographic imaging plate system. *Journal of neurochemistry*, 63(6):2240–2247, 1994.

[154] Marie Hautiere, Delphine Vivier, Paul Dorval, Donovan Pineau, Dimitri Kereselidze, Caroline Denis, Amaury Herbet, Narciso Costa, Claire Bernhard, Victor Goncalves, et al. Preoperative pet imaging and fluorescence-guided surgery of human glioblastoma

using dual-labeled antibody targeting eta receptors in a preclinical mouse model: A theranostic approach. *Theranostics*, 14(16):6268, 2024.

[155] Michael Weller, Martin van den Bent, Matthias Preusser, Emilie Le Rhun, Jörg C Tonn, Giuseppe Minniti, Martin Bendszus, Carmen Balana, Olivier Chinot, Linda Dirven, et al. Eano guidelines on the diagnosis and treatment of diffuse gliomas of adulthood. *Nature reviews Clinical oncology*, 18(3):170–186, 2021.

[156] Walter Stummer, Uwe Pichlmeier, Thomas Meinel, Otmar Dieter Wiestler, Friedhelm Zanella, and Hans-Jürgen Reulen. Fluorescence-guided surgery with 5-aminolevulinic acid for resection of malignant glioma: a randomised controlled multicentre phase iii trial. *The lancet oncology*, 7(5):392–401, 2006.

[157] Vibeke A Larsen, Helle J Simonsen, Ian Law, Henrik BW Larsson, and Adam E Hansen. Evaluation of dynamic contrast-enhanced t1-weighted perfusion mri in the differentiation of tumor recurrence from radiation necrosis. *Neuroradiology*, 55(3):361–369, 2013.

[158] Roger Stupp, Warren P Mason, Martin J Van Den Bent, Michael Weller, Barbara Fisher, Martin JB Taphoorn, Karl Belanger, Alba A Brandes, Christine Marosi, Ulrich Bogdahn, et al. Radiotherapy plus concomitant and adjuvant temozolomide for glioblastoma. *New England journal of medicine*, 352(10):987–996, 2005.

[159] Giuseppe Minniti, Maximilian Niyazi, Filippo Alongi, Piera Navarria, and Claus Belka. Current status and recent advances in reirradiation of glioblastoma. *Radiation Oncology*, 16(1):36, 2021.

[160] Kenta Masui, Paul S Mischel, and Guido Reifenberger. Molecular classification of gliomas. *Handbook of clinical neurology*, 134:97–120, 2016.

[161] Rupesh Kotecha, Yazmin Odia, Atulya A Khosla, and Manmeet S Ahluwalia. Key clinical principles in the management of glioblastoma. *JCO oncology practice*, 19(4):180–189, 2023.

[162] Roger Stupp, Sophie Taillibert, Andrew Kanner, Santosh Kesari, Steven A Toms, Gene H Barnett, Karen L Fink, Antonio Silvani, Frank S Lieberman, Jay-Jiguang Zhu, et al. Tumor treating fields (ttfields): A novel treatment modality added to standard chemo-and radiotherapy in newly diagnosed glioblastoma—first report of the full dataset of the ef14 randomized phase iii trial., 2015.

[163] Bichun Xu, Xianzhi Zhao, Yiyin Liang, Weiwei Zhang, Liang Chen, Yusheng Ye, Jie He, Jiaojiao Tong, Yangyang Gong, Judong Luo, et al. Definitive radiotherapy for

local and metastatic lesions in prostate cancer patients with oligometastases. *Frontiers in Oncology*, 15:1662567, 2025.

[164] Sabrina Digiovanni, Martina Lorenzati, Olga Teresa Bianciotto, Martina Godel, Simona Fontana, Muhlis Akman, Costanzo Costamagna, Pierre-Olivier Couraud, Annalisa Buffo, Joanna Kopecka, et al. Blood-brain barrier permeability increases with the differentiation of glioblastoma cells in vitro. *Fluids and Barriers of the CNS*, 21(1):89, 2024.

[165] Sagun Parakh, Joseph Nicolazzo, Andrew M Scott, and Hui Kong Gan. Antibody drug conjugates in glioblastoma–is there a future for them? *Frontiers in Oncology*, 11:718590, 2021.

[166] Henry S Friedman, Michael D Prados, Patrick Y Wen, Tom Mikkelsen, David Schiff, Lauren E Abrey, WK Alfred Yung, Nina Paleologos, Martin K Nicholas, Randy Jensen, et al. Bevacizumab alone and in combination with irinotecan in recurrent glioblastoma. *Journal of Clinical Oncology*, 41(32):4945–4952, 2023.

[167] Shasha Lv, Erik Teugels, Jan Sadones, Sylvia De Brakeleer, Johnny Duerinck, Stephanie Du Four, Alex Michotte, Jacques De Greve, and Bart Neyns. Correlation of egfr, idh1 and pten status with the outcome of patients with recurrent glioblastoma treated in a phase ii clinical trial with the egfr-blocking monoclonal antibody cetuximab. *International journal of oncology*, 41(3):1029–1035, 2012.

[168] Ilse AC Spiekman, Birgit S Geurts, Laurien J Zeverijn, Gijs F De Wit, Vincent Van Der Noort, Paul Roepman, Wendy WJ De Leng, Anne ML Jansen, Benno Kusters, Laurens V Beerepoot, et al. Efficacy and safety of panitumumab in patients with raf/ras-wild-type glioblastoma: results from the drug rediscovery protocol. *The oncologist*, 29(5):431–440, 2024.

[169] Xiao-Jing Du, Xian-Ming Li, Lin-Bo Cai, Jian-Cong Sun, Si-Yang Wang, Xi-Cheng Wang, Xiao-Lin Pang, Mei-Ling Deng, Fang-Fang Chen, Zhi-Qiang Wang, et al. Efficacy and safety of nimotuzumab in addition to radiotherapy and temozolomide for cerebral glioblastoma: a phase ii multicenter clinical trial. *Journal of Cancer*, 10(14):3214, 2019.

[170] Céline Chevaleyre, Anthony Novell, Nicolas Tournier, Ambre Dauba, Steven Dubois, Dimitri Kereselidze, Erwan Selingue, Benoit Jego, Bernard Maillère, Benoit Larrat, et al. Efficient pd-l1 imaging of murine glioblastoma with fus-aided immunopet by leveraging fcrn-antibody interaction. *Theranostics*, 13(15):5584, 2023.

[171] Eleanor Martin, Jean-François Aubry, Mark Schafer, Lennart Verhagen, Bradley Treeby, and Kim Butts Pauly. Itrusst consensus on standardised reporting for transcranial ultrasound stimulation. *Brain Stimulation*, 17(3):607–615, 2024.

[172] Kenneth B Bader, Frederic Padilla, Kevin J Haworth, Nicholas Ellens, Diane Dalecki, Douglas L Miller, Keith A Wear, Bioeffects Committee of the American Institute of Ultrasound in Medicine, Kenneth Bader, Jason T Nomura, et al. Overview of therapeutic ultrasound applications and safety considerations: 2024 update. *Journal of Ultrasound in Medicine*, 44(3):381–433, 2025.

[173] Golo Petzold. Role of ultrasound methods for the assessment of nafld. *Journal of clinical medicine*, 11(15):4581, 2022.

[174] Douglas L Miller, Nadine B Smith, Michael R Bailey, Gregory J Czarnota, Kullervo Hynynen, Inder Raj S Makin, and Bioeffects Committee of the American Institute of Ultrasound in Medicine. Overview of therapeutic ultrasound applications and safety considerations. *Journal of ultrasound in medicine*, 31(4):623–634, 2012.

[175] Likai Yuan, Qianqian Li, and Zhen Li. Effects of ultrasound for bio-applications. *Advanced Sensor Research*, 3(8):2300199, 2024.

[176] Dawid Przystupski and Marek Ussowicz. Landscape of cellular bioeffects triggered by ultrasound-induced sonoporation. *International journal of molecular sciences*, 23(19):11222, 2022.

[177] Veronica Zelli, Alessandra Corrente, Chiara Compagnoni, Francesco Colaianni, Martina Sara Miscione, Monica Di Padova, Daria Capece, Gaetano Barbato, Edoardo Alesse, Francesca Zazzeroni, et al. Ultrasound as a new method for the release and identification of novel micrornas and proteins as candidate biomarkers in pancreatic cancer. *Cancers*, 17(12):1979, 2025.

[178] Jessica Cornice, Daria Capece, Mauro Di Vito Nolfi, Monica Di Padova, Chiara Compagnoni, Daniela Verzella, Barbara Di Francesco, Davide Vecchiotti, Irene Flati, Alessandra Tessitore, et al. Ultrasound-based method for the identification of novel microrna biomarkers in prostate cancer. *Genes*, 12(11):1726, 2021.

[179] Bryan C Fuchs, Tsutomu Fujii, Jon D Dorfman, Jonathan M Goodwin, Andrew X Zhu, Michael Lanuti, and Kenneth K Tanabe. Epithelial-to-mesenchymal transition and integrin-linked kinase mediate sensitivity to epidermal growth factor receptor inhibition in human hepatoma cells. *Cancer research*, 68(7):2391–2399, 2008.

[180] Jae-Gahb Park, Jae-Ho Lee, Myung-Soo Kang, Kyu-Joo Park, You-Me Jeon, Hyun-Ju Lee, Hae-Sung Kwon, Hyun-Sook Park, Kyong-Sook Yeo, Kuhn-Uk Lee, et al. Characterization of cell lines established from human hepatocellular carcinoma. *International journal of cancer*, 62(3):276–282, 1995.

[181] AM Pfeifer, Katherine E Cole, Duane T Smoot, Ainsley Weston, John D Groopman, Peter G Shields, Jean-Michel Vignaud, Michel Juillerat, Michael M Lipsky, and Benjamin F Trump. Simian virus 40 large tumor antigen-immortalized normal human liver epithelial cells express hepatocyte characteristics and metabolize chemical carcinogens. *Proceedings of the National Academy of Sciences*, 90(11):5123–5127, 1993.

[182] Marjan Norouzzadeh, Yas Kalikias, Zinat Mohamadpur, Loghman Sharifi, and Maryam Mahmoudi. Determining population doubling time and the appropriate number of hepg2 cells for culturing in 6-well plate. *Int Res Bas Sci*, 10(3):299–303, 2016.

[183] Akira Yokoi, Juntaro Matsuzaki, Yusuke Yamamoto, Yutaka Yoneoka, Kenta Takahashi, Hanako Shimizu, Takashi Uehara, Mitsuya Ishikawa, Shun-ichi Ikeda, Takumi Sonoda, et al. Integrated extracellular microrna profiling for ovarian cancer screening. *Nature communications*, 9(1):4319, 2018.

[184] Fumihiko Urabe, Juntaro Matsuzaki, Yusuke Yamamoto, Takahiro Kimura, Tomohiko Hara, Makiko Ichikawa, Satoko Takizawa, Yoshiaki Aoki, Shumpei Niida, Hiromi Sakamoto, et al. Large-scale circulating microrna profiling for the liquid biopsy of prostate cancer. *Clinical cancer research*, 25(10):3016–3025, 2019.

[185] Yusuke Yamamoto, Shunsuke Kondo, Juntaro Matsuzaki, Minoru Esaki, Takuji Okusaka, Kazuaki Shimada, Yoshiki Murakami, Masaru Enomoto, Akihiro Tamori, Ken Kato, et al. Highly sensitive circulating microrna panel for accurate detection of hepatocellular carcinoma in patients with liver disease. *Hepatology communications*, 4(2):284–297, 2020.

[186] Wataru Usuba, Fumihiko Urabe, Yusuke Yamamoto, Juntaro Matsuzaki, Hideo Sasaki, Makiko Ichikawa, Satoko Takizawa, Yoshiaki Aoki, Shumpei Niida, Ken Kato, et al. Circulating mirna panels for specific and early detection in bladder cancer. *Cancer science*, 110(1):408–419, 2019.

[187] Davide Vecchiotti, Mauro Di Vito Nolfi, Francesca Veglianti, Francesca Dall'Aglio, Hafiz Nadeem Khan, Irene Flati, Daniela Verzella, Daria Capece, Edoardo Alesse, Adriano Angelucci, et al. A 3d bioprinting approach to studying retinal müller cells. *Genes*, 15(11):1414, 2024.

[188] Michele Patrizii, Monica Bartucci, Sharon R Pine, and Hatem E Sabaawy. Utility of glioblastoma patient-derived orthotopic xenografts in drug discovery and personalized therapy. *Frontiers in oncology*, 8:23, 2018.

[189] William H Hicks, Cylaina E Bird, Jeffrey I Traylor, Diana D Shi, Tarek Y El Ahmadieh, Timothy E Richardson, Samuel K McBrayer, and Kalil G Abdullah. Contemporary mouse models in glioma research. *Cells*, 10(3):712, 2021.

[190] Susann Hetze, Ulrich Sure, Manfred Schedlowski, Martin Hadamitzky, and Lennart Barthel. Rodent models to analyze the glioma microenvironment. *Asn Neuro*, 13:17590914211005074, 2021.

[191] Vu Long Tran, Anthony Novell, Nicolas Tournier, Matthieu Gerstenmayer, Arnaud Schweitzer-Chaput, Claudia Mateos, Benoit Jego, Alizée Bouleau, Hervé Nozach, Alexandra Winkeler, et al. Impact of blood-brain barrier permeabilization induced by ultrasound associated to microbubbles on the brain delivery and kinetics of cetuximab: An immunopet study using 89zr-cetuximab. *Journal of Controlled Release*, 328:304–312, 2020.

[192] Clifford S Patlak, Ronald G Blasberg, and Joseph D Fenstermacher. Graphical evaluation of blood-to-brain transfer constants from multiple-time uptake data. *Journal of Cerebral Blood Flow & Metabolism*, 3(1):1–7, 1983.

[193] E Merit Reyes-Reyes, Yun Teng, and Paula J Bates. A new paradigm for aptamer therapeutic as1411 action: uptake by macropinocytosis and its stimulation by a nucleolin-dependent mechanism. *Cancer research*, 70(21):8617–8629, 2010.

[194] Ine Lentacker, Ine De Cock, R Deckers, SC De Smedt, and CTW Moonen. Understanding ultrasound induced sonoporation: definitions and underlying mechanisms. *Advanced drug delivery reviews*, 72:49–64, 2014.

[195] Xiaofei Song, Zie Wang, Yan Jin, Yong Wang, and Wenbing Duan. Loss of mir-532-5p in vitro promotes cell proliferation and metastasis by influencing cxcl2 expression in hcc. *American journal of translational research*, 7(11):2254, 2015.

[196] Xiao Wang, Shasha Liu, Ling Cao, Tengfei Zhang, Dongli Yue, Liping Wang, Yu Ping, Qianyi He, Chaoqi Zhang, Meng Wang, et al. mir-29a-3p suppresses cell proliferation and migration by downregulating igf1r in hepatocellular carcinoma. *Oncotarget*, 8(49):86592, 2017.

[197] Guohui Wang, Shaihong Zhu, Yonghong Gu, Qian Chen, Xinrong Liu, and Hua Fu. Microrna-145 and microrna-133a inhibited proliferation, migration, and invasion, while

promoted apoptosis in hepatocellular carcinoma cells via targeting fscn1. *Digestive diseases and sciences*, 60(10):3044–3052, 2015.

[198] Mariarosaria Incoronato, Anna Maria Grimaldi, Peppino Mirabelli, Carlo Cavaliere, Chiara Anna Parente, Monica Franzese, Stefania Staibano, Gennaro Ilardi, Daniela Russo, Andrea Soricelli, et al. Circulating mirnas in untreated breast cancer: an exploratory multimodality morpho-functional study. *Cancers*, 11(6):876, 2019.

[199] Fatma Ibrahim Dwedar, Reham Said Shams-Eldin, Salwa Nayer Mohamed, Ayman Farouk Mohammed, and Salwa Hamdi Gomaa. Potential value of circulatory microrna10b gene expression and its target e-cadherin as a prognostic and metastatic prediction marker for breast cancer. *Journal of clinical laboratory analysis*, 35(8):e23887, 2021.

[200] Lanyun Zhou, Wei Wang, Fenfen Wang, Siqi Yang, Jiaqi Hu, Bingjian Lu, Zimin Pan, Yu Ma, Mengyue Zheng, Liyuan Zhou, et al. Plasma-derived exosomal mir-15a-5p as a promising diagnostic biomarker for early detection of endometrial carcinoma. *Molecular cancer*, 20(1):57, 2021.

[201] Michiro Muraki. Soluble fas ligand, soluble fas receptor, and decoy receptor 3 as disease biomarkers for clinical applications: A review. *AIMS Medical Science*, 9(2):98–267, 2022.

[202] Hua Guo, Ying-tang Gao, Qin Zhang, Li Jing, Tong Liu, Wen-xia Shi, Dao-kuan Zhai, Xiang Jing, and Zhi Du. Expression and clinical significance of livin protein in hepatocellular carcinoma. *Disease markers*, 35(5):489–496, 2013.

[203] R. Kozuka, Y. Nakagawa, Y. Tanaka, et al. Soluble immune-checkpoint proteins as predictors of hepatocellular carcinoma development during nucleos(t)ide analogue treatment. *Scientific Reports*, 12:13625, 2022.

[204] L. Lorente, A. Jakovljevic, I. González-Pinto, et al. High serum soluble cd40l levels before liver transplantation are associated with increased mortality in hepatocellular carcinoma patients. *Journal of Critical Care*, 43:316–320, 2018.

[205] N. V. Hanh, P. H. Thu, et al. Poorly differentiated hepatocellular carcinoma cells exhibit increased soluble cd40 levels. *Biomedical Journal*, 48:100752, 2025.

[206] G. Gruden, P. Carucci, V. Lolli, et al. Serum heat shock protein 27 levels in patients with hepatocellular carcinoma. *BMC Cancer*, 12:483, 2012.

Tesi redatta con il cofinanziamento dell'Unione europea-*NextGeneration EU*
Piano Nazionale di Ripresa e Resilienza Missione 4 – Componente 1 –
Investimento 4.1. del PNRR – "Ricerca PNRR" – CUP E11I22000160001